SAND2014-19004R

SANDIA REPORT

SAND#
UUR
Printed February 2014

Hybrid-renewable processes for biofuels production: concentrated solar pyrolysis of biomass residues

Anthe George, Manfred Geier, Daniel Dedrick

Prepared by
Sandia National Laboratories
Albuquerque, New Mexico 87185 and Livermore, California 94550

Sandia National Laboratories is a multi-program laboratory managed and operated by Sandia Corporation, a wholly owned subsidiary of Lockheed Martin Corporation, for the U.S. Department of Energy's National Nuclear Security Administration under contract DE-AC04-94AL85000.

Sandia National Laboratories

Issued by Sandia National Laboratories, operated for the United States Department of Energy by Sandia Corporation.

Available to DOE and DOE contractors from
U.S. Department of Energy
Office of Scientific and Technical Information
P.O. Box 62
Oak Ridge, TN 37831

Telephone: (865) 576-2087
Facsimile: (865) 576-5728
E-Mail: reports@adonis.osti.gov
Online ordering: http://www.osti.gov/bridge

Available to the public from
U.S. Department of Commerce
National Technical Information Service
5301 Shawnee Rd
Alexandria, VA 22312

Telephone: (800) 553-6847
Facsimile: (703) 605-6900
E-Mail: orders@ntis.gov
Online order: http://www.ntis.gov/help/ordermethods.aspx#online

SAND200X-XXXX
Unlimited Release
February 2014

Hybrid-renewable processes for biofuels production: concentrated solar pyrolysis of biomass residue

Anthe George, Manfred Geier, Daniel Dedrick
08367
Sandia National Laboratories
P.O. Box 5800
Albuquerque, New Mexico

ABSTRACT

The viability of thermochemically-derived biofuels can be greatly enhanced by reducing the process parasitic energy loads. Integrating renewable power into biofuels production is one method by which these efficiency drains can be eliminated. There are a variety of such potentially viable "hybrid-renewable" approaches; one is to integrate concentrated solar power (CSP) to power biomass-to-liquid fuels (BTL) processes. Barriers to CSP integration into BTL processes are predominantly the lack of fundamental kinetic and mass transport data to enable appropriate systems analysis and reactor design. A novel design for the reactor has been created that can allow biomass particles to be suspended in a flow gas, and be irradiated with a simulated solar flux. Pyrolysis conditions were investigated and a comparison between solar and non-solar biomass pyrolysis was conducted in terms of product distributions and pyrolysis oil quality. A novel method was developed to analyse pyrolysis products, and investigate their stability.

ACKNOWLEDGMENTS

This work was supported by the Laboratory Directed Research and Development program at Sandia National Laboratories. Sandia National Laboratories is a multi-program laboratory managed and operated by Sandia Corporation, a wholly owned subsidiary of Lockheed Martin Corporation, for the U.S. Department of Energy's National Nuclear Security Administration under contract DE-AC04-94AL85000.

We thank Christopher Shaddix, SNL and Rafael Kandiyoti, Imperial College London, for their constructive comments during this work and, Trevor Morgan, at the Hawaiian institute of technology for his contributions to the method development studies in this work.

CONTENTS

1.0 Introduction

The viability of thermochemically-derived biofuels can be greatly enhanced by reducing the process parasitic energy loads. Gasification processes are globally endothermic, requiring 20-45% of the feedstock[i] to be consumed allothermally. Additionally, in air-blown gasification, high CO_2 and N_2 dilute the product syngas. Likewise pyrolysis processes also require external energy to progress. Integrating renewable power into biofuels production is one method by which these energy efficiency drains can be eliminated. There are a variety of such potentially viable "hybrid-renewable" approaches; one is to integrate concentrated solar power (CSP) to power biomass-to-liquid fuels (BTL) processes, both during pyrolysis and/or gasification operations as well as downstream. Barriers to CSP integration into BTL processes are predominantly the lack of fundamental kinetic and mass transport data to enable appropriate systems analysis and reactor design.

There is currently little understanding of the fundamental behavior of biomass particles subjected to solar flux. When considering thermochemical conversion of carbonaceous feedstocks, many parallel as well as sequential reactions involving neighboring particles need to be considered. In these complex reactions final product distribution is a function of the time-temperature-pressure distribution, as well as history, of the reaction mixture. Pyrolysis experiments are therefore very sensitive to the heating method, flow patterns, design of reaction zone and configuration of the sample (shape, size, composition), and data are often an artifact of the methods used to produce them. The paucity of data on solar treatment of biomass is exacerbated by the fact that, to-date, attempts have not been made to decouple these secondary effects from reactor design. In this work we proposed to develop a reactor scheme that simulates solar influx onto biomass particles but minimizes these artifact effects, allowing high quality fundamental data to be obtained. This will enable rational science-based design of process scale-up, rather than the post-hoc approaches taken to-date. Part of this investigation necessitated the development of methods to analyse the bio-oil in its entirety. Current analytical techniques do not adequately cope with the heavier components of pyrolysis oils and gasification tars, and it is thought that it is these components which contribute to the instability of the bio-oils (one of the main challenges associated with these types of fuels). Therefore techniques were developed

that could give more information on the higher molecular weight components in thermochemically derived liquids, and the aging and stability of gasification tars were investigated via the techniques developed, in order to highlight their effectiveness in this context.

Other than process energy, feedstock is another important parameter in biofuels production. Lignocellulosic biomass typically consists of 20-30% lignin. Utilizing lignin that is currently a waste stream from the lignocellulosic biofuels process to produce biofuels would have an enormous impact on the economics of the biorefinery, which only uses the cellulose portion of the biomass. Feedstock cost is one of the main economic barriers to the uptake of biofuels technologies, so using a waste stream as the feedstock to the CSP process would make a significant contribution to the process viability. In this research we investigated the pyrolysis of lignin. Thermochemical conversion is particularly challenging due to the high quantities of char produced. One of the great advances in plant science is the ability to manipulate the structure of the growing plant. Lignin itself has been shown to be altered in the plant cell wall, in terms of both its degree of polymerization, the amount of lignin that can produce a viable plant and also the structure of the lignin. In this study we investigated genetically modified lignins to ascertain if the thermochemical conversion in these plants produces a different quality bio-oil and if this bio-oil is of a superior quality (or has the potential to be superior) compared to the conversion of the wild-type plant.

2.0 Simulated concentrated solar pyrolysis reactors and bio-oil production

Thermochemical behavior, particularly pyrolysis behavior is highly dependent on reactor configuration. Three reactors were developed in this study to enable the investigation of different aspects of solar thermochemical conversion of biomass. The first reactor, (Figure 2.1) was the most complex system and was designed to allowed the careful study of thermochemical behavior by minimizing to as great an extent as possible mass transfer limitations within fuel particles that inhibit volatile release and promote char formation. This is particularly important when investigating the conversion of biomass to fuel as here char conversion should be minimized and liquids yield maximized. The fluidizing medium in this instance was found to lower the achievable temperature in the system, which whilst higher than required for typical pyrolysis processes is lower than would be desirable when simulating higher temperature gasification. Therefore a second fixed bed reactor was developed which would remove the heat-transfer from the fuel particle to the flowing gas and allow for gasification studies to be conducted (Figure 2.2). Higher temperature gasification reactions are somewhat less sensitive to particle size and mass transfer limitations associated with lower temperature biomass pyrolysis reactions attempting to maximize oil yield and therefore a fixed bed was deemed to be appropriate for this type of study. Finally to allow for comparison between the solar case and conventional pyrolysis systems a furnace type pyrolysis reactor was designed (Figure 2.3). These reactors are described below.

2.1 Fluidized and fixed bed solar thermochemical conversion reactors and conventionally heated batch pyrolysis reactor

Several assumptions and requirements were made in order to arrive at the best approximation for a concentrated solar powered fuel conversion reactor. All the reactors in this investigation were custom fabricated from quartz, which although can be fragile, is used in this instance because a) it is transparent to the simulated solar radiation, b) allows for an inert atmosphere for the pyrolysis oils (preventing catalytic reactions occurring when pyrolysis products come into contact with metals) and c) also

for easy recovery of any condensed material on the reactor. An added benefit is the possibility of allowing visual monitoring and imaging of the system whilst the experiment is underway.

The heat source for this system was intended to simulate concentrated solar power. Typically argon lamps are often used for this purpose, but due to budget considerations IR lamps were investigated as suitable alternatives. To enable an even distribution of light to the biomass particles a columnated light source was required at a narrow wavelength range. The wavelength chosen would need to be transparent to quartz. Research Inc Strip IR 5360 lamps were used. Figure 2.4 depicts the columnated light produced from a single lamp and how a configuration of several lamps can be used to improve the density of the radiance. In this system two lamps were used. The tungsten emitter in the lamps has an operating temperature of up to 2205 °C with a spectral energy peak wavelength of 1.15 microns (Figure 2.5). The power outlet of these heaters was 1000W at 240 V. The heater consists of a specular aluminum reflector that directs the infrared energy generated by one ceramic end-seal 'T-3 style' quartz halogen lamp factory-installed in the heater. The quartz halogen lamps heat up and cool down instantly in response to power control signals. They reach 90 percent of full operating temperature within three seconds of a cold start. The radiant energy dissipates to ten percent five seconds after the power supply is disconnected.

Despite the responsive nature of the lamp, fast pyrolysis needs to be controlled to within milliseconds, and we have this requirement here. Therefore a shutter system was designed and controlled by LABVIEW, whereby a heat resistant shield made of refractory material was designed. Using this shutter system and LABVIEW the exposure of the biomass particles to the heat source can be controlled to +/- 5 ms.

The operation of the fluidized bed reactor given the design described is as follows: the feeding tube and lamp cooling water systems are activated, after which the hot fluidizing gas (nitrogen, 180 °C) is passed through the reactor. The fluidizing gas is heated to below the pyrolysis temperature of the particles as the short reaction times, and high heating rates required to conduct these fundamental studies could not be achieved with the lamp set-up in this reactor scheme, if the experiment was starting from "cold". A carrier gas at the top of the reactor of low flowrate (Figure 2.1) is then

introduced into the reactor. The charge of biomass particles are introduced into the fluidized zone via opening a simple ball valve and are carried through by the small flowrate of the aforementioned gas. The experiment is now ready to proceed. By means of LABVIEW, the lamps are switched on and after 3 seconds the shutters are opened. The fluidized biomass particles are exposed to the heat source for the prescribed time after which the shutters are automatically closed. Any solids (char and unreacted biomass) is collected in the char-trap after the fluidizing gasses have been switched off. The volatile pyrolysis products are condensed in a tar-trap, and in theory after the tar trap a gas analyser could quantify the permanent gases from the experiment. However, this facility was not available for these experiments and gas yields were quantified by difference. To compare the pyrolysis product distribution from the solar heated and non-solar heated case a furnace based pyrolysis reactor was designed (Figure 2.3).

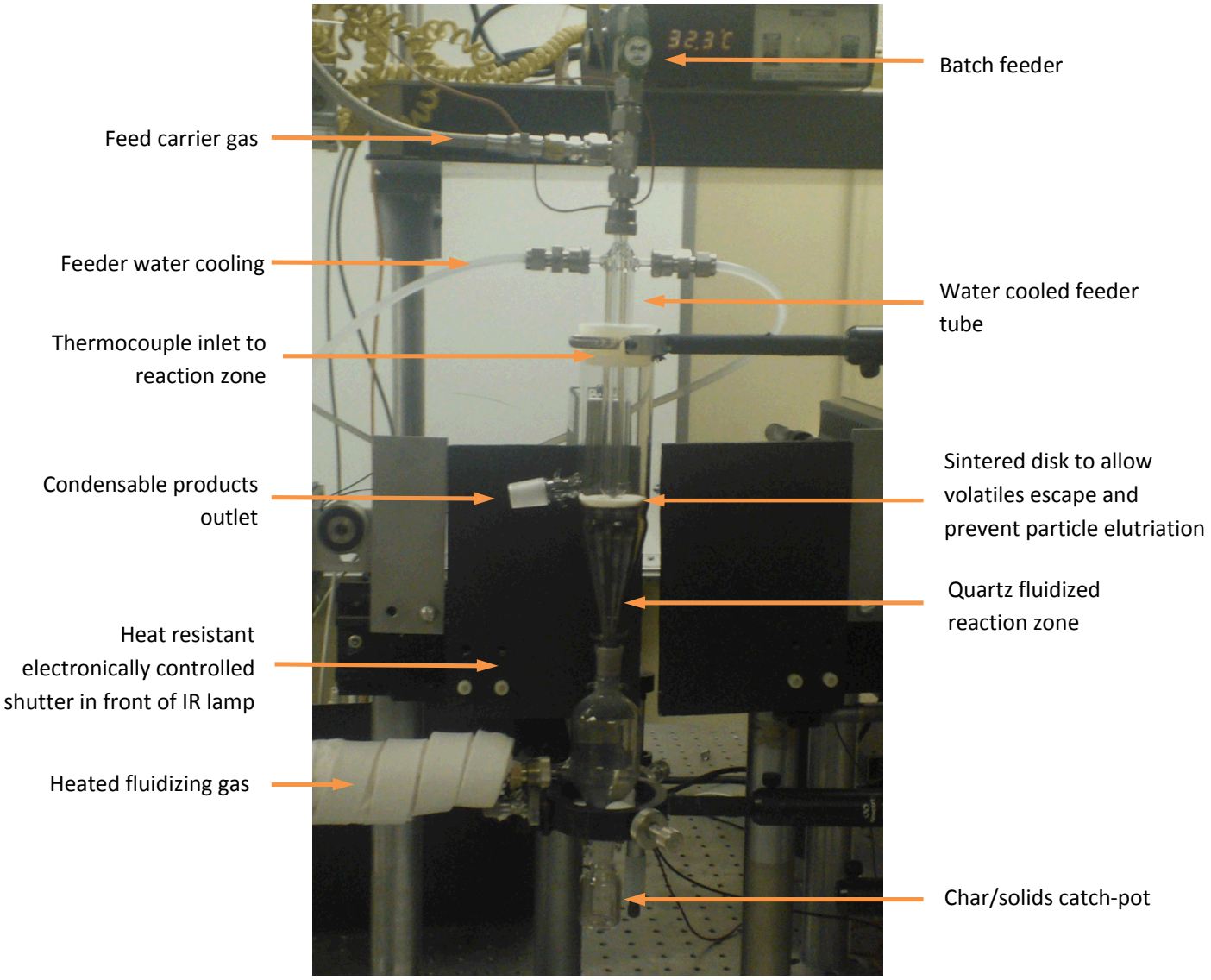

Figure 2.1 Fluidized solar pyrolysis reactor, illustrating key operating components

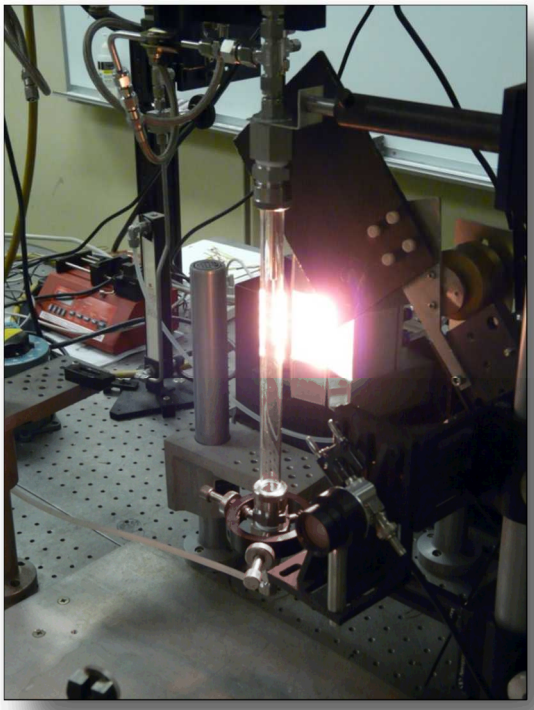

Figure 2.2 Fixed bed solar pyrolysis reactor, showing electronically controlled shutter carrier gas in-let and volatile (bio-oil) outlet.

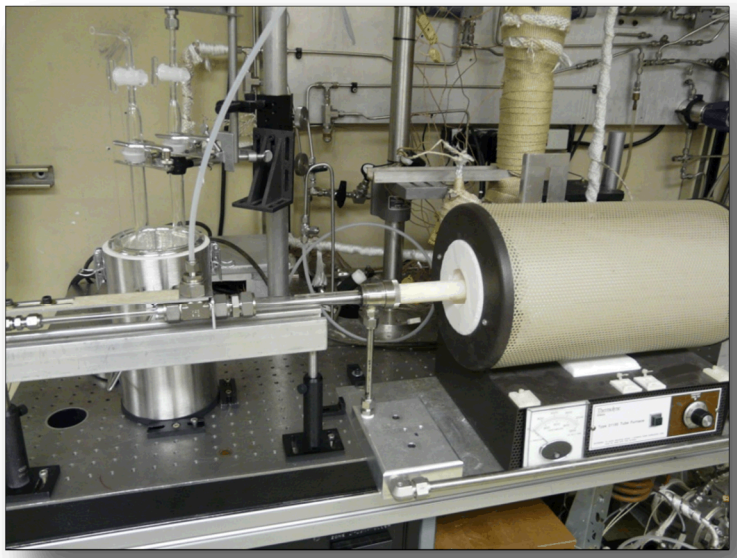

Figure 2.3 Columnated solar pyrolysis reactor, showing electronically controlled shutter carrier gas in-let and volatile (bio-oil) outlet.

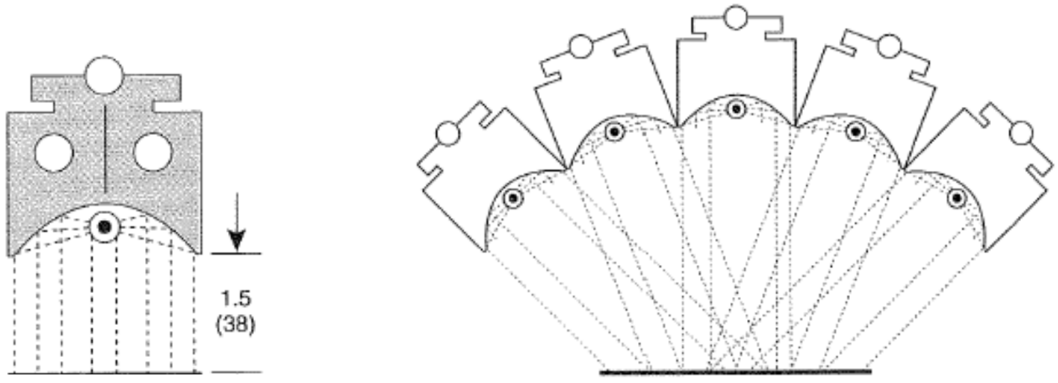

Figure 2.4 Columnated IR radiation produced by IR lamp and multi-lamp configuration for increasing density of radiation to target. In this work a two lamp configuration was used.

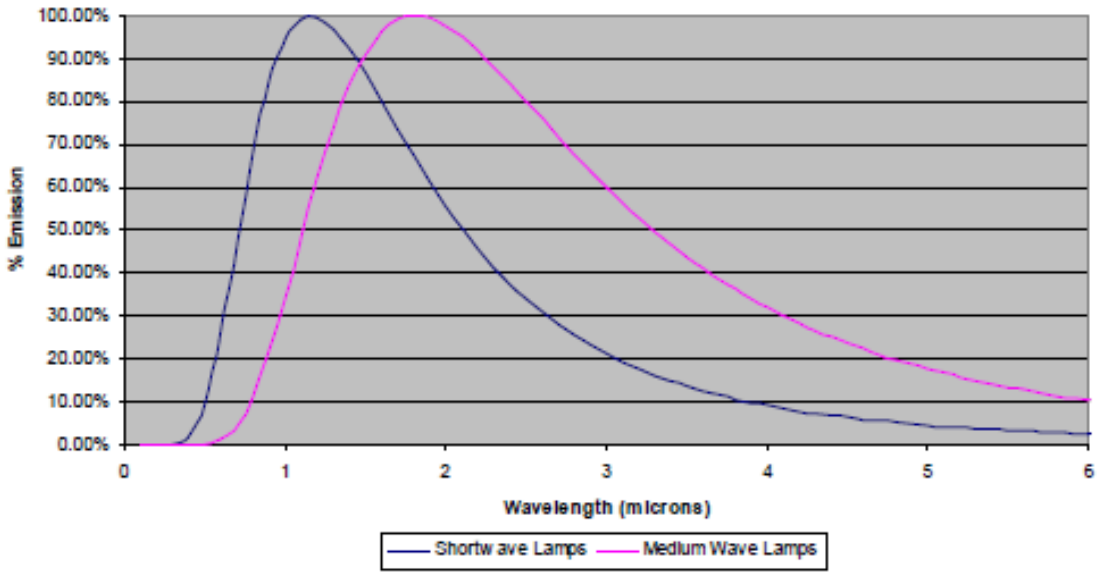

Figure 2.5 Emission range of IR lamp used in fluidized solar pyrolysis reactor. Peak emission is approximately 1 μm which allows for transmittance through quartz and isa representative wavelength for solar radiation.

2.2 Materials

Switchgrass (Panicum virgatum) was provided by Dr. Daniel Putnam, University of California at Davis. Switchgrass was ground by a Wiley Mill through a 2 mm screen and separated by a vibratory sieve system (Endecotts, Ponte Vedra, FL). The switchgrass fractions falling between 60 and 80 mesh were collected for use in this study. The

biomass was dried in a convection oven at 50 degrees Celsius for 24 hours before use. Analytical grade reagents (Sigma) were used throughout.

2.3 GC-FID Analysis

For pyrolysis oil analysis, a Varian GC3800-FID with a Varian 'FactorFour' capillary column (VF-5ms 30M, 0.25mM ID, DF = 0.25) was used to quantitatively examine the tars. 5 μL injection volume (split ratio 50), helium carrier gas (2 mL/min), injector temperature 325°C, column starting temperature of 50°C for 4 minutes, 25°C/min ramp to 150°C, 5°C/min ramp to 325°C, held at 325°C for 2 minutes. FID detector temperature was 325°C. For the GC analysis a volume of the isopropanol-tar solution was taken before the sample was vacuum dried. Further details of peak identification, standards and calibration are provided in S3.

2.4 Product distribution

Switchgrass was pyrolysed at varying conditions (residence time and temperature), table 2.1. This data is compared with experiments conducted in the wire-mesh reactor described in section 4.1. Particle heating rate calculations are always challenging in thermochemical conversion experiments. The challenge with the solar reactor system designed here is that the heating rate of the particle could not be as accurately inferred as in the wiremesh, as the temperature being measured was the bulk temperature in the reaction zone. Nevertheless heating rates up to 500 °C per second could be achieved with lamp power at 80% of maximum, with a heated inlet gas of 180° C with the fluidized system and 1200 °C for the static system. For the char tar and gas product distributions, char is defined as the solids material recovered after reaction, tar as the condensable liquid material recovered in the trap after reaction and the permanent gas yield was calculated by difference. Reactions were repeated in quadruplicate, and measurement uncertainties were in most cases <5% but always <10% and data are given on a dry, ash free basis.

Table 2.1 pyrolysis of switchgrass using simulated solar irradiation via an IR lamp

Reactor type	Peak temperature (°C)	Holding time (s)	Char (wt.%)	Tar (wt.%)	Gas (wt.%)
Solar	400	5	24.3	48.34	27.36
Solar	400	30	22.1	47.6	30.3
Solar	550	5	17.8	50.1	32.1
Solar	550	30	17.4	50.4	32.2
Wire-mesh	400	5	19.9	52.8	27.3
Wire-mesh	400	30	19.2	52.6	28.2
Wire-mesh	550	5	18.4	53.5	28.1
Wire-mesh	550	30	18.3	53.2	28.5

In general the solar system showed greater sensitivity to parameter change than the wire-mesh reactor. With regard to variations in temperature, it appears for the solar system that for both holding times char yields decreased with increasing temperature and whilst both tar and gas yields increased. Pyrolysis product yields are generally thought to be more affected by heating rate than temperature, but at 400 °C it is likely that the higher solids yields are due to unreacted material, rather than a greater production of char. This is bourne out by the lower char yields in the solar reactor at longer residence times at both temperature tests.

The data above show that holding time did not make a difference in the case of the wire-mesh reactor for char production at a particular temperature but was a more significant variable in the solar system at 400 °C. However, particularly at higher temperatures, the tar yields were reduced at longer holding times In the solar reactor. The wire-mesh was designed to approximate an ideal system in terms of secondary tar reactions and cracking. It appears for the solar system, heat transfer within the particle is more efficient leading to lower char yields, however, the evolved products are further cracked to permanent gases. Further investigation of the heat transfer phenomena via this radiative system at these lower temperatures would be most interesting.

3.0 Method development for analyzing heavy pyrolysis oils and bio-oil stability

3.1 Challenges in bio-oil characterization

A known issue with pyrolysis oil and liquid products from gasification is accurate characterization of the molecular structure, particularly of the heavier components of the biomass which sample instability. This is particularly challenging if these components are to be used for bio-fuel production which, as with all fuels, will need to have stable attributes that fall within certain standard values. A method was developed to characterize heavier components in biomass by evaluating the heaviest tars produced in the co-gasification of biomass with coal. A description of the study and results are shown in this section.

Gasification has been recognised as one of the most efficient thermochemical processes for converting solid fuels into energy [1]. Despite this high efficiency, relatively few power stations have adopted this technology, due to economic and downstream technical drawbacks. The environmental concerns about the levels of carbon dioxide in the atmosphere have provoked a renewed interest [1-8]. However, several unsolved problems related to fixed- and fluidised-bed biomass gasification remain which hamper the implementation of the technology. Of main concern for any application of the synthesis gas is the presence of impurities such as tar, NH_3, HCl, HCN, H_2S and COS [1]. In particular, the amount of tar produced reduces the carbon conversion and efficiency and causes significant operational problems due to deposition on exhaust lines [1, 9]. There are also difficulties with their subsequent storage and processing [1, 5-10].

Gasification tars also contain high levels of polyaromatic hydrocarbons (PAHs) that are recognised carcinogens by the environmental protection agency (EPA [11]). A number of gas cleaning systems are commercially available and in routine operation, but these are costly and not currently optimised [8-10].

At present, tars from the co-gasification of biomass and coal, as well as from pure biomass, are being produced on a small but increasing scale after synthesis gas cleaning. Recovered gasification tars are typically re-used as boiler-fuel. This is not necessarily environmentally favourable or cost effective [12, 13]. Moreover, the increased emphasis

on using biomass as a substitute for coal for power generation will lead to greater amounts of tars being generated in the future. These will need to be used, stored, or otherwise disposed. Gasification tars from biomass, which contain higher quantities of oxygen than those from coal, will have analogous issues to biomass pyrolysis liquids with regard to their storage, upgrading and/or use.

Biomass pyrolysis liquids are composed of a complex mixture of oxygenated hydrocarbons (e.g. alcohols, aldehydes, carboxylic acids, esters, ethers, ketones, phenols and sugar derivatives) with 15-30 wt% water from the original moisture and as reaction product [1, 14, 15]. The effects due to ageing on biomass pyrolysis liquids have been widely studied. Reactions occur between oxygenated compounds, volatile components are lost due to evaporation leading to an increase of molecular weight, and changes in water content and viscosity can result in phase separation [1, 14-22]. The probable reaction pathways involved in the ageing process have been reported to confer possible changes to bulk properties such as boiling range, density and viscosity [14]. However, limited information is available regarding changes on the molecular level.

Ageing studies of biomass pyrolysis liquids have focused on the analysis of the trends in molecular weight, based on size exclusion chromatography or viscosity, and on the determination of the water content [14, 15]. Less attention has been paid to the study of chemical composition through techniques such as GC/GC-MS, FT-IR and NMR [19, 23, 24]. The influence of storage temperature and solvent addition on the stability of oils and tars has been widely examined, typically based on viscosity data which can only provide indicative information on other important properties [14-16, 25, 26]. Several approaches to improve the stability of pyrolysis oils have been reported [15, 27]. The addition of a polar solvent is a common approach to improve the stability of tars during storage and can result in a twenty fold decrease in the ageing rate, reduction in viscosity and acidity, as well as increasing heating value and miscibility with fossil fuels [15, 18, 23, 26]. The upgrading of biomass pyrolysis liquids by addition of alcohols at room temperature has been conducted at the industrial scale since 1995 [28]. Similarly, the storage of gasification and pyrolysis tars in alcohol solution at reduced temperature (5°C) has been reported to minimise ageing reactions [14].

Standard analytical methods are available for the recovery [29] and characterisation [30] of tars from gasification, which enable comparisons to be made between different reactor configurations and fuels. The standard methods however, are based on gas chromatography (GC) and the gravimetric weight of the tar. This limits the analysis to materials that are volatile at GC column conditions. In general, little is known about the composition of materials labelled as 'tars' in terms of molecular mass distribution, average molecular mass or structure, beyond information available from GC methods [1, 8, 12, 13, 31]. For compounds present in gasification tars the typical GC upper limit is ~350 u for aromatic compounds and ~600 u for aliphatic compounds, C60-C70 or a little higher (C100), using high temperature GC [32-34]. The smaller molecular weight components typically constitute between 30-60 wt% of the entire sample (depending on reaction conditions and feedstock), so there exists a large gap in understanding of the important remaining portion of the tar [12].

Studies in the literature reveal that more advanced analytical techniques have rarely been applied to gasification tars and in particular those from biomass. This is despite the fact that biomass and coal gasification tars have been of studied since the 1990s and have been indentified as a key issue to be addressed for improving energy conversion [35-37]. This point has also been reiterated more recently in a comprehensive review of the chemistry of thermochemical processes used to synthesise transportation fuels from biomass [1]. Much of the early work using advanced analytical methods focused on coal tars and pitch [36, 37], petroleum maltene and asphaltenes [38], coal [39], partial oxidized aromatic hydrocarbons [40] and products from wood pyrolysis [41-43]. Most of these studies focus on the identification of small to medium sized molecules (<800 u) [39-42], in some cases using GC based methods [39, 41] or in combination with liquid chromatography [40, 42].

Some of these early studies looked at the higher mass molecules (>1000 u) in attempts to more fully characterise the samples [36-38, 43, 44] mostly based on laser desorption-MS (LD-MS). These studies showed evidence for molecular mass greater than 2000 u in a wood tar pitch [44], wood pyrolysis liquids [43], coal tars [36, 37] petroleum asphaltenes [38, 45] and pyrolysis products from waste plastics [46]. However, no studies using LD-MS on biomass gasification tars, or tars from co-gasification with coal, could be found in the literature. In addition, great progress has been made in optimizing

the experimental conditions for LD-MS and interpretation of the results, in particular when applied to complex samples such as those mentioned above, as detailed in a recent review article [47].

More recently ion cyclotron resonance mass spectrometry (ICR-MS) has received attention for studying complex samples such as oils and tars due to unprecedented level of mass resolution, typically to 0.1 ppm of mass, at masses of a few hundred mass units. The method has been applied to coal tar pitch [48], carbon black [49], products from pyrolysis of shale oils [50], heavy bitumen derived samples [51], and petroleum asphaltenes [52]. The method was able to provide extremely valuable and detailed information for molecular mass up to a maximum of 1200 u (typically < 800 u) in all these samples. However, the method is known to suffer from selective sampling (incomplete sampling) issues, which is not fully understood [47]. In addition, all the samples mentioned above are known to contain higher mass molecules than detected by ICR-MS. It cannot therefore be used to determine average mass estimates or mass distributions for complex mixtures of hydrocarbons. These points and the wider benefits and limitations of ICR-MS have been addressed in a recent review article [47].

Similar problems persist when trying to fully characterise pyrolysis derived liquids and tars from biomass, coal and petroleum residues, in terms of molecular mass distribution, average molecular mass or structural composition by other advanced MS methods [12, 13, 47]. Typically, the standard method for gasification tar analysis is also used on pyrolysis liquids [8, 29]. In many of the studies mentioned above that looked at materials beyond the GC range, size exclusion chromatography (SEC) was used for molecular weight determination, with tetrahydrofuran (THF) as eluent and solvent, often with a refractive index detector [14, 15, 27, 43]. These SEC systems have been shown to be incapable of resolving small to medium sized poly-aromatic hydrocarbons in terms of molecular size or mass [53-55]. This is thought to be due to THF acting as a weak solvent for the samples in question and enabling interactions with the SEC column, and also the usefulness of refractive index for detection is questionable. A number of studies have addressed these, and the wider issues, over the last decade for coal, petroleum, biomass and bitumen derived oils, tars and pitches [12, 13, 31, 53-57] and a review of these studies has been reported [47].

The aforementioned investigations demonstrated that N-methyl-2-pyrrollidinone (NMP) was a superior SEC eluent and solvent for tars that contain high aromaticity and fewer hetero-atoms such as coal or biomass derived gasification oils/tars [47]. Despite their high oxygen content, pyrolysis liquids from biomass can also be analysed with NMP as the SEC eluent [58, 59].

It is important to note that using SEC with NMP eluent does not provide complete information or quantification of molecular mass distributions, although it has proved a valuable tool for making relative comparisons between similar samples and is better understood than other SEC systems [47, 53, 55]. It is important that the limitations of the technique are understood and accounted for when interpreting SEC results to avoid over-interpretation of data.

Therefore, there remains a great need in the gasification and pyrolysis communities to obtain more accurate information on molecular weight distributions and structural features of liquid/solid products beyond the 1000 u mass range [12, 13, 47]. To this end, a recently reported analytical approach was assessed [31, 47, 56, 60]. This methodology has been successfully applied to the determination of average molecular mass number estimates, molecular mass distributions and detailed structural information on petroleum and coal tar pitch derived maltenes and asphaltenes [47, 56, 60, 61] as well as bitumen (oil/tar sand) samples and solubility sub-fractions [47, 62].

The study at hand assesses the validity of the above mentioned analytical approach [31, 47, 56, 60] for tars from the co-gasification of a soft wood (pine) and a Polish black (sub-bituminous) coal. To study the validity of the above methods, we attempted to identify changes in composition (in terms of molecular mass distribution and aromatic structural features) after ageing the tars under different storage conditions. Findings from the scoping study are reported. It is intended that data from this scoping study would first determine if using this methodology is justified, and secondly, assess if this new methodology can spur further research in the future.

Changes due to aging in the composition of gasification tars are expected to be less significant compared to changes imparted on tars from the use of catalysts, thermal upgrading processes, or seen during the ageing of biomass pyrolysis liquids. Therefore, if the methods used here are sensitive enough to identify changes in gasification tars due

to ageing then they would likely also be suitable for studying all the processes mentioned above.

3.2 Materials and methods

The tars used for this study were recovered from a 20 kW_{th} internal circulating fluidised bed gasification and combustion reactor [63, 64] using the tar protocol (TP) method [29]. The collected tars were then subjected to different storage conditions where temperature, ageing time and exposure to light were varied; these samples are defined in Section 2.4. The results from analysing these samples are presented as follows:

1. A mass balance, showing tar yields, GC-FID analysis and ultimate analysis of the bulk samples.
2. Planar chromatography (PC) [31, 56] was used to fractionate the bulk samples, and data observed from the PC fractions (without further chemical analysis) are presented.
3. PC fractions from the different tars were then subjected to further analysis using SEC and LD-MS to determine molecular mass distribution estimates. Synchronous fluorescence spectroscopy (UV-F) was used to compare relative extents of conjugation. Finally, the data were combined to make possible interpretations, in terms of chemical reactivity of the tars based on known chemistry from the literature. These methods were based on those developed in previous studies [31, 47, 56, 60].
4. LD-MS was then used to analyse the bulk tars, and data compared with the PC for a more robust interpretation of the whole material.
5. Finally, the aged samples exhibited precipitation. The final component of this study was to analyse this precipitated solid tar material to gain further insight into the tar ageing process.

3.2.1 Standards and solvents

Polystyrene, amongst other polymer and PAH standards, was used to calibrate the SEC system as previously reported [53, 54]. The solvents were from VWR,

(chloroform, heptane and acetone as HPLC grade), Rathburn Chemicals Ltd., Walkerburn, Scotland, UK (NMP – peptide synthesis grade) and used without further purification.

3.2.2 Tar generation

The tar was generated using a 20 kW_{th} internal circulating fluidised bed (ICFB) gasifier which has been described elsewhere [63, 64]. Gasification tests were performed using pellets made from a blend of pine wood (oven dried, ~12 wt% moisture) and a black Polish sub-bituminous coal (~8 wt% moisture), at a ratio of 7:3 wt%. The properties of the fuel are given in Supporting Information (S) Section S1. The cylindrical pellet size was 2 mm in diameter and 6 mm in length. These were fed at a rate of 4.0 kg per hour.

The tar was collected under steam gasification conditions at 800°C, with a flow rate of 3.75 Nm^3/h of steam and 3.0 Nm^3/h of air to the gasifier; air to fuel equivalence ratio 0.15; steam to fuel ratio 0.75. The combustor was operated with an air flow rate of 11 Nm^3/h. The fluidised bed contained approximately 12 kg of inert silica sand of particle size 0.2-0.4 mm. Gas residence time in the bed was 1-2 seconds and 3-5 seconds in the freeboard.

3.2.3 Tar recovery

The tar sample was recovered using the tar protocol (TP) method [29, 30]. The method uses an impinger train where a slipstream of the producer gas is passed through a series of seven bottles containing isopropanol, some at -20°C and others at 40°C. Approximately 0.1 Nm^3 of the producer gas was passed through the impinger train over a period of one hour during stable operation. The isopropanol tar solution was pooled from the seven impinger bottles and filtered within two hours of collection to remove particulates (i.e. char and bed material). A 1 μm glass fibre filter was used; the filtrate was a single phase solution.

3.2.4 Tar storage

To study the effect of storage conditions on the composition of tar, the tar solutions were stored under four different conditions, where the time, temperature and exposure to light were varied, as described below for each sample:

$T_{N2\text{-}0h}$: The tar sample recovered in isopropanol was frozen in liquid nitrogen within 2 hours of recovery and stored in this way. Immediately prior to the analysis, the sample was thawed in the dark at 5°C and then vacuum dried. This is deemed to be "fresh tar".

$T_{5C\text{-}6m}$: The isopropanol tar solution was stored for 6 months at 5°C, in the absence of light, prior to being vacuum dried and analysed.

$T_{20C\text{-}6m}$: The isopropanol tar solution was kept at room temperate (~20°C), in the absence of light for 6 months, prior to being vacuum dried and analysed.

$T_{20C\text{-}6m\text{-}L}$: The remainder of the tar solution was left at room temperature in the fume cabinet and thereby exposed to indirect sunlight for 6 months prior to being vacuum dried and analysed.

Whilst these conditions were chosen in order to be systematic in varying temperature, time and exposure to light, results from sample $T_{20C\text{-}6m}$ showed similar data to those obtained from $T_{5C\text{-}6m}$. Therefore, for brevity and clarity, the presented work will focus on the samples that showed the most significant differences between one-another and highlight the benefits of using this analytical approach: $T_{N2\text{-}0h}$, $T_{5C\text{-}6m}$ and $T_{20C\text{-}6m\text{-}L}$. The results from $T_{20C\text{-}6m}$ are *not* shown or discussed explicitly since the findings are similar to those for $T_{5C\text{-}6m}$.

Additionally, to study the effect of time during storage, aliquots of all the tar solutions were taken for GC analysis after 20 hrs, 3 days, 20 days and 6 months, and compared to those from the fresh tar solution immediately after it was thawed from liquid nitrogen ($T_{N2\text{-}0h}$). The results obtained after 3 and 20 days storage provided limited information and therefore will *not* be discussed herein, although they are reported in S3. The GC analysis of the fresh tar ($T_{N2\text{-}0h}$) was performed before any precipitate was observed to have formed, while for the 20 hours old samples precipitate had already formed and was removed before performing the GC analysis. Therefore, comparing results for $T_{N2\text{-}0h}$ with the samples aged for 20 hours gives a comparison of the tar composition before and after precipitation.

As an additional check, the thawed $T_{N2\text{-}0h}$ sample, which was observed to form precipitate within 14 hours of standing (at 5°C in the dark), was also analysed by GC after removing the precipitate. It should be noted that the exact point in time when the

precipitate formed was not determined. Moreover, this 14 hour old sample was only used to examine changes in the tar's GC composition before and after precipitation and was *not* subjected to further analyses.

The main focus of this study is the application of LD-MS, SEC and UV-F to the analysis of the tar samples. Only the fresh tar ($T_{N2\text{-}0h}$) and the 6 month aged tars were analysed by all of these techniques, not the intermediate samples mentioned above which were analysed by GC only. A summary of the nomenclature, storage conditions and analytical techniques that were applied to each sample are listed in Table 1.

Table 1, Nomenclature of the tar samples, their storage conditions and the analytical techniques applied.

Label	Storage			Analytical Technique					
	Temp (°C)	Sun-Light	Age	GC	Recovered Dry weight	UA	UV-F	SEC	LD-MS
$T_{N2\text{-}0h}$	-196	No	<5 hrs	X	X	X	X	X	X
$T_{N2\text{-}14h}$	-196	No	14 hrs*	X	-	-	-	-	-
$T_{5C\text{-}20h}$	5	No	20 hrs	X	X	-	-	-	-
$T_{5C\text{-}6m}$	5	No	6 months	X	X	X	X	X	X
$T_{20C\text{-}20h\text{-}L}$	20	Yes	20 hrs	X	X	-	-	-	-
$T_{20C\text{-}6m\text{-}L}$	20	Yes	6 months	X	X	X	X	X	X

* 14 hrs refers to the time the sample was stored in a fridge (5°C) after being thawed from liquid nitrogen

3.2.5 Bulk sample preparation and tar yield calculation

Gravimetric analysis and tar yield calculations were performed based on the standard method described in detail elsewhere [29, 30] and only briefly summarized here, using the following steps to provide four fractions:

1. GC Total: The tar-isopropanol solution was directly analysed by GC to quantify the material in the GC range.

2. Precipitate: The tar-isopropanol solutions were filtered using a glass-fibre filter of 1 μm to recover any precipitate. The precipitate was washed with five lots of fresh isopropanol (10 mL each) before being dried in a fan assisted oven at 105°C until no solvent remained, approximately 2 hours. This fraction was weighed to yield the precipitate weight in the solution
3. Recovered Dry: The filtrate after the precipitated material was removed was vacuum dried for 4 hours at a temperature of 75°C and 10^{-3} bar. This material was weighed to determine the mass of the dried, recovered matter. Any light material would be lost due to vacuum drying.
4. GC Recovered Dry: The Recovered Dry fraction was then redissolved and analysed by GC. The difference between the GC Total and the GC Recovered Dry fraction is the mass of volatiles lost during vacuum drying.

The Total Tar may be calculated as follows:

$$Total\ Tar = Volatiles + Precipitate + Recovered\ Dry$$

Where: Volatiles = GC Total – GC Recovered Dry

The bulk sample used in all further analysis was the "Recovered Dry" fraction, i.e. the tar without precipitate or light volatiles. Vacuum drying was used here as the solvent cannot be completely removed by other means. Additionally, vacuum drying was employed to remove the most volatile components from the samples so that a better comparison could be made between SEC and LD-MS mass estimates. Without this vacuum treatment the samples for SEC and LD-MS would be quite different due to the high vacuum in the LD-MS sample chamber leading to the loss of molecules with mass of less than ~200 u. It is important to note, however, that the drying process could result in changes in the sample composition (due to reactions) and it is not possible to isolate these effects from those that occurred during storage alone.

3.2.6 Planar chromatography (PC) fractionation

The bulk (dried) tar samples described above were fractionated by using planar chromatography to aid in their analysis. Aluminium backed PC plates of 20 cm^2 with silica gel thickness of 250 μm (Whatman, UK) were used. The plates washed with acetone and then chloroform before use. The tar was dosed onto the PC plate as a solution in chloroform; multiple sample doses were added at the origin of the plate to increase the amount of sample. All samples were completely soluble in chloroform. The PC plate was successively developed with chloroform, acetone, and heptane, being dried every time before the application of a new solvent. Figure 1 gives an example of the mobility-fractions for the tar $T_{N2\text{-}0h}$, Figure S2.1 shows images of the PC plates from all three tars and provides further information. Each sample was eluted with the same solvent three times consecutively, to the same height, before moving on to the next solvent. No attempt was made to quantify the PC fractionation due to the inherent difficulties involved; although the apparent abundances from visual inspection are described in Section 3.2.

In order to optimize the sample fractionation, a series of tests were performed to select the solvents and order of elution. The aim of the PC separation was to provide relatively few discrete mobility-fractions and to isolate some material at the origin, which in previous studies was composed of the highest mass species [31, 56].

This material, which was immobile in all of the eluents, was denoted as PC fraction F1. Subsequent fractions of material with increasing mobility (higher up the PC plate) were taken at regular intervals and grouped by number based on the solvent they were mobile in. Fraction F2 was acetone mobile but chloroform and heptane immobile; Fraction F3 was chloroform mobile, but heptane immobile. The material at the furthest solvent front was labelled fraction F4 (heptane mobile); cf. Figure 1 and S2.1 for images of the plates with the numbering scheme overlaid.

For LD-MS analysis the different mobility-fractions were cut out from the PC plate and directly adhered to the LD-MS target.

For SEC and UV-F analysis the samples were recovered by removing the silica from the plates and extracting this with NMP. The resulting NMP solution was filtered (1μm).

3.2.7 Ultimate analysis (UA)

The carbon, hydrogen, sulphur and nitrogen contents of the dried bulk tar samples were determined with a LECO-CHNS-932 microanalyzer. The oxygen content was obtained directly using a LECO-VTF-900 furnace coupled to the microanalyzer. These samples contained *no* moisture and *no* ash. Duplicate analyses showed deviation from the mean were less than +/- 0.5% of the absolute value.

3.2.8 Gas-chromatography (GC-FID)

GC was used to study the smaller molecules in the samples. The GC analysis of the fresh tar ($T_{N2\text{-}0h}$) was performed immediately after thawing. The sample was inspected after 14 hours (at 5°C in the absence of light) and it was observed that precipitate had formed. Therefore the precipitate was removed by filtration and GC analysis was performed on the supernatant. Comparing the GC results from $T_{N2\text{-}0h}$ and after 14 hours storage gives a comparison of the tar composition before and after precipitation. As an additional check, the samples stored at 5°C in the dark and at 20°C in the presence of indirect sunlight, which were observed to form precipitate within 20 hours of standing, was also analysed by GC after removing the precipitate (Table 3). It should be noted that these samples were *not* checked between the ages of 5-20 hours due to practical experimental constraints.

A Varian GC3800-FID with a Varian 'FactorFour' capillary column (VF-5ms 30M, 0.25mM ID, DF = 0.25) was used to quantitatively examine the tars. 5 µL injection volume (split ratio 50), helium carrier gas (2 mL/min), injector temperature 325°C, column starting temperature of 50°C for 4 minutes, 25°C/min ramp to 150°C, 5°C/min ramp to 325°C, held at 325°C for 2 minutes. FID detector temperature was 325°C. For the GC analysis a volume of the isopropanol-tar solution was taken before the sample was vacuum dried. Further details of peak identification, standards and calibration are provided in S3.

3.2.9 Size exclusion chromatography (SEC)

The operating conditions and methodology have been reported elsewhere [53, 54]. Briefly, a Mixed-D column (5 µm particle size, 300 mm x 7.5 mm i.d.) packed with polystyrene/ polydivinylbenzene beads, was operated at 80°C with a Knauer M100 isocratic HPLC pump. NMP was used as eluent (0.5 mL min^{-1}) and solvent.

Material eluting from the column was detected by UV-absorbance at 270, 300, 350, and 370 nm. The results obtained at 300 nm are considered representative of the main trends observed at all wavelengths; only those results will be shown and discussed. The SEC system was calibrated using standard polystyrene (PS), polymethylmethacrylate (PMMA) and polysaccharide (PSAC) samples, as well as small standard PAH, O-PAH and N-PAH compounds [53-55].

In the conversion of elution time to mass estimate, the materials eluting early from the column (<15 minutes) which is excluded from column porosity cannot be accurately accounted for. This is because the nature of this early eluting (apparently high mass) material remains uncertain and is thought to have a hydro-dynamic volume which departs from those of the calibration materials, possibly due to three-dimensional conformation where size is not easily related to molecular mass [53, 55]. Previous work on similar materials has shown this early eluting material (<15 minutes) to be of higher average molecular mass (>2500 u) than the later eluting materials [55]. These aspects and the application of this calibration are described in said publications and outlined in S4.

3.2.10 Laser desorption / ionisation mass spectrometry (LD-MS)

A Bruker Daltonics Reflex IV MALDI-TOF mass spectrometer was used for LD-MS. No matrices were used because the samples in this study behave as self-matrices [31, 56]. No matrix deflection voltage was used; a nitrogen laser of 337 nm was employed. The method applied in this study has also been described in detail elsewhere [31, 56].

Linear-mode was used with a delayed ion extraction (DIE) time of 0, and 600 ns. The mass range was m/z 0-300,000; Ion source 2 = 16.5 kV and Lens = 9.5 kV. The digital gain (DG) was set to its lowest level (1x). In all cases shown, 10 spectra were added using the pulsed ion extraction method on the same point. 50 spectra were also added for some of the samples; these spectra were found to match those where only 10 spectra were summed, with an increased signal-to-noise ratio. Due to time considerations the addition of 10 spectra of each analysis was considered satisfactory for the purpose of this study.

A HIMAS detector (Bruker's 'high-mass detector') operating in the linear mode was used to investigate the higher molecular mass region. Detection of high mass ions can be enhanced through the use of a variable high mass accelerator (HMA) voltage.

When the bulk samples were analysed, the ion intensity of the smaller mass ions was reduced (to avoid overloading the HIMAS detector) by reducing the high mass accelerator voltage from the maximum value of 10 kV to 6 kV. At the same time, the laser power was increased beyond that necessary for ionisation of the small molecules of the samples. This is to examine the influence of laser power on the mass distribution, which is generally significant. A laser power of 30-50% (of the maximum available) was typically found to be adequate to ionise the samples. The bulk tar samples were applied to the LD-MS target neat following the procedure described elsewhere [31, 56]. Mainly the results obtained with a DIE of 600 ns will be reported and discussed in relation to the 'bulk' samples, for the reasons outlined in S5.

During the examination of the PC mobility-fractions, the HMA voltage was set to its maximum value (10 kV) in all cases. By desorbing the sample directly from the silica surface of the PC plate, high laser powers could be applied with no resulting significant change of the mass spectra, apart from producing flat-topped peaks due to overloading of the detector. For the PC fractions, only LD-MS spectra acquired in linear-mode with no DIE are shown. A clean silica surface from the PC plate was found to give no observable ion current under any of the LD-MS operating conditions used [56].

A major obstacle to the use of LD-MS is the variability of the data depending on the conditions and the operator [31, 56]. The approach used in this study was found to give consistent findings independent of the operator. Four operators recorded the data reported. This provides a degree of confidence in the reproducibility of the approach. The results from LD-MS are not quantitative.

3.2.11 UV-fluorescence spectroscopy (UV-F)

The Perkin-Elmer LS55b luminescence spectrometer was set with a slit width of 5 nm, to scan at 500 nm min^{-1}; synchronous mode fluorescence spectra were acquired at a constant wavelength difference of 20 nm. A quartz cell with 1 cm path length was used. The procedure has been described elsewhere [31, 47, 65].

The spectrometer featured automatic correction for changes in source intensity as a function of wavelength. Emission, excitation, and synchronous spectra of the samples were obtained in NMP solution for all of the samples; only synchronous spectra are shown. Solutions were diluted with NMP to avoid self-absorption effects: dilution was increased until the fluorescence signal intensity began to both decrease in intensity and the relative intensities of the different maxima in the spectra ceased to change. The UV-F spectra are displayed as peak normalised because this enables relative comparisons between the samples; the results are not quantitative.

To ease the discussion of the UV-F data the results will be described with reference to the approximate number of conjugated aromatic rings that would fluoresce at the equivalent wavelength to the sample in question. This is based on a recently noticed correlation between the peak maximum from UV-F in synchronous mode, and the number of conjugated aromatic rings as determined by NMR and average structural parameter calculations for coal and petroleum derived samples [47, 60]. The maximum intensity of fluorescence shifts steadily to longer wavelengths by about 30 nm per additional aromatic ring in a conjugated aromatic system, where 1 ring = 270 nm, 2 rings = 300 nm, and so on.

It should be noted however, that some of the tar samples contain slightly more oxygen than the coal and petroleum derived samples studied previously, which could affect the UV-F results. The influence of oxygen on the UV-F spectrum of large PAH molecules (>500 u), however, is not well enough understood to be able to comment on its effects in detail. The definitions outlined above are not a literal description of chromophores such as those present in the tars but as a means to discuss qualitative differences between samples and their dominant features. Further details are provided in S6 regarding the interpretation of the UV-F results and the influence of oxygen.

3.3 Results and discussion

3.3.1 Tar-yields, GC-FID and ultimate analysis

The tar $T_{N2\text{-}0h}$ and the aged samples were analyzed by means of the standard approach (GC-FID and gravimetric yield) [30] as described in Section 2.5. $T_{N2\text{-}0h}$ was analysed immediately after being thawed from liquid nitrogen storage; T_{5C} and T_{20C} were both analysed after 20 hours and 6 months of storage; the results are summarized in Table 2. $T_{N2\text{-}0h}$ was the only sample that was analysed before any precipitation occurred, whereas precipitate was observed for all other tar solutions within 20 hours of resting. The precipitate was removed from the solutions before they were analysed.

The yields are presented in Table 2 for each tar as determined after different periods of storage, results are normalised to grams per normal cubic meter of the producer gas (g/Nm3). Error determination is described in S3.

Table 2: Tar yields after different durations of storage (g/Nm^3 producer gas)

	Sample Age	T_{N2}	T_{5C}	T_{20C}
		g/Nm^3		
GC Total	0 hours	5.2		
	20 hours		4.6	4.9
	6 months		2.3	2.9
Precipitate	0 hours	0.0		
	20 hours		0.06	0.09
	6 months		0.03	0.07
	Total		*0.09*	*0.16*
Recovered Dry	0 hours	1.3		
	20 hours		1.4	1.4
	6 months		1.8	1.9
GC Recovered Dry	0 hours	0.6		
	20 hours		0.6	0.6
	6 months		0.2	0.2
Volatiles	0 hours	3.9		

	20 hours		3.2	3.5
	6 months		0.5	1.0
Total Tar	0 hours	5.9		
	20 hours		5.5	5.8
	6 months		4.0	4.8

Relative deviations +/- 5 % for GC, 15% for Recovered Dry, and 30% for precipitate.

Blank denotes not applicable.

The main findings from studying the tar yields (Table 2) were that $T_{N2\text{-}0h}$ contains the greatest proportion of molecules in the GC range and the lowest in the gravimetric range, with no occurrence of precipitation. After 6 months storage $T_{5C\text{-}6m}$ and $T_{20C\text{-}6m\text{-}L}$ show a decrease in the quantity of GC range molecules (from ~5 g/Nm^3 to ~2.5 g/Nm^3) and an increase in Recovered Dry tars (from 1.3 g/Nm^3 to 1.8-1.9 g/Nm^3), compared to $T_{N2\text{-}0h}$ (errors are given in the footnote to Table 2 and S3). Precipitate was observed in these samples. These results are an indication of a change in mass distribution of the stored samples towards higher average molecular masses, which is in accordance with reported studies of pyrolysis liquids [15, 16, 18, 19, 21, 22].

The differences between the GC results from $T_{5C\text{-}6m}$ and $T_{20C\text{-}6m\text{-}L}$ were relatively minor after 20 hours of storage (Table 3). Both samples also exhibit the presence of precipitate, to a slightly larger extent in $T_{20C\text{-}6m\text{-}L,}$ although the error in the determination has to be considered (cf. Table 2 and S3). The tar solutions were regularly checked over a 3 month period and no further precipitation was observed; however, when the tar solutions were collected after 6 months storage precipitate was apparent in both cases.

To determine if the precipitate (after 20 hours and 6 months) contained any GC range species its dichloromethane soluble fraction was examined; no evidence of GC range molecules was found. Therefore, aggregation of small molecules can be ruled out as a mechanism for the precipitate formation.

By comparing the tar yields for the stored tars (T_{5C} and $T_{20C\text{-}L}$) after 20 hours and 6 months, a large reduction in the GC range components is evident, by ~ 2.0-2.5 grams

per Nm^3 for both samples (Table 2). If those molecules had reacted to form larger ones they would be observed by an equivalent increase in the 'Recovered Dry' and 'precipitate' yields. However, the gravimetric yields only increased by <1 gram per Nm^3 and the precipitates were less than 200 mg per Nm^3. It is likely that the discrepancy is due to some of the GC range compounds being lost to the glassware during storage. This is thought to be due to attraction and adhesion of molecules to the glass surface, not necessarily due to reactions followed by lose to the surfaces. Other factors affecting the quantification include evaporation of solvent and/or volatile compounds over the 6 month storage period and water formation during the ageing reactions (not quantifiable by GC). In future studies it would be beneficial to determine the water content using e.g. a Karl-Fischer titration [66].

The tar solutions were stored in ground glass stoppered bottles and sealed with parafilm; however, some loses due to evaporation are still thought to have occurred after 6 months of storage and during sampling. This is thought to be the case as the greatest changes were in the naphthalene concentration which is quite volatile and is unlikely to be reactive under the storage conditions.

To see if GC can provide information on the precipitation process, the thawed $T_{N2\text{-}0h}$ solution was examined before any precipitation occurred, and then again after precipitation had occurred (after filtration to remove the precipitate). The precipitate formed within 14 hours of standing in the dark at 5°C after thawing. No significant differences were observed for GC tars in T_{N2} before and after precipitation (Table 3). Specifically, comparing these results with those from the 20 hours old samples, which had precipitated material, shows that only small changes occurred in the GC tars (Table 3). There is a slight decrease in acenaphthylene and phenanthrene, the decrease in naphthalene is only slightly greater than the deviation. The only other statistically significant changes are a slight increase in the amounts of benzo[a]pyrene, indeno[1,2,3]pyrene and benzo[g,h,i]pyrene.

Of the molecules detected in the GC range acenaphthylene and phenanthrene are likely to be the most reactive, but there was little evidence for these having reacted in the 14 hour old sample (Table 3). This suggests the difference observed in the 20 hours

old samples were not related to the formation of precipitate and were most probably due to losses of material to the glassware and other experimental errors. It would seem that the precipitate is primarily formed by reactions between molecules that are not detected by GC.

These results and the tar yields are discussed further in S3, as are the sources and scales of the errors. The weight of the precipitate from tar T_{N2} after 14 hours could not be determined due to the small volume of solution frozen in liquid nitrogen; hence, not enough material could be recovered to weigh.

Table 3, GC-FID results for the tar samples before vacuum drying, displayed as mg per cubic meter of producer gas. Relative errors were less than +/- 5%.

Sample Name		T_{N2}		T_{5C}	T_{20C}
		mg/Nm³			
		0h	14h	20h	20h
Naphthalene		3000	3000	2600	2700
Acenaphthylene		710	700	640	670
Acenaphthene		10	10	10	10
Fluorene		50	60	40	50
Phenanthrene		460	450	380	410
Anthracene		90	90	80	80
Fluoranthene		230	240	220	240
Pyrene		240	250	220	240
Chrysene		30	30	20	30
Benzo[a]anthracene		30	40	30	30
Benzo[k]fluoranthene		30	40	30	30

Benzo[b]fluoranthene	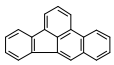	10	10	10	10
Benzo[a]pyrene		40	60	40	40
Indeno[1,2,3-cd]pyrene	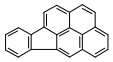	30	40	20	20
Dibenz[a,h]anthracene		5	10	5	5
Benzo[g,h,i]perylene		5	30	5	20
Total EPA 16		5000	5100	4400	4600
Unknowns		280	280	230	270
GC Total		5300	5400	4600	4900

Ultimate analysis (UA) was used to gain further information about the tars. The results obtained for samples $T_{N2\text{-}0h}$, $T_{5C\text{-}6m}$ and $T_{20C\text{-}6m\text{-}L}$ (Table 4) show an increase in the amount of oxygen in $T_{20C\text{-}6m\text{-}L}$ compared to $T_{5C\text{-}6m}$ and a corresponding decrease in hydrogen. $T_{N2\text{-}0h}$ shows the highest C/H ratio. The amount of oxygen in $T_{N2\text{-}0h}$ was greater than in the cold stored tar, but less than the room temperature sample. The trends in the UA results were repeatable. Table 5 represents the same results in terms of the number of atoms in a molecule with a mass of 500 u, it can be seen that the number of oxygen atoms ranges from 0.2 to 1.4 per molecule, whereas there are 36 to 38 carbon atoms.

Taken together these results indicate that in $T_{N2\text{-}0h}$ (no precipitate) there are significant quantities of highly aromatic PAH and oxygen containing PAH compounds. After precipitation (i.e. the aged samples), less carbon is detected in the molecules that remained in solution and more hydrogen, and the C/H decreased. Therefore it would seem that the most highly aromatic compounds had precipitated. In $T_{5C\text{-}6m}$ less oxygen was found than in the fresh tar which suggests many of the O-PAH compounds have also precipitated. The material that remained in solution for $T_{5C\text{-}6m}$ has a lower C/H ratio than the dissolved tars in $T_{20C\text{-}6m\text{-}L}$ which suggests the molecules are less aromatic. In $T_{20C\text{-}6m\text{-}L}$ more oxygen was observed than in $T_{N2\text{-}0h}$ which indicates this sample has precipitated

mainly PAHs and possible undergone additional reactions with oxygen from the air or the solvent during its storage.

The increase in nitrogen and sulphur content of dissolved tars observed with ageing suggests that molecules containing N or S do not precipitate as readily as those that do not contain them; therefore N and S become concentrated in the solution. However, the absolute differences in N and S between the samples are minor, Table 5. As these findings are somewhat unexpected and only duplicate analyses of each tar was possible (due to limited amounts of sample), future studies should investigate these aspects more closely to confirm these results. In addition, the precipitate could not be examined by UA in this study because the amount of sample recovered from the filter was insufficient for the analysis. In future studies, a different filtration method will be employed and larger sample volumes treated so that UA can be performed on the precipitate.

Table 4, Ultimate analysis of the vacuum dried tars, $T_{N2\text{-}0h}$ and after 6 months storage.

Element	$T_{N2\text{-}0h}$	$T_{5C\text{-}6m}$	$T_{20C\text{-}6m\text{-}L}$
	Wt.%	Wt.%	Wt.%
C	91.5	86.6	86.9
H	5.5	11.6	7.3
N	0.3	0.6	0.6
S	0.5	0.8	0.7
O	2.2	0.5	4.5

Deviation estimated at +/- 0.5% of the absolute value, based on two repeats.

Table 5, Number of atoms in a tar molecule with a mass of 500 u, for $T_{N2\text{-}0h}$ and after 6 months storage.

Element	$T_{N2\text{-}0h}$	$T_{5C\text{-}6m}$	$T_{20C\text{-}6m\text{-}L}$

	Number of atoms		
C	38	36	36
H	28	58	37
N	0.1	0.2	0.2
S	0.08	0.13	0.11
O	0.7	0.2	1.4
C/H	1.4	0.6	1.0

Summarizing the results from the standard/commonly applied techniques (GC, gravimetric weight and UA) for studying tars and oils from gasification and pyrolysis, changes to higher mass materials in the aged samples can be implied. However, the differences observed could in principle also be due to other reasons, such as changes in polarity/solubility with ageing. This could reduce the amount of compounds detected by GC and produce precipitate. The information obtained from these techniques can thus only be regarded as indicative. In addition, there was no evidence for a significant change in the GC-FID results in tar T_{N2} before and after precipitation of material, Table 3. To obtain more detailed information about changes in molecular mass distribution or structural features (conjugation) due to ageing, techniques such as SEC, LD-MS and UV-F can prove useful, as will be demonstrated below.

3.3.2 PC fractionation of the Recovered Dry tars

To aid the investigation of the vacuum dried tars and the material they contain beyond the range of GC the Recovered Dry material as defined in Section 2.5 was fractionated via planar chromatography (PC). The methodology behind this analytical approach has been reported elsewhere [31, 47, 56]. Images of the PC plates bearing the tar samples after development are shown in S2, Figure S2.1. An example is shown below in Figure 1 for the tar $T_{N2\text{-}0h}$:

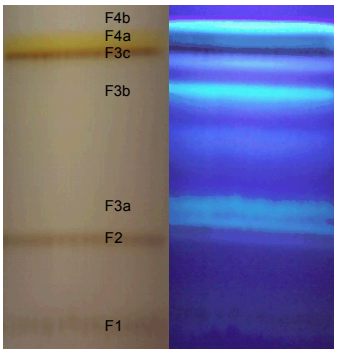

Figure 1, PC plate bearing the vacuum dried tar $T_{N2\text{-}0h}$ after being eluted with chloroform (F3) followed by acetone (F2) and finally heptane (F4). The image on the left-hand side was taken under white light, and the right-hand side under UV-light (260 nm).

The PC fractionation is not quantitative; nonetheless, it was possible to make a relative comparison between the apparent amounts of material in each mobility-fraction by visual inspection. The apparent order of abundance of the PC mobility-fractions was determined internally for each tar sample and is listed below (the main fluorescent bands are shown in bold):

$T_{N2\text{-}0h}$	F3c ≥ F4a ≥ **F4b** ≥ **F3b** > **F3a** ≥ F2 > F1
$T_{5C\text{-}6m}$	F1 > F2 ≥ **F4b** ≥ F4a > F3c (no F3b, no F3a)
$T_{20C\text{-}6m\text{-}L}$	F2 ≥ F1 > **F3b** > F3c > F4a (trace **F4b**, no F3a)

Where F1 = immobile, F2 = acetone mobile / chloroform and heptane immobile, F3 chloroform mobile / heptane immobile, F4 heptane mobile; the labels c, b and a refer to material with decreasing mobility in the same solvent as denoted by the corresponding number – i.e. they are *not* associated to repeated elution with the same solvent.

By comparing the apparent order of abundance for $T_{N2\text{-}0h}$ with those of the aged tars indicative information regarding changes in composition can be obtained. Only significant differences are mentioned. $T_{N2\text{-}0h}$ contains less of the immobile material (F1)

relative to its other fractions than was the case for the 6 month aged samples. It was also evident that there was some fluorescent material associated with the immobile material (F1) in $T_{N2\text{-}0h}$ that was not seen for the other samples.

The aged samples all appeared to contain similar amounts of immobile material, although $T_{5C\text{-}6m}$ was the only tar that appeared to contain more material in fraction F1 than in F2. Another clear difference was observed between $T_{5C\text{-}6m}$ and $T_{20C\text{-}6m\text{-}L}$, where the main fluorescent band from $T_{5C\text{-}6m}$ was F4b (not observed for $T_{20C\text{-}6m\text{-}L}$) while for $T_{20C\text{-}6m\text{-}L}$ it was F3b (not observed for $T_{5C\text{-}6m}$). In addition, the highly fluorescent material observed in F3a of the fresh tar was not seen in the 6 month aged tars. These findings are difficult to interpret on their own (i.e. without the data LD-MS, SEC and UV-F will provide). However, they do provide clear evidence of a change in composition of the tar upon ageing that is dependent on the storage conditions. Further details regarding the planar chromatography results are given in S2.

3.3.2.1 SEC, LD-MS and UV-F analyses of PC fractions

To examine the Recovered Dry tars comprehensively their PC mobility-fractions were analysed by SEC, LD-MS and UV-F. The findings from these analyses were used to determine the mass range and extent of aromatic conjugation for each tar. As these are not standard reference techniques for analyzing tars (they are in the validation phase of development) the complete data sets for each sample are presented in the supporting information (S7-S9). For brevity, a summary of the key findings from the analysis of the PC fractions is presented below with a complete account provided in S7. To aid the comparison of the equivalent PC fraction from different samples the LD-MS, SEC and UV-F results are displayed by PC fraction in S8. To observe trends between PC fractions from a single sample the results are also shown by sample in S9. Some of these figures are also shown in the article to highlight the main findings.

Table 6 summarizes the mass estimates from SEC and LD-MS for the PC fractions; the methodology for estimating average mass and mass ranges/distributions has been described previously [47, 55, 56]. To discuss the results and draw conclusions the following assumptions are used, but this does not however discount other possible

assumptions and interpretations. Further work is needed to confirm the assertions outlined below.

1. The results from $T_{N2\text{-}0h}$ are considered to represent the molecules originally present in the tar.

2. When UV-F signal is observed in a PC fraction from $T_{N2\text{-}0h}$ but the same signal is not observed in the equivalent fraction from the aged tars (for example PC fraction F3c, Figure 2a), the molecules containing the chromophore responsible for the fluorescence are assumed to have reacted (either with another tar molecule, or with the solvent or oxygen in the air). Hence these molecules have different mobility during PC and are found in different locations or as precipitate.

3. The most probable ageing reactions are those involving tar molecules with highly conjugated aromatic systems either with themselves or with oxygen that is present in the solvent or the air. These reactions are unlikely to cause a significant change in the chromophore (conjugation) present in the original tar molecule when observed by UV-F if they proceed as shown in Figure 3a. We note that the addition of a carboxyl group to aromatics as shown in Figure 3b (in the presence of sunlight) can have two effects, depending on the position they have on the ring system. An added carboxylic group can either destroy conjugation, or increase conjugation (causing a red shift) [67], cf. S6 for further detail. However, due to the low oxygen contents of these tars, these effects are unlikely to significantly influence the results.

4. Some of the UV-F results show that molecules with significantly greater conjugation are produced during ageing (such as those in the precipitate or F1 from $T_{5C\text{-}6m}$, discussed below). In these cases, it is possible that PAH molecules have reacted with one another resulting in larger, higher mass molecules with increased aromatic conjugation (the role of oxygen in this process is

unknown). There are no reports of the formation of aromatic carbon-carbon bonds, or of deoxygenation as shown in Figure 3a, happening at room temperature. There is also limited information for oxygen acting in a way that increases conjugation in large aromatic molecules (>500 u) at room temperature. However, the shift of fluorescence to higher wavelengths with ageing has to be a result of one of these interpretations, or from a combined effect.

5. Fragmentation of some molecules occurs during LD-MS analysis. This is probably due to non-conjugated bonds (such as aliphatic or oxygen containing bridges) between aromatic cores. Structures such as these were identified in recent studies of petroleum samples as being the most difficult to observe by LD-MS due to excessive fragmentation [47, 56, 61].

6. When SEC shows evidence for larger molecules than witnessed from LD-MS this is an indication that the larger molecules fragment during ionization, hence the mass of the parent molecule is not detected or is greatly underestimated by LD-MS.

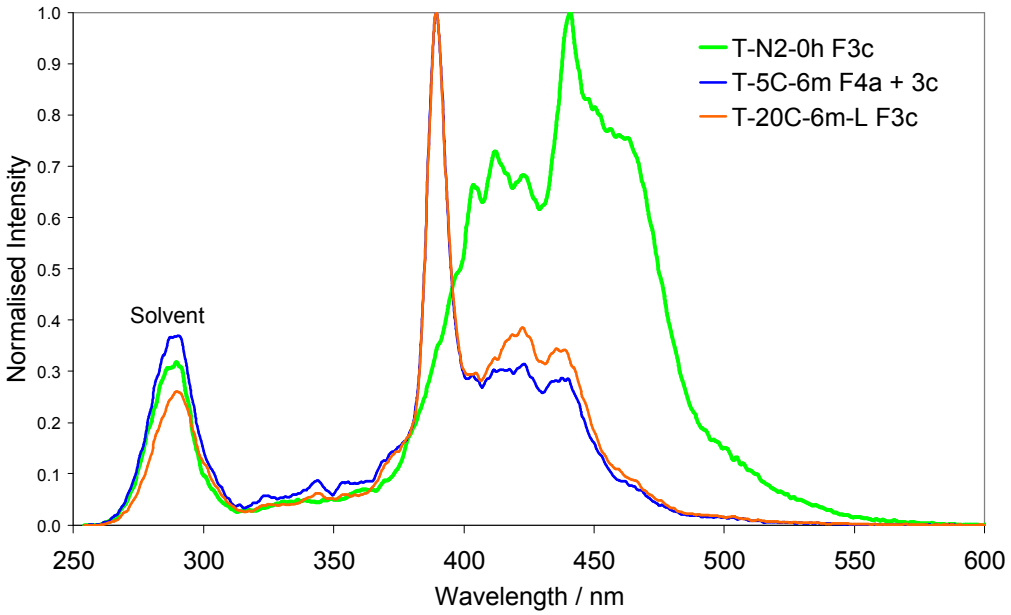

Figure 2a, Synchronous UV-F spectra (peak normalised) of PC fraction F3c.

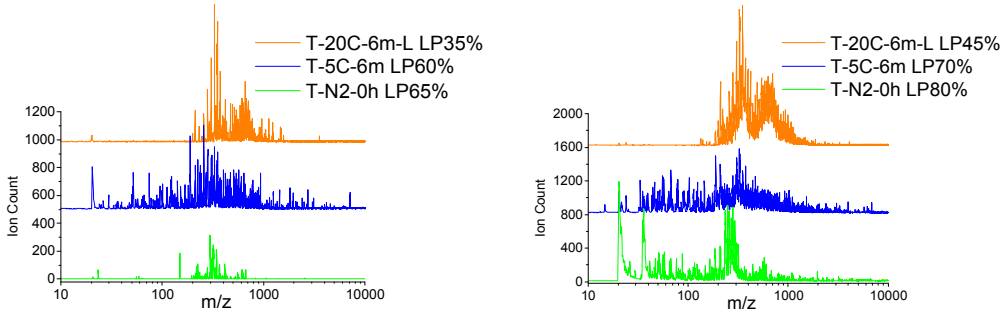

Figure 2b, LD-MS spectra of PC fraction F3c at low and high laser power (left and right respectively), no DIE, HMA voltage was 10 kV.

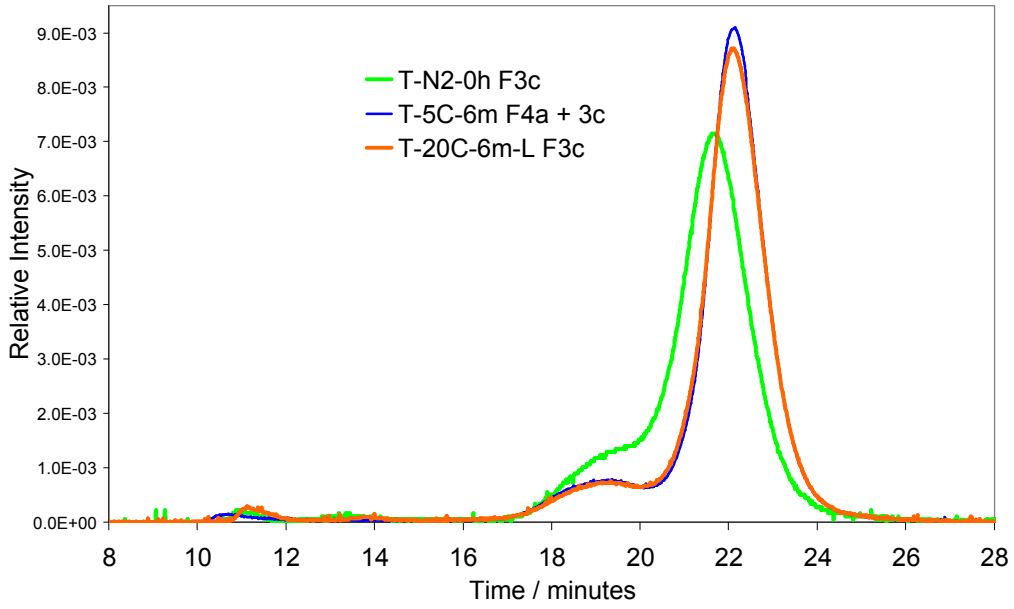

Figure 2c, SEC chromatograms (area normalised) of PC fraction F3c at 300 nm.

In addition to the assumptions above, information from the literature can also give insight into possible mechanisms of reaction, and this is discussed here before the data are interpreted below. From the little that is known about reaction mechanisms of large PAHs, alkyl aromatics and oxygen containing aromatic molecules, it is the molecules containing the largest conjugated chromophores that are thought to be the most reactive [47, 60, 68-70]. Oxygen can react with molecules such as these, under mild conditions (260-290°C [69]), and is thought to cause cross-linking through carboxylic (Figure 3a) and possibly ether bridges between aromatic compounds [14, 68].

It has been reported that PAHs with aliphatic hydrogen are the most reactive during oxidative thermal treatments of oils and pitches [70, 71]; i.e. polymerization reactions between PAHs appear to proceed via cross-linking where the active sites are mainly located on the aliphatic groups (the radical chain mechanism). The amount of oxygen in the reaction products increases by a few weight percent; whereas the changes in mass distribution and aromaticity are more profound than would be expected due to the incorporation of oxygen alone [60, 69, 71]. The exact role of oxygen remains unclear.

It is known however, that further thermal treatment (>440-460°C) of the reaction products from oxidative thermal treatment can lead to removal of oxygen and results in

an increase in aromaticity as shown in Figure 3a, and the size of fused aromatic carbon ring systems [68-71]. There is no reported evidence however, of this happening at room temperature. It should be noted that the incorporation of oxygen into alkyl aromatics and their decomposition as described above, and shown in Figure 3a, would not significantly alter the conjugation of the molecules and is unlikely to significantly influence their UV-F spectrum (in synchronous mode). This is because previous NMR and UV-F studies of samples similar to those being examined here (anthracene oil and their air-blown reaction products [31, 60, 69, 71]) found the aromatic cores were the least effected during the first phase of air-blowing reactions; the reactions occur mainly at aliphatic sites in the molecules that contain the largest aromatic chromophores, as mentioned above. These types of reactions proceed in the absence of light.

In the presence of sunlight a different mechanism can occur leading to incorporation of oxygen into PAH molecules through reactions with oxygen from the air [72-74]. The mechanism proposed is through singlet oxygen formed by energy transfer from a PAH molecule in its triplet state (formed via UV-VIS photo-excitation of the PAH ground state followed by inter system crossing). The oxygen can bond to the PAH giving peroxides which are in turn photolyse to give carbonyls and eventually hydroxyls [72]. Figure 3b displays a simplified example of the photo-oxidation of phenanthrene to phenanthrene quinone [72]. Despite the depicted apparent simplicity it is important to recall that the formation and breaking of peroxides implies the possibility of a large range of (radical) reactions including further oxidation with ground state oxygen to form e.g. more peroxides, radicals, carbonyls and hydroxyl groups, but also fragmentation and polymerisation of molecules.

Hydroxyl groups on PAH molecules can react further leading to polymerization processes occurring as described in reference [14]; this provides a comprehensive review of possible reactions of oxygenated hydrocarbons that occur in biomass pyrolysis oils. However, most of the reactions described therein are unlikely to occur in the gasification tars being examined due to their much lower oxygen contents (less than 5 wt%) than biomass pyrolysis oils (15-30 wt%). Therefore, the influence of oxygen on the results from these tars will be relatively minor. In addition, without information on the oxygen content of the precipitate it is futile to speculate on oxygen's role in the ageing of

this tar, or without NMR, FT-ICR-MS and FT-IR data. It is intended to address these aspects in future studies.

In gasification and pyrolysis tars and oils free radicals are also likely to play a role in ageing reactions; however, no information is available on their yield in these tars or their role during ageing. Additionally, the tar molecules recovered from gasification are not thermodynamically stable, as their residence time at the high temperature in the gasifier is insufficient for equilibrium to be reached [1]; it is therefore also possible that part of the aging involves molecules re-arranging slowly to more energetically favourable configurations, that they would have reached more quickly at high temperature in the gasifier. However, detailed information on these processes is not available for the sizes and structures of molecules being investigated here. In addition, traces of ash or char could remain in the tar solution even after filtration and if present could well play a role in the ageing processes.

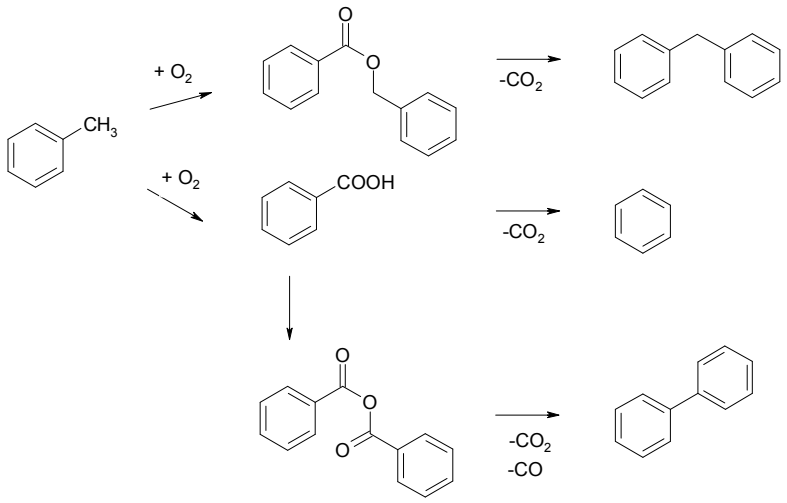

Figure 3a, Simplified schematic example of the incorporation of oxygen into alkyl aromatics and decomposition leading to cross-linking or increased levels of aromaticity [68].

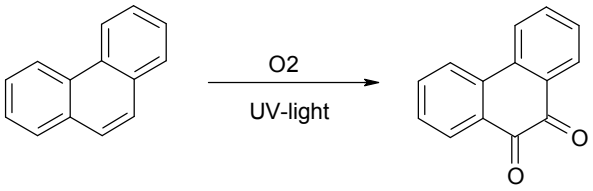

Figure 3b, Example of the photo-oxidation of phenanthrene to phenanthrene quinone [72].

Table 6, Molecular mass estimates for the PC fractions of the Recovered Dry tars from SEC and LD-MS. The results are presented as peak maximum values for the main bands of signal in order of abundance; for the LD-MS results the range over which ions were observed is also given.

		$T_{N2\text{-}0h}$		$T_{5C\text{-}6m}$		$T_{20C\text{-}6m\text{-}L}$	
		SEC	LD-MS	SEC	LD-MS	SEC	LD-MS
Fraction	Definition	Mass / u	Mass m/z	Mass / u	Mass m/z	Mass / u	Mass m/z
F4b	Peak Max	150	210	140	200		
	Range		<200-400		<200-300		
F4a	Peak Max	190	260	180+	250	160	325
	2nd Peak	1100	500	1000+	600	1000	650
	Range		<200-600		220-1500		250-1250
F3c	Peak Max	220	275	180+	330	180	350
	2nd Peak	900		1000+		1000	650
	Range		250-550		200-1100		220-1100
F3b	Peak Max	275	<200			460	
	2nd Peak	900				>2000	<200
	3rd Peak	>2000					
	Range		<200-400				<200-750
F3a	Peak Max	220	<200				
	2nd Peak	900					

	3rd Peak	>2000					
	Range		<200-800				
F2	Peak Max	210	550	200	700	650	600
	2nd Peak	650		600		>2000	
	3rd Peak	>2000		>2000			
	Range		200-1300		220-1500		220-1500
F1	Peak Max	>2000	650	>2000	725	>2000	725
	2nd Peak	1000	900	1300		1100	
	Range		200-2000		250-2000		300-1900

+SEC results for F3c and F4a from $T_{5C\text{-}6m}$ are from the combined F3c and F4a fractions as they could not be recovered separately.

Combining SEC, LD-MS, and UV-F analysis: When results for equivalent PC mobility-fractions where compared from the different samples it was generally found they did not contain identical molecular masses or structures (as was anticipated). Often they shared common features but show significant differences in either mass distribution or extents of conjugation (or occasionally both) due to the ageing conditions. It is thus an important finding that it is not correct to simply assume that equivalent PC mobility-fractions represent the same component(s) in different tar samples.

For example, Figures 2a-2c show the UV-F, LD-MS and SEC spectra, respectively, for PC fraction F3c from the fresh and aged tars. A significantly different UV-F spectrum was obtained from F3c from the fresh tar than the aged tars. Larger aromatic chromophores were observed in $T_{N2\text{-}0h}$ than in the aged tars. Differences between the LD-MS spectra are also apparent, where F3c from $T_{N2\text{-}0h}$ showed the lowest m/z peak maximum, a narrower distribution at low laser power and extensive fragmentation when a higher laser power was used as well as some new ions at m/z >400. $T_{5C\text{-}6m}$ showed a similar m/z peak maximum to $T_{N2\text{-}0h}$ but has a much greater tendency to fragment during ionization and produce a wider m/z range of ions. No fragment ions

were observed from PC fraction F3c of $T_{20C\text{-}6m\text{-}L}$ and a greater abundance of higher mass ions (m/z >400) were detected here than in the other tars, Figure 2b.

SEC shows that fraction F3c from the fresh tar contains more larger-sized molecules than the same fraction from the aged tars (Figure 2c). The two aged tars gave almost identical SEC chromatograms; whereas their LD-MS spectra are noticeable different. This is partly due to the lower resolution of SEC than LD-MS and may be evidence of the largest molecules observed by SEC (in $T_{N2\text{-}0h}$) fragmenting during LD-MS analysis. Further work is needed to better understand the differences observed between the SEC and LD-MS results.

It is possible that the molecules containing the largest aromatic chromophores present in F3c of the fresh tar react upon ageing and are no longer found in the F3c fraction of the aged tars. Although, the two aged tars appear to be very similar by SEC and UV-F, LD-MS indentifies clear differences. The molecules in $T_{20C\text{-}6m\text{-}L}$ are more stable during ionisation whilst those in $T_{5C\text{-}6m}$ are less stable. The material observed in this fraction in the aged samples contains molecules with less-conjugated chromophores than were present in same fraction from $T_{N2\text{-}0h}$.

It should be noted that the trends observed for PC fraction F3c of the different tars are not representative of the behaviour of the other fractions; each fraction showed subtle and unique differences. However, for brevity only a summary of the findings is presented below with the full account provided in S7 and the figures presented in S8.

Inspection of the complete set of LD-MS results reveals further differences in the tendency for fragmentation or susceptibility towards laser ionisation (i.e. strength of laser power needed to observe satisfactory signal) for the different PC fractions, and different tars. $T_{20C\text{-}6m\text{-}L}$ was least prone to fragmentation and its ions were easiest to observe. $T_{5C\text{-}6m}$ showed the greatest tendency to fragment and was the most difficult to observe. In general, the more mobile fractions were most likely to fragment. The LD-MS results also provide some confirmation of the mass estimates derived from SEC (cf. Table 6 and S7, Tables S7.1 – S7.7).

All the tar samples showed evidence of containing molecules with masses <200 u to >2000 u. There were distinct differences however, in their mass distribution before and after ageing depending also on the storage conditions. In general, there was a shift to

higher masses in the aged tars compared to the fresh tar, and for $T_{20C\text{-}6m\text{-}L}$ relative to $T_{5C\text{-}6m}$ i.e. heavier material in warmer conditions and the presence of light. Many of the PC fractions were composed entirely of materials beyond the range of GC, such as fractions F1 and F2, cf. Table 6, Figures S8.5a and S8.6a.

Examining the extents of conjugation present in the tars (via UV-F) shows that conjugated 4-6 aromatic ring systems dominate in almost all cases. It should be noted however, that fluorescence quantum yields are dramatically lower for conjugated aromatic ring systems that contain more than ~8 rings as discussed in S6 and elsewhere [47, 55], which means, if present, they are always underestimated. The fresh tar contains more aromatic molecules with high degree of conjugation than the aged tars when the mobile PC fractions (F3 and F4) are compared. Correspondingly, when comparing the least mobile fractions (F1 and F2), the reverse is typically found for the aged tars, where they contain more aromatic molecules with high degree of conjugation than in the fresh tar (there are exceptions, cf. S7). PC fraction F1 of $T_{5C\text{-}6m}$ contained the largest conjugated systems of all the tar samples (equivalent to an average of 8 conjugated aromatic rings).

When the UV-F spectra for all the PC mobility-fractions from all the tars are considered the following observations can be made:

i) The chromophores responsible for the fluorescence observed at 340-360 nm in $T_{N2\text{-}0h}$ F4b move to F3b in $T_{20C\text{-}6m\text{-}L}$, and possibly to F1; whereas for $T_{5C\text{-}6m}$ they remain in F4b.

ii) The chromophores responsible for the fluorescence observed at 440-550 nm in $T_{N2\text{-}0h}$ F3c appears to move to F3b and F1 in $T_{20C\text{-}6m\text{-}L}$; and to F1 for $T_{5C\text{-}6m}$.

iii) The chromophores identified in the precipitate (cf. Section 3.4, Figures 6a-d) and $T_{5C\text{-}6m}$ F1 (Figure 4a) showed maximum fluorescence intensity at >450 nm (>6 conjugated aromatic rings); these chromophores seem to originate from PC

fractions F4a, F3c, F3a and F2 in $T_{N2\text{-}0h}$, (Figure 4b); the evidence for this is discussed further in S7 and in the final summary (Section 3.5).

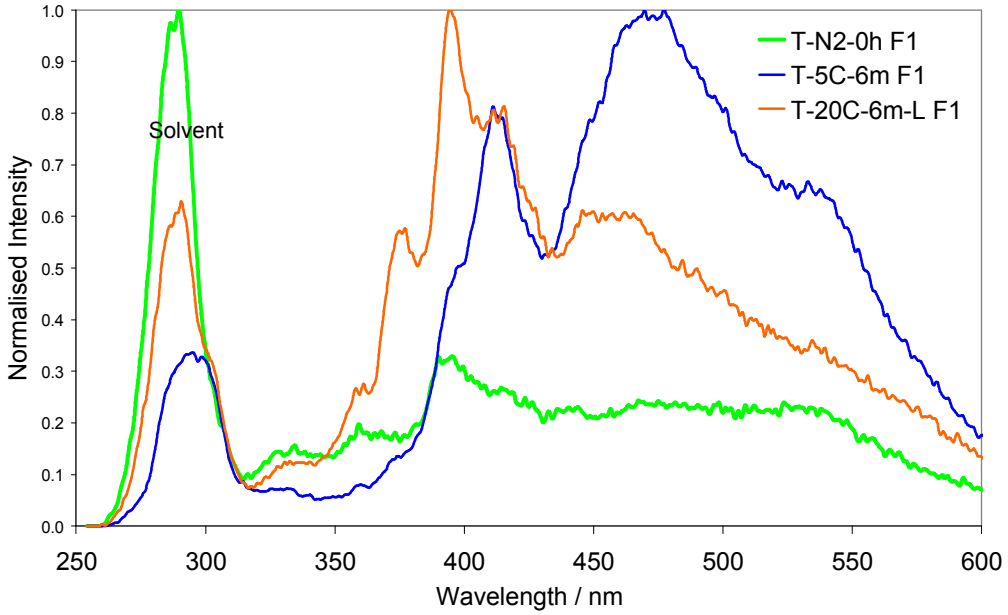

Figure 4a, Synchronous UV-F spectra (peak normalised) of PC fraction F1; for $T_{N2\text{-}0h}$ there was weak signal due to sample low abundance.

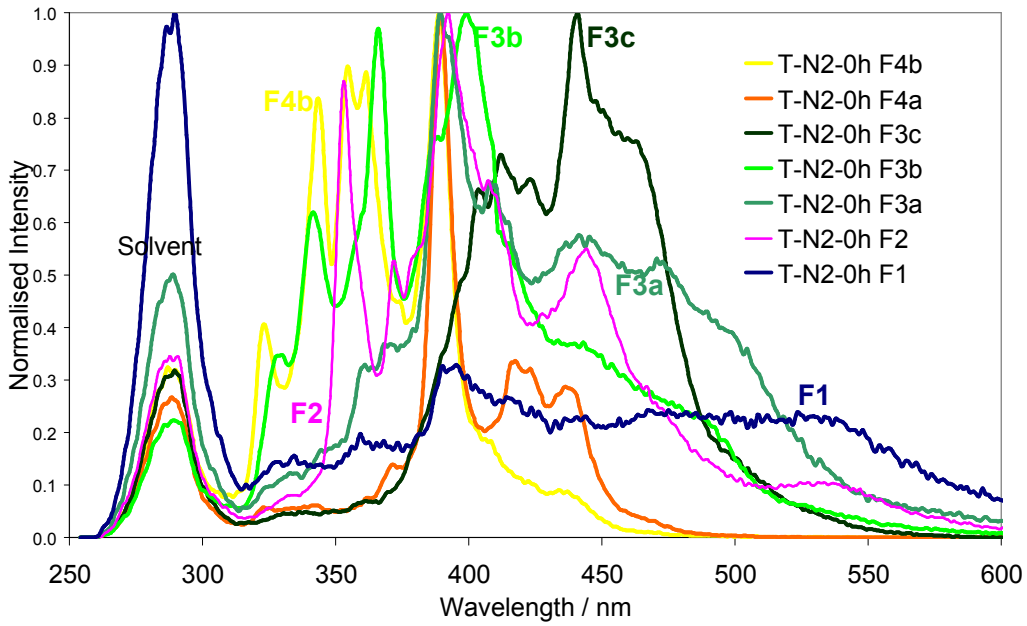

Figure 4b, Synchronous UV-F spectra (peak normalised) of the PC fractions from $T_{N2\text{-}0h}$.

Although the UV-F results are difficult to interpret they do show that changes in conjugation occur during ageing in addition to there being a change in the distribution of the tars on the PC plate. However, it is not possible to determine whether this is solely due to changes in aromaticity or a result of the incorporation of oxygen into the molecules as mentioned previously. It was often the case that the biggest differences between an equivalent PC fraction from the fresh and aged tars were observed by UV-F. Information on relative extents of conjugation is difficult to obtain by other methods. NMR could provide more detailed information and would greatly aid the interpretation of the UV-F results; however, the difficulty of recovering the requisite quantity of sample from planar chromatography hampers studies via NMR.

In future studies, column chromatography fractionation could be performed to obtain quantitative information; however, this will not be directly comparable to a PC fractionation as the mechanisms of separation differ. It would be best to do this in parallel to a PC fractionation as it is more difficult to perform LD-MS analysis on fractions recovered from column chromatography than from PC [31].

From a visual comparison of the PC plates bearing the fractionated tar some initial assertions were drawn. $T_{N2\text{-}0h}$ had very little immobile material (F1), larger quantities of F3c and F2, and no precipitate was observed before the sample was dried. Therefore, it is possible that it was the dark band of material denoted as F3c that was involved in reactions with F4b and F3b to generate the material that is labelled F1 and precipitate in the aged samples. The interpretation of the UV-F results as described above (and in S7) concurs with these assertions when combined with the mass estimates (from SEC and LD-MS, S9), i.e. these are the PC fractions that showed the biggest differences after ageing. It is suggested that it was mainly PC fractions F4b and F3c that react with one another to generate F1 and the precipitated materials during ageing; fractions F3b, F3a and perhaps F2 also seem to be involved in these reactions but to a lesser extent.

The results also imply that different processes occurred when the tar was stored at room temperature in the presence of indirect sunlight than when stored at 5°C in the absence of light. This is as opposed to the same changes occurring in both samples, but slower in the case of the sample stored at 5°C. When stored at 5°C all of the material seen as F3b in $T_{N2\text{-}0h}$ disappears, probably due to reactions forming material that can mobilize to another fraction or precipitate. Meanwhile, storing the tar at room temperature and exposed to indirect sunlight resulted in the absence of fraction F4b and a changed in composition of F3b; significant differences were also observed between the respective F1 and F2 fractions. These differences are probably related to the altered oxygen contents of the aged tars (Table 4) and the influence of sunlight, or a lack of it, on the reaction mechanism available to the tar molecules, as discussed earlier in Section 3.2.1.

It is interesting here also to speculate if the photochemistry of biomass may give clues to the photochemistry of its tars. The photochemistry of biomass and in particular lignin has been widely studied, due to its susceptibility to absorb both visible and near UV light [75]. The resulting excited states have shown to enable lignin depolymerisation in the presence of oxygen. After light absorption the molecules in their excited state can form radical species, usually by cleavage of the common β-O-4 aryl ether linkage, which then readily react with oxygen to form new chromophores. At the temperature at which

the gasification tars were produced here, the lignin in the pine is highly modified but may contain some β-O-4 aryl ether linkages present in the original biomass.

No oxygenated species were identified from the GC analysis of the tars. This implies oxygen is concentrated in the molecules beyond the range of GC. On the other hand, oxygenated hydrocarbons are known to co-elute with pure hydrocarbons during GC and this may explain their absence [76]. These aspects warrant further investigations; and are discussed further in S7.

An unexpected finding was that tar $T_{20C\text{-}6\ m\text{-}L}$, which has the highest oxygen content of the three tars and a greater C/H ratio than $T_{5C\text{-}6\ m,}$ contains aromatic molecules with low degree of conjugation. Even more surprising is that $T_{20C\text{-}6m\text{-}L}$ was the most stable towards LD-MS analysis (least prone to fragmentation, with the most easily observable ions). In contrast, $T_{5C\text{-}6m}$ has the least oxygen (although the absolute difference is small, Tables 4 and 5) and the lowest C/H ratio but contains the most aromatic molecules with the highest degrees of conjugation of the three tars; it also showed the greatest tendency towards fragmentation during LD-MS analysis.

The results described above appear to be evidence of photo-oxidation reactions having occurred during storage of the tar. The presence of indirect sunlight resulted in partial photo-oxidation of tar $T_{20C\text{-}6m\text{-}L}$, via the mechanism described earlier in Section 3.2.1 and displayed in Figure 3b. It would seem that the incorporation of oxygen groups into these predominantly aromatic molecules improves there susceptibility towards laser desorption and ionization, and destroys (or reduces) aromatic conjugation. Whereas tar $T_{5C\text{-}6m}$ was not exposed to light, therefore it reacted mainly via a different mechanism leading to molecules with greater molecular masses and less oxygen content (remaining in solution). These molecules also contain aromatic chromophores which have high degrees of conjugation, but they were not stable towards laser desorption and ionisation.

These observations show that the C/H ratio which is typically used to estimate the aromaticity of tar samples does not give information regarding the extents of aromatic conjugation. For example, the C/H ratio shows a trend of $T_{N2\text{-}0h}$>$T_{20C\text{-}6m\text{-}L}$>$T_{5C\text{-}6m}$, however, UV-F showed the extent of conjugation to be $T_{5C\text{-}6m}$>$T_{N2\text{-}0h}$>$T_{20C\text{-}6m\text{-}L}$. In addition, the relationship between extent of aromatic conjugation and susceptibility to

LD-MS analysis is contrary to that which would be expected based on previous studies of lignin (in preparation for publication), petroleum, bitumen and coal derived samples [31, 47, 55, 56, 60]. Where lignin is the most difficult to analyse followed by bitumen, with petroleum and coal-derived samples the easiest. However, in those previous studies all the samples were stable under the same conditions as used to age the gasification tars in the present study. Additional studies are required to understand the relevance of these observations.

3.3.3 Bulk analyses of Recovered Dry tar

To enable a significantly more robust interpretation of LD-MS data, the PC fraction data must be considered in tandem with bulk sample LD-MS data, rather than either of these approaches alone. This has been discussed in detail elsewhere [31, 47, 56]; briefly, whilst information gained from the bulk tars is considered more representative than results from PC fractionation alone, the LD-MS analysis of the bulk tars gives highly variable results depending on the conditions used [31, 47, 56]. This is demonstrated in Figures S10.1 and S10.2 for $T_{5C\text{-}6m}$ and $T_{20C\text{-}6m\text{-}L}$. Therefore combined information from both data sets is used in interpretation of results.

Figures 5a-c show the chromatograms and spectra from the analysis of the bulk Recovered Dry tars $T_{N2\text{-}0h}$, $T_{5C\text{-}6m}$ and $T_{20C\text{-}6m\text{-}L}$ by SEC, LD-MS and UV-F, respectively. The LD-MS spectra displayed in Figure 5b were selected after analysing low to high laser powers and the influence of different 'delayed ionisation extraction' times on the results, an example of these tests and their results is given in S10. The choice of which spectra to use to represent the sample was based on the information gained from the examination of the PC fractions, cf. S7 to S9, as described previously [56].

SEC reveals that $T_{N2\text{-}0h}$ contains smaller sized molecules, on average, than the aged tars (Figure 5a). The aged tars ($T_{5C\text{-}6m}$ and $T_{20C\text{-}6m\text{-}L}$) show very similar SEC chromatograms to one-another and give almost identical mass spectra from LD-MS (Figure 5b), with $T_{20C\text{-}6m\text{-}L}$ possibly containing more higher-mass (m/z) ions. The differences observed are subtle but noticeable. With the information obtained from the analysis of the PC fractions, it can be safely concluded that there is a trend towards higher average mass materials: $T_{N2\text{-}0h} < T_{5C\text{-}6m} < T_{20C\text{-}6m\text{-}L}$.

UV-F spectra of the different bulk tars are similar (main peak ~390 nm, equivalent to 5 aromatic rings – Figure 5c); the main difference is that $T_{N2\text{-}0h}$ shows slightly more fluorescence at wavelengths greater than 400 nm (>5 rings), followed by $T_{5C\text{-}6m}$ with $T_{20C\text{-}6m\text{-}L}$ giving the weakest signal in that region. This could be related to the aromatic molecules with the highest degrees of conjugation, originally present in $T_{N2\text{-}0h,}$ having reacted and precipitated from the aged samples. This explains the decrease in fluorescence at >400 nm in those samples (this confirms the findings from the PC fractions – S7).

When the UV-F spectrum from the bulk sample is compared to its PC fractions it can be seen that the bulk samples resemble their F3c and F4a PC fractions (the most mobile, low mass materials). This is consistent with previous observations where signal from larger aromatic chromophores is difficult to observe in the presence of less conjugated aromatics. This is thought to be related to a reduction in the quantum yields as the aromatic systems become more conjugated [55, 56, 61, 77].

The analysis of the bulk tars reveals that only limited information could be obtained about the changes that have occurred during ageing and highlights the importance of fractionating the tars prior to their analysis. It is important to note that fractionation of the tars by PC cannot readily be done quantitatively; therefore, it is beneficial to analyze the bulk samples as well as their PC fractions.

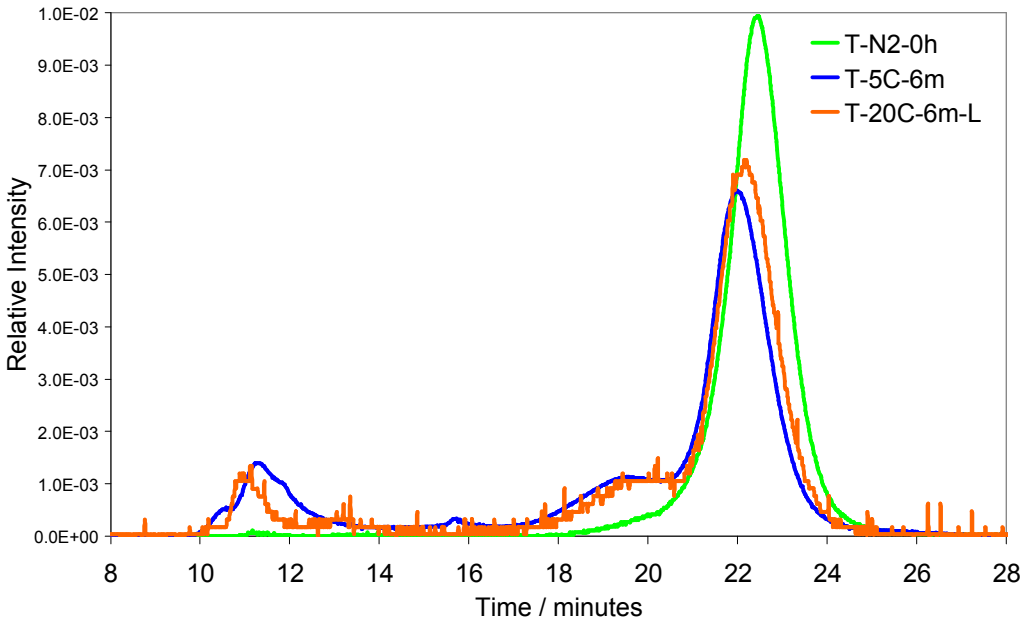

Figure 5a, Area normal size exclusion chromatograms of the bulk tars $T_{N2\text{-}0h}$, $T_{5C\text{-}6m}$, and $T_{20C\text{-}6m\text{-}L}$, detection at 300nm.

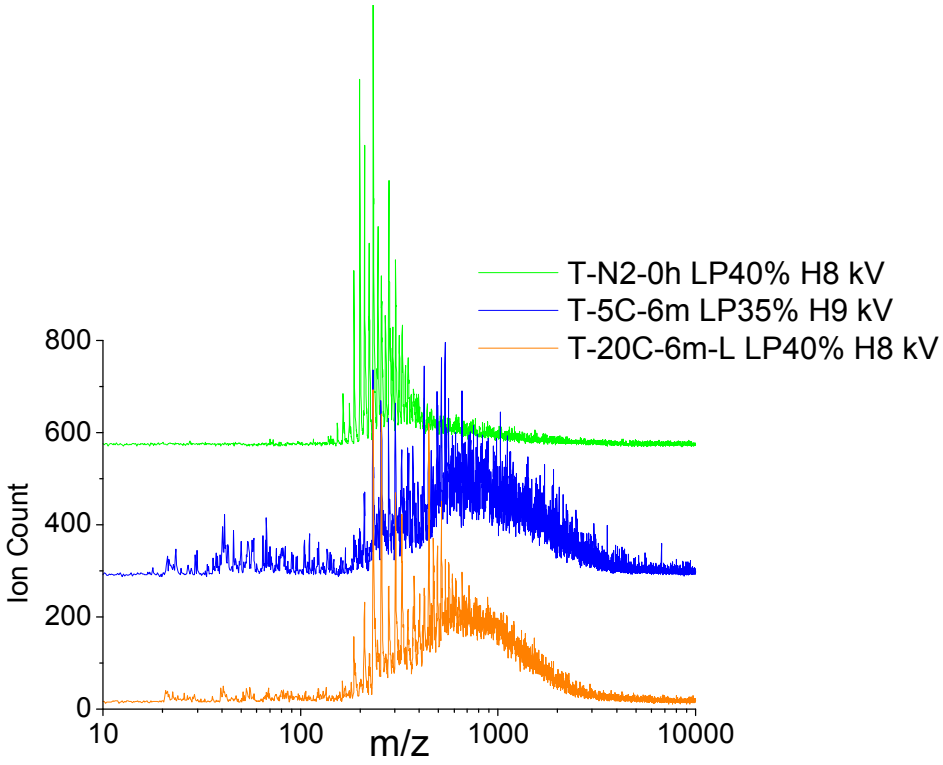

Figure 5b, LD-MS spectra of bulk tars $T_{N2\text{-}0h}$, $T_{5C\text{-}6m}$, and $T_{20C\text{-}6m\text{-}L}$ with no DIE, laser power (LP) and high mass accelerator (H) voltage are shown in the legend.

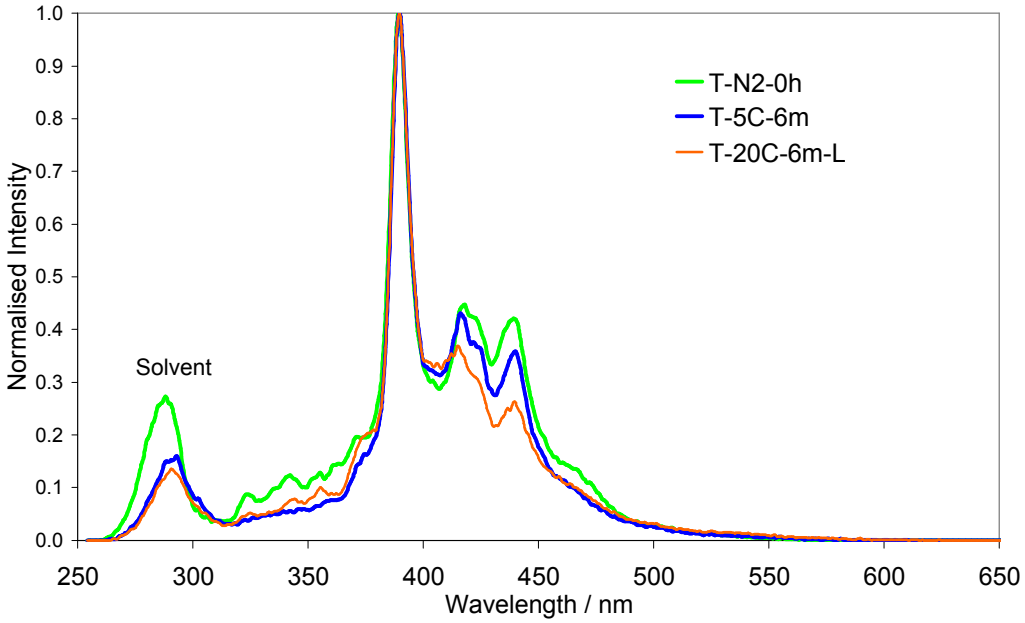

Figure 5c, Peak normalised synchronous UV-F spectra of the bulk tars $T_{N2\text{-}0h}$, $T_{5C\text{-}6m}$, and $T_{20C\text{-}6m\text{-}L}$.

3.3.4 Precipitated materials analyses

SEC and UV-F results from the analysis of the precipitates that formed within 20 hours, and after 6 months of storage of the tars are displayed in Figures 6a-d. It should be noted that the precipitated materials were fully soluble in NMP at the concentrations used. For $T_{N2\text{-}0h}$ the precipitate was recovered after 14 hours storage in a fridge after being thawed from liquid nitrogen – this sample is labelled $T_{N2\text{-}14h\text{-}ppt}$. LD-MS was not applied to the analysis of the precipitates as part of this scoping study; however, it would provide additional useful information and will be considered in future.

Figure 6a shows the SEC chromatograms from the precipitate recovered after 20 hours storage of T_{5C} ($T_{5C\text{-}20h\text{-}ppt}$) and T_{20C} ($T_{20C\text{-}20h\text{-}ppt}$) and 14 hours for T_{N2} ($T_{N2\text{-}14h\text{-}ppt}$), alongside tar $T_{20C\text{-}6m\text{-}L}$ to highlight the differences between the spectra from the tars and the precipitates. Evidence of a small but steady increase in the size of the molecules present in the precipitate can be seen

from $T_{N2\text{-}14h\text{-}ppt}$ < $T_{5C\text{-}20h\text{-}ppt}$ < $T_{20C\text{-}20h\text{-}ppt}$. All the precipitates contain molecules of larger size than those present in the tars.

Comparing the precipitate from 20 hours storage to that recovered after 6 months shows virtually no change in size distribution for $T_{5C\text{-}6m}$; however, for $T_{20C\text{-}6m\text{-}L}$ there is a shift to larger molecules in the precipitate recovered after 6 months, cf. Figures 6a and 6b.

UV-F reveals that all the 20 hour precipitates gave spectra almost identical to one another, and the precipitate from T_{N2} (14 hour precipitate) showed slightly less fluorescence at wavelengths greater than 470 nm (> 7 conjugated aromatic rings), Figure 6c. The spectra from the precipitates were significantly different to those from the bulk tars or their PC fractions, with the exception of $T_{5C\text{-}6m}$ PC fraction F1 which gave an almost identical spectrum (Figure 4a).

Comparing the UV-F spectra obtained from the precipitate after 6 months storage to that after 20 hours shows that for $T_{5C\text{-}6m}$ there is no discernable difference; for $T_{20C\text{-}6m\text{-}L}$ there is an increase in fluorescence at ~500 nm, cf. Figures 6c and 6d. The analysis of the precipitate shows that this material was not originally present in the fresh tar and must therefore be the product of reactions between the tar molecules (or with the solvent, or dissolved oxygen) during their storage. It is likely that greater differences could be detected between the precipitated materials if planar chromatography and LD-MS had also been used, as for the liquid tar samples; however, that was beyond the scope of the present investigation. In addition, ultimate analysis would provide valuable information and will be used in future studies.

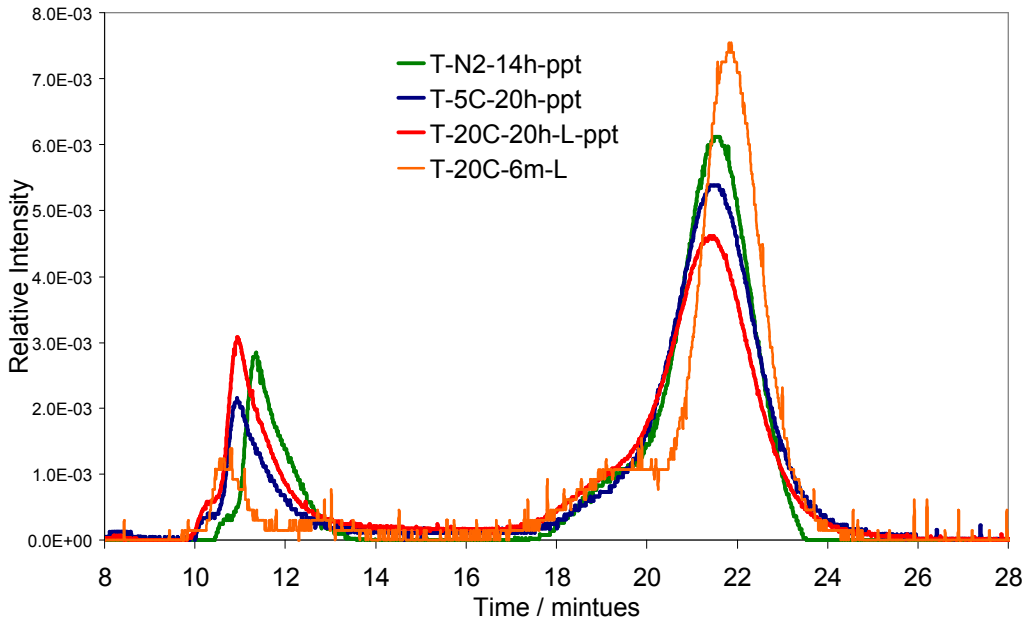

Figure 6a, Area normal size exclusion chromatograms of the precipitate after 20 hours from, T_{5C} and T_{20C}, and T_{N2} recovered after 14 hours after thawing from liquid nitrogen, the bulk tar $T_{20C\text{-}6m\text{-}L}$ is shown for comparison, detection at 300nm.

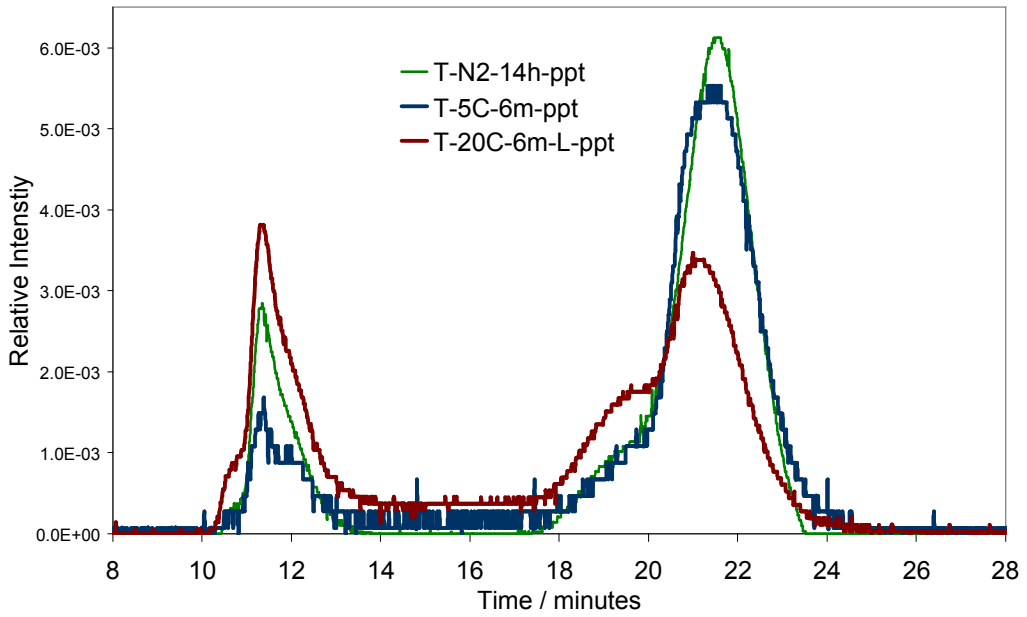

Figure 6b, Area normal size exclusion chromatograms of the precipitate from $T_{20C\text{-}6m\text{-}L}$, $T_{5C\text{-}6m}$ after 6 months storage, and the PPT from $T_{N2\text{-}14h}$ (after 14 hours storage).

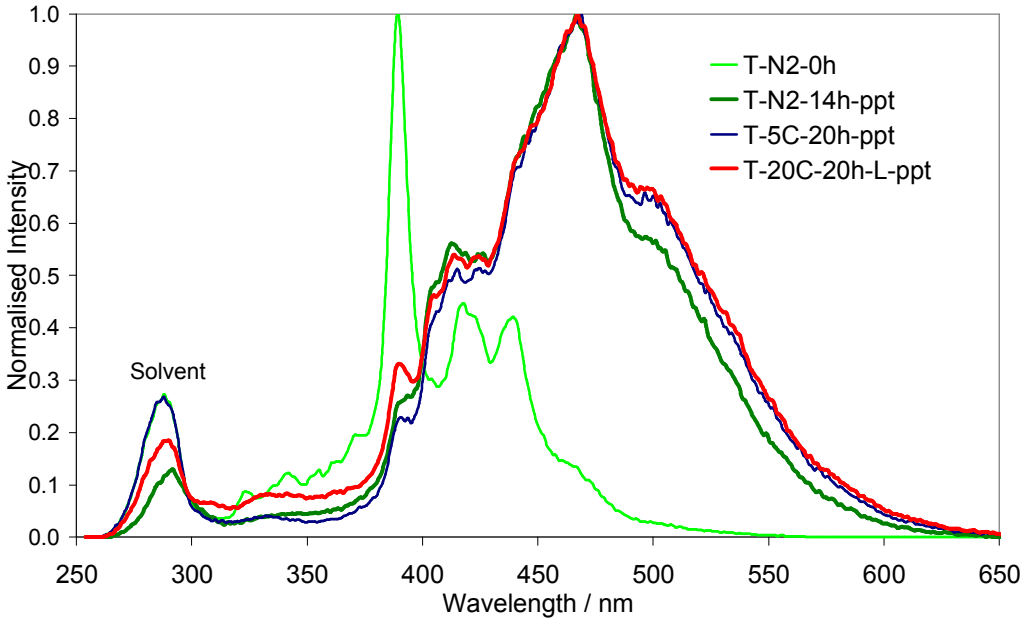

Figure 6c, Peak normalised synchronous UV-F spectra of the precipitate after 20 hours storage of the tar solutions T_{5C} and $T_{20C,}$ and after 14 hours for T_{N2}, along with the fresh tar $T1_{N2\text{-}0h}$ for comparison.

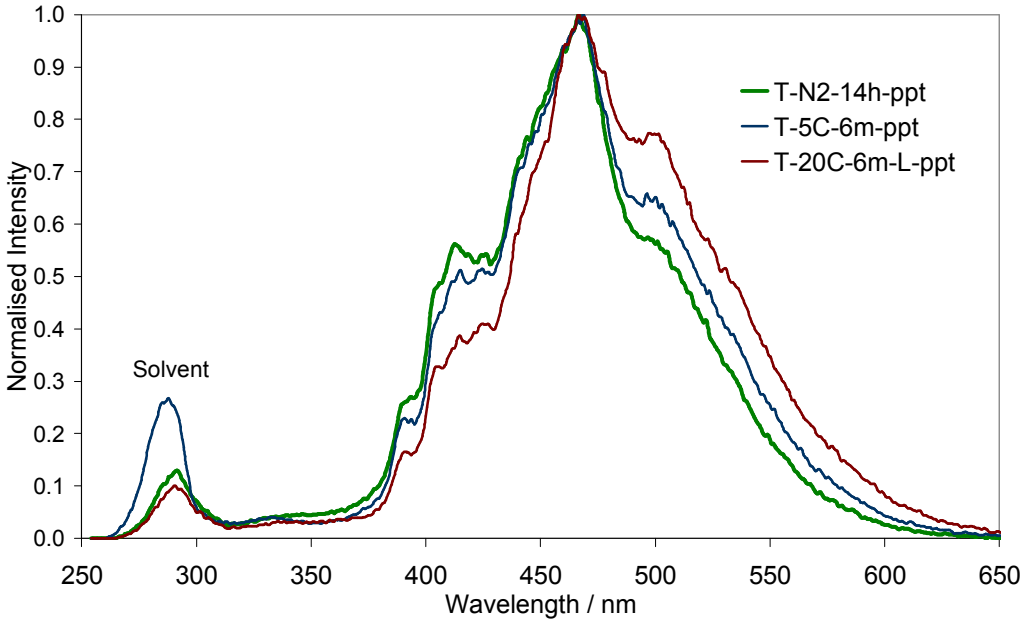

Figure 6d, Peak normalised synchronous UV-F spectra of the precipitate after 6 months storage of the tar solutions $T_{20C\text{-}6m\text{-}L}$, and $T_{5C\text{-}6m;}$ and 14 hrs precipitate from $T_{N2\text{-}14h}$.

3.3.5 Summary

When all the findings from the analyses of the tars, their PC fractions and the precipitated materials are considered together inferences can be made regarding the changes that occurred during ageing under different storage conditions.

The results strongly suggest evidence of aging reactions taking place and that PC fraction F1 in the aged tars is composed mostly of reaction products of aging. This is because there was a very low abundance of F1 in the fresh tar, so little so, that it was difficult to obtain satisfactory SEC and UV-F results. There is evidence that F1 of the aged tars contains higher molecular masses and different chromophores than the fresh tar (Figures 4a and S8.6a-c); this is most evident for PC fraction F1 from $T_{5C\text{-}6m}$. There was no precipitation noted in the fresh tar and the precipitate from the aged samples was found to contain molecules of higher mass (larger size) and with greater conjugation than the material in the fresh tar (Figures 5a-c and 6a-d). This is all evidence of a series of reactions occurring during ageing which result in an increase in molecular mass and conjugation in the tars. The precipitates recovered after 20 hours from the $T_{5C\text{-}6m}$ and $T_{20C\text{-}6m\text{-}L}$ samples contained molecules of similar size distribution and extents of conjugation. After 6 months the precipitate from $T_{5C\text{-}6m}$ showed little change by SEC or UV-F, whereas $T_{20C\text{-}6m\text{-}L}$ had increased in size (mass) and contained more aromatic molecules with high degree of conjugation (Figures 6a-d).

It was determined that the largest aromatic chromophores (8 conjugated aromatic rings, UV-F peak max 475 nm) and largest molecules were found in PC fraction F1 of $T_{5C\text{-}6m}$ (Figures 4a, 6b, 6d and S8.6b). PC fraction F1 from $T_{20C\text{-}6m\text{-}L}$ contained molecules approximately the same size as F1 from $T_{5C\text{-}6m}$, however the chromophores are much less conjugated, on average (5 aromatic rings versus 8). The precipitate recovered from $T_{20C\text{-}6m\text{-}L}$ contained the next largest molecules and sizes of conjugated chromophores (7-8 rings, 460 nm), which were slightly larger than those from the $T_{5C\text{-}6m}$ precipitate. At the same time $T_{20C\text{-}6m\text{-}L}$ contained less conjugated chromophores than $T_{5C\text{-}6m}$ or the fresh tar.

LD-MS analysis of the PC fractions shows that fraction F1 from the fresh tar has an average mass (peak max. m/z) of ~650 and the aged tars m/z ~725, with a shift in the distribution towards higher masses in the aged tars, extending to at least m/z 2000 (Table 6). Comparing these masses to the average number of aromatic rings as determined by UV-F ($T_{N2\text{-}0h}$ 5 aromatic rings, $T_{5C\text{-}6m}$ 8 rings and $T_{20C\text{-}6m\text{-}L}$ 5 rings) it can be determined that these molecules probably contain more than one aromatic core (as 5 rings = ~250 u and 8 rings = ~400 u), i.e. more probably archipelago- and island-like structural configurations rather than continental [61]. However, NMR and ultimate analysis data are needed to determine the amounts of aromatic and aliphatic material, ideally for each PC fraction, but there were sample limitations to conducting NMR.

When the results for bulk tars and their PC fractions are considered together, it can be determined that $T_{N2\text{-}0h}$ contains significant quantities of aromatic molecules with high degree of conjugation and after precipitation (i.e. the aged samples) the C/H ratio decreased. Therefore it would seem that the most highly aromatic compounds had precipitated. In $T_{20C\text{-}6m\text{-}L}$ more oxygen was observed than in $T_{N2\text{-}0h}$ which indicates mainly PAHs had precipitated and possibly undergone additional reactions with oxygen from the air or the solvent during its storage. In $T_{5C\text{-}6m}$ less oxygen was found than in the fresh tar. This suggests many of the oxygen containing PAH compounds have also precipitated. The C/H ratio of $T_{5C\text{-}6m}$ (0.62) and $T_{20C\text{-}6m\text{-}L}$ (0.99) implies that the latter is more aromatic; however, UV-F reveals it is $T_{5C\text{-}6m}$ that contains molecules with greater extents of conjugation (Figure S9.1c, S9.2c and S9.3c). $T_{20C\text{-}6m\text{-}L}$ shows evidence of containing slightly higher molecular masses and larger molecules. This sample is much more stable during LD-MS analysis than $T_{5C\text{-}6m}$ (Figure S9.2a-b and S9.3a-b).

The results suggest that the ageing process for $T_{20C\text{-}6m\text{-}L}$ proceeded via a different mechanism than that for $T_{5C\text{-}6m}$. Indeed, it is probable that the presence of indirect sunlight on $T_{20C\text{-}6m\text{-}L}$ induces photo-oxidation reactions which cannot occur in $T_{5C\text{-}6m}$ stored cold in the dark. It is less probable that the results are simply due to kinetic effects where tar $T_{20C\text{-}6m\text{-}L}$ has reached a

thermodynamically more stable state than $T_{5C\text{-}6m}$ due to enhanced kinetics from higher temperatures. In other words, it is unlikely that the ageing / polymerization reactions are progressing through the same mechanism but have progressed to a lesser extent in $T_{5C\text{-}6m}$ than in $T_{20C\text{-}6m\text{-}L}$. It is rather the case that there are a number of reaction mechanisms occurring simultaneously with competing influences from kinetic, thermodynamic, and photochemical effects when samples are stored exposed to light.

$T_{5C\text{-}6m}$ and $T_{20C\text{-}6m\text{-}L}$ did not show statistically significant differences in degree of precipitation. It is not possible to derive conclusive information regarding the ageing mechanism from this study due to the lack of key information such as the oxygen content of the precipitate and ideally for the PC fractions. In addition, NMR studies are required to aid the interpretation of the UV-F results and to reveal mechanistic information. However, to perform all of these analyses comprehensively a large amount of tar (>10 g) would be required.

However, the investigations here demonstrate that detailed information can be obtained by the combined use of SEC, LD-MS and UV-F methods, which can identify differences between tars that are difficult to obtain by other approaches. UV-F and LD-MS are very sensitive techniques that can provide evidence for the presence of large molecules (>1000 u) and those with highly-conjugated chromophores (>7 conjugated aromatic rings equivalent) that are formed during ageing. The methods are able to identify these materials, even when they are present in low abundance, if used in conjunction with planar chromatography. Knowledge of the presence of these high mass molecules and/or aromatic molecules with high degrees of conjugation in tars and oils, even in low quantities, is essential when considering their properties and further use. These tars and oils have applications in many processes including combustion, reforming and upgrading but these large molecules can cause problems of char formation/coking in engines/boilers or poisoning of catalysts.

3.4 Conclusions

The tars recovered in this study using the tar protocol method rapidly exhibited instability, with precipitate forming within 14 hours of standing; this was independent of storage at 5°C or at 20 °C. Only storing the solution in liquid nitrogen halted this process.

The study revealed that the molecules that contained the largest sizes of conjugated aromatic ring systems, rather than the molecules with the greatest masses, were primarily involved in ageing reactions, resulting in precipitation occurring.

Storing the tar isopropanol solution in the dark at reduced temperature (5°C) appears to result in a different ageing reaction mechanism to that when the sample is left at room

temperature and exposed to indirect sunlight. There are probably numerous mechanisms occurring, and for the sample exposed to indirect sunlight there is evidence of additional photo-oxidation reactions. From this preliminary investigation these details cannot be determined with certainty and the influence of sunlight and oxygen should be investigated further.

The differences observed between these biomass/coal mixture samples were greater than anticipated from previous studies of coal, petroleum and bitumen derived materials [47]. However, it remains difficult to definitively interpret the results, which highlights the complexity of attempting to elucidate the molecular properties of tars or their ageing mechanisms.

An important finding of this scoping study is that the combined analytical approach including SEC, LD-MS and UV-F, which was originally developed for studying heavy samples such as pitches and asphaltenes rather than oils and tars [47], can be equally well applied to these (lower molecular weight) biomass tars. In fact, the methodology could provide clearer information for tars and oils than pitches and asphaltenes, as the molecules here have a more suitable mass and size range for study via SEC, LD-MS and UV-F (mass range <5,000 u and chromophores < 10 rings). However, the higher oxygen content of biomass tars compared to that of heavier samples such as pitches and asphaltenes makes results interpretation less exact.

Future studies should include NMR, FT-ICR-MS and FT-IR analyses to aid the interpretation of the UV-F results and to clarify the findings in general. Ultimate analysis of the bulk precipitate, and ideally also the PC fractions, would provide additional valuable information.

Through the application of the combined analytical approach outlined here it is possible to build up a detailed understanding of tar samples and other similar biomass, coal or petroleum derived liquids in terms of molecular mass range, average mass estimates and extents of aromatic conjugation. For a more thorough understanding of the aging process these methods should be combined with those currently being developed for bio-oils.

One of the more troublesome aspects of getting useful energy from tars is their high viscosity and their tendency to age into even more viscous material, such that learning details about the chemical routes of ageing and how to prevent that chemistry from happening can have important implications for utilizing tars.

3. S: Supporting information

S1; Fuel Properties

S2; Planar Chromatography Images

S3; Tar Yields, GC and UA Further Discussion

S4; SEC Calibration and Interpretation

S5; LD-MS Additional Information

S6; Synchronous UV-F Interpretation

S7; PC Fractions SEC, LD-MS and UV-F Results

S8; Figures, by PC Fraction (SEC, LD-MS and UV-F)

S9; Figures, by Sample (SEC, LD-MS and UV-F of PC fractions)

S10; Figures, LD-MS of the Bulk Tars

S3.1; Fuel properties

The fuel properties reported in Table S1.1 below were determined in previous studies [1]. Approximate contents of cellulose, hemi cellulose and lignin in a typical pine wood sample is 48.0, 23.5 and 28.5 wt% respectively (excluding extractives, 3.9 wt%) [2].

Table S1.1, Properties of the fuels used to generate the tar samples

Fuel	Polish coal		Pine wood chips
Origin	Poland		Portugal
Type	bituminous coal		softwood

Proximate analysis			
Fixed C, %	54.9		13.6
Volatiles, %	28.8		74.5
Ash, %	8.6		0.3
Moisture, %	7.7		11.6
Ultimate analysis			
C, % daf	79.1		51.6
H, % daf	4.5		4.9
S, % daf	0.5		0.2
N, % daf	1.3		0.9
Cl, % daf	0.4		0.07
O, % daf	14.2		42.4

Deviations determined as within +/-0.5%, absolute.

S3.2; PC fractionation

Images of the planar chromatography plates bearing the three tar samples are shown in Figure S2.1.

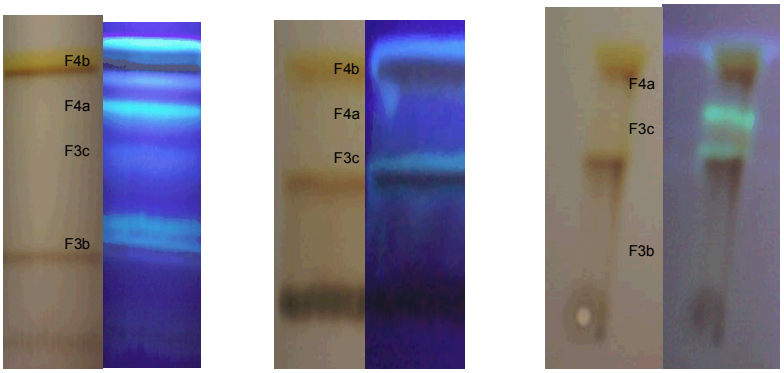

$T_{N2\text{-}0h}$ $T_{5C\text{-}6m}$ $T_{20C\text{-}6m\text{-}L}$

Figure S2.1, PC plates bearing the vacuum dried tar samples after being eluted with chloroform (F3) followed by acetone (F2) and finally heptane (F4). The image on the left-hand side was taken under white light, and the right-hand side under UV-light (260 nm).

The main bands of material are labelled as follows:

F1 = immobile (dark band)

F2 = acetone mobile / chloroform and heptane immobile (dark band)

F3 = chloroform mobile / heptane immobile (dark and fluorescent bands)

F4 = heptane mobile (yellow and fluorescent bands)

Note: In Figure S2.1 the small silver circle visible for $T_{20C\text{-}6m\text{-}L}$ F1, under 'white light' is due to the aluminium backing-plate showing through due to loss of the silica coating. In addition, the lighter colour of $T_{20C\text{-}6m\text{-}L}$ observed under UV when compared to the other images was due to the photo being taken during the day time, whereas the others were taken at night. Caution is required when trying to draw conclusions from the images of the

PC plates displayed in Figure S2.1 as the photos are not of high enough resolution to convey the full extent of the visual information that was observed and described in the manuscript (which was based on the examination of a greater number of PC plates).

Chloroform was the first eluent used which resulted in one main band of dark material at the solvent front (F3c) and numerous weaker bands further down the plate (F3b and F3a being the mains ones), many of which were highly fluorescent in the green, yellow, orange and blue (this *cannot* be clearly seen from the photographs displayed in Figure S2.1). Less emphasis was placed on the separation and identification of these mobile components, the aim was to isolate the higher mass components and to generate a few representative bands to aid the characterisation of the parent samples.

S3.3; Tar yields, GC and UA further discussion

Error in the tar yields: By examining the tar yields in Table 2 it is apparent there are errors in the mass balances presented. This is noticeable when comparing the 20 hour GC results to those after 6 months of storage, as discussed in the main text (Section 3.1). The deviations in the determinations of the 'recovered dry' tar weight and the weight of the precipitate were also fairly significant (+/- ~15 and 30 % respectively). For the recovered dry tar yield, the errors were due to the limited volume and low concentration of the solution as well as the high volatile content of the tars; the actual weights being determined were in the tens of milligrams range at best. Similarly, the quantity of precipitate recovered was in the milligram range.

GC-FID experimental – additional information: Before each set of analyses a standard solution (containing the 16 PAHs indentified as carcinogens by the Environment Protect Agency, EPA-16) was used for peak identification and area calibration. Dodecane was used as an internal quantitative standard. All the results were normalised to grams of tar per normal cubic meter of exhaust producer gas from the gasifier (g/Nm^3). To check the repeatability of the results triplicate samples were analysed from each stock solution and the scatter found to be less than +/- 2% (relative standard deviation - RSD). Table

S3.1 presents the concentrations of the quantified compounds (EPA-16) in the tar. Unknown peaks were included in the calculation of the total GC tar yield. This was achieved by comparing the combined area counts of the unknowns to naphthalene, the calculated g/Nm^3 was then halved and that amount reported. Benzene, toluene and xylene were *not* accounted for by the GC method used.

GC results: Some information can be inferred from the analysis of the relative peak intensities, to see how the tars change with ageing. There is a strong trend showing a decrease in the amount of GC range molecules with ageing, Table S3.1; however, there was no evidence for an equivalent increase in the corresponding gravimetric tar yields or precipitate. Therefore, it seems unlikely that these loses are due to reactions between GC ranges molecules resulting in higher mass species; it is more probably a result of evaporation or losses to the glassware as discussed in the manuscript. This is thought to be the case because the greatest changes were in the naphthalene concentration which it is unlikely to be reactive under the storage conditions.

Examination of the GC results for tar $T_{N2\text{-}0h}$ before and after precipitate confirms that no significant change can be detected (cf. the 0 and 14 hour samples, Table S3.1). The biggest changes were a slight decrease in acenaphthylene and phenanthrene, although, these are within the scatter of the results. The only changes larger than the scatter were a slight increase in the amounts of benzo(a)pyrene, indeno(1,2,3)pyrene and benzo(g,h,i)pyrene, and a small decrease in the amount of naphthalene, as described in the manuscript.

Tar components more volatile than naphthalene were *not* examined; it is possible that the apparent increase in the amount of benzo(a)pyrene, indeno(1,2,3)pyrene and benzo(g,h,i)pyrene was due to some of the more volatile compounds (than naphthalene) reacting, possibly with naphthalene to form these species, and/or due to solvent evaporation or loss of other volatile components. However, it would be surprising if naphthalene was reactive under these conditions.

Table S3.1, GC-FID results for the tar samples before vacuum drying, displayed as mg per cubic meter of producer gas

Sample Name	T_{N2}			T_{5C}				T_{20C}			
Units	mg/Nm³										
Sample Age	*0h*	*14h*	*20d*	*20h*	*3d*	*20d*	*6m*	*20h*	*3d*	*20d*	*6m*
Naphthalene	3000	3000	2800	2600	2700	2800	1000	2700	2900	2700	1500
Acenaphthylene	710	700	680	640	630	680	400	670	680	660	420
Acenaphthene	10	10	10	10	10	10	10	10	10	10	5
Fluorene	50	60	50	40	50	50	20	50	50	50	20
Phenanthrene	460	450	470	380	400	440	230	410	420	420	230
Anthracene	90	90	100	80	80	90	40	80	90	90	40
Fluoranthene	230	240	250	220	220	230	140	240	230	230	150
Pyrene	240	250	250	220	220	240	150	240	230	230	150
Chrysene	30	30	30	20	30	30	20	30	30	30	20
Benzo(a)anthracene	30	40	40	30	40	40	20	30	40	40	20
Benzo(k)fluoranthene	30	40	40	30	40	30	20	30	40	30	20
Benzo(b)fluoranthene	10	10	10	10	10	10	5	10	10	10	10
Benzo(a)pyrene	40	60	50	40	50	50	40	40	50	50	40
Indeno(1,2,3)pyrene	30	40	30	20	30	30	20	20	30	30	20
Dibenzo(a,h)anthracene	5	10	5	5	5	5	5	5	5	5	5
Benzo(g,h,i)perlyene	5	30	30	5	30	5	20	20	30	30	20
Total EPA 16	5000	5100	4800	4400	4500	4700	2100	4600	4900	4600	2700
Unknowns	280	280	270	230	250	240	170	270	250	220	180
GC Total	5300	5400	5100	4600	4750	4900	2300	4900	5150	4800	2900

Relative errors were less than +/- 5%

S3.4; SEC calibration and interpretation

The SEC elution time was converted to mass using a five point PS calibration performed on the day of analysis. This equation (Eq 1) was applied from 15.0 – 20.7 minutes. After this time a calibration based on small poly aromatic hydrocarbon (PAH) standards (Eq 2) was used, based on previous studies [3-5]. The equation from the PAH standards (Eq 2) was applied to the 20.7 – 24.0 min region. 24.0 minutes relates to a mass of about 100 u; any signal in the region 24-25 minutes was given a value of 100 u. 25 minutes is the permeation limit for this column. Materials eluting earlier than 15.0 minutes were assigned an estimated mass of 2500 u. The reasons for this are briefly described in the following section.

Equations used to convert SEC elution time to mass:

Eq 1: 15.0 – 20.5 minutes region: $y = 9.683-0.346.x$ PS calibration

Eq 2: 20.5 – 24.0 minutes region: $y = 6.902-0.210.x$ PAH calibration

Where $y = \log_{10}(MM)$; and x = elution time in minutes

12.0 – 15.0 minutes region: >2,500 u average mass LD-MS calibration.

24.0 – 25.0 minutes region: Value kept constant at 100 u

Comment on the disparity between the SEC and LD-MS mass estimates: There is an apparent disparity between the mass estimates derived from a SEC PS calibration with those from LD-MS measurements when analysing complex hydrocarbon mixtures [3-6].

This is thought to arise for a number of reasons as described in a recent review article [6]. In brief, it has previously been shown that the material which elutes in the excluded region (<15 minutes) of this SEC system has a higher average mass than the materials eluting in the retained region (15-25 minutes), for similar materials. However, it is difficult to accurately determine the mass of the excluded material, as discussed elsewhere [3-6]. The PS calibration appears to greatly overestimate the mass of the excluded material observed by SEC, an LD-MS study found average masses (m/z) of 2500 - 3500 when the excluded SEC material was examined in isolation of retained material; whereas, the SEC PS calibration indicated masses >100,000 u. In addition, when there is some retained SEC material also present in the sample being analysed by LD-MS, as for these samples, it tends to dominate the LD-MS spectra even when it is present in lower abundance (mass discrimination and other factors [3, 5-9]).

S3.5; LD-MS additional information

For the LD-MS analysis all the samples were investigated using a 0 (zero) and 600 ns delayed ion extraction (DIE) time. Spectra were also recorded in reflector-mode (results not shown). It is prudent to examine the samples by as wide a range of conditions as possible to aid interpretation. The LD-MS results presented in the manuscript were those obtained under the following conditions:

For the PC fractions: only spectra obtained in linear-mode operation with a HMA voltage of 10 kV, no DIE time and with varying levels of laser power applied, are displayed. These conditions are based on previous studies [3, 7]. Briefly, the purpose of the analysis of the PC fractions is to obtain information on the mass range of the sample. Therefore, the conditions are selected to aid the observation of the fragment ions and the highest mass components (ions).

For the bulk tars: the aim was to obtain mass spectra that more accurately represent the mass distribution of the sample in its entirety. Therefore, only spectra obtained in linear-mode operation with the following conditions are reported, DIE time of 600 ns and where the HMA voltage was reduced as the laser power was increased. These conditions are used to aid the detection of the higher m/z ions and avoid overloading the detectors with low m/z ions.

A few LD-MS spectra are presented that were obtained under different conditions to those described above to highlight certain points; in these instances the conditions will be stated in the text.

The use of the peak of maximum intensity (peak max.) to estimate average mass values from SEC and LD-MS was considered sufficient for the purposes of this scoping study (i.e. to draw relatively comparisons) based on previous experience [3, 6, 7]. Details of the methods used to determine molecular mass estimates are also provided in said publications.

S3.6; Synchronous UV-F interpretation

The approach used to interpret the UV-fluorescence results is based on previous investigations. A number of studies have reported that UV-F spectra show bathochromic shifts (to *longer* wavelengths, red-shift) and emit lower fluorescence intensities with increasing sizes of conjugated aromatic ring systems [5, 8, 10, 11]. More recent work also supports these conclusions. A qualitative relationship has been noted between the wavelength of maximum fluorescence and number of conjugated aromatic rings in a polynuclear aromatic (PNA) system, as determined by synchronous mode UV-F and NMR spectroscopy, respectively [6]. This was for a number of coal, petroleum and bitumen derived oils, tars, pitches and asphaltenes, and their solubility sub-fractions [3, 10, 12-14]. This correlation was drawn from a comprehensive review of UV-F spectroscopy and other analytical techniques useful for analysis complex hydrocarbon mixtures [6].

Figure S6.1 and Table S6.1 demonstrate the relationship between synchronous UV-fluorescence spectra for a series of coal and petroleum derived samples with their number of conjugated aromatic rings (determined by NMR) superimposed on the peak with maximum intensity of fluorescence. The maximum intensity of fluorescence shifts steadily to longer wavelengths by approximately 30 nm per additional aromatic ring in a conjugated aromatic system, based on NMR results [3, 10, 12-14]. Fluorescence intensities in the UV-fluorescence spectrum of the samples 4P1 and 5P1 were very low

and showed a broad distribution, ranging from 350 to more than 650 nm. These findings suggest the presence of molecules containing a wide range of chromophores, some corresponding to polycyclic aromatic ring systems with more than 10 conjugated rings – as determined by ^{13}C-nmr [6, 14].

It should be noted that oxygen and other substituents on aromatic ring systems also influence fluorescence characteristics. Limited information is available however, regarding their influence on the fluorescence of poly aromatic hydrocarbons with molecular masses greater than ~400 u. A summary of some relevant fundamental aspects of UV- fluorescence are given below, further details can be found elsewhere [15].

When substituent groups are introduced to an aromatic molecule the effect on fluorescence characteristics depends on position on the ring they occupy as well as their functionality. Electron-accepting unsaturated functional groups, such as -COOH, -NO_2, -C=O, NH2, or -C=S-R can influence fluorescence characteristics of PAH's. Such groups have low lying vacant π* orbitals which *can* become occupied by an excited electron from the aromatic ring. Electron density is transferred from the ring to the substituent (intramolecular charge transfer). Another complication is the introduced of C=O, C=S, -NO_2, or hetero-atoms (N, S). Each of these groups processes a lone pair of electrons in an orbital parallel to the plane of the aromatic ring, which can be promoted. This can have profound effect on fluorescence, dramatically reducing fluorescence intensity [15].

When groups containing 'n' electrons (n = non-bonding electrons, as in C=O) are conjugated with a π electron group, the effect is the same as increasing aromatic conjugation on fluorescence characteristics. Therefore, addition of C=O groups to PAHs and alkyl-aromatics results can result in a red shift of the fluorescence (to longer wavelengths), depending on the position they occupy. Aromatic carbonyl compounds are strongly influenced by the low-lying (n, π*) singlet excited states (as n-to-π* transition is 100x less intense than π-π *); therefore, this significantly reduces fluorescence quantum yield [15].

Auxochromes, which generally do not absorb significantly in the 200-800 nm region will affect the fluorescence spectrum of the chromophore to which it is attached. OH is an auxochrome; however, it typically has a minor influence on the chromophore it is

attached to [15]. Ether groups typically have no influence on conjugation or fluorescence.

Due to the complex nature of fluorescence characteristics in large PAH molecules it was not possible to account for the influence of oxygen on the UV-F results of the tars being studied or in the correlation described above and shown in Figure S6.1 and Table S6.1. To simplify the discussion of the UV-F results the term 'number of conjugated aromatic rings' or 'number of rings' will be used in reference to the wavelength where the peak of maximum fluorescence intensity is observed, using the correlation provided in Table S6.1. In should be noted that this is *not* meant as a literal description of the chromophore, it is only used to make relative comparisons between samples. The changes in fluorescence characteristics referred to could also be due to the influence of oxygen or other substituents, not necessarily changes in aromatic conjugation alone.

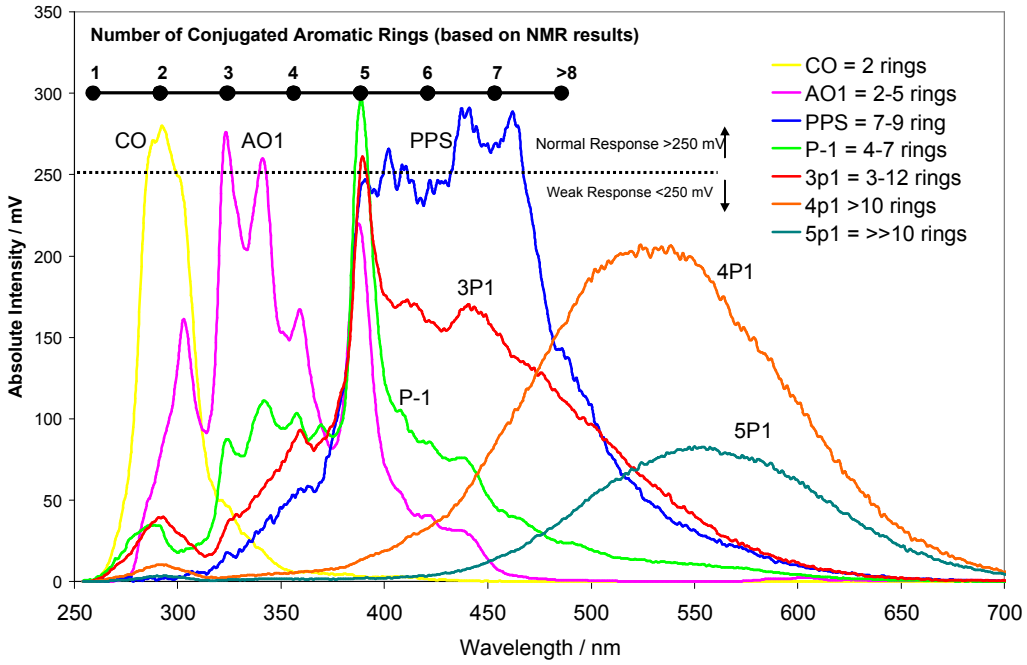

Figure S6.1, Synchronous UV-F spectra (absolute intensity - mV) of sample fractions showing correlation with conjugated aromatic rings as determined by NMR. CO is creosote oil, AO1 anthracene oil, PPS pyridine soluble fraction of coal tar pitch, P-1 a synthetic pitch-like material, 3P1, 4P1 and 5P1 are solubility fractions of P-1. [3, 10, 12-14].

Table S6.1, Correlations between the average numbers of rings in polynuclear aromatic ring systems (determined by NMR) and the wavelengths of maximum fluorescence intensity in the UV-fluorescence spectra [6]

Wavelength of peak with maximum intensity	Approximate Number of Aromatic Rings	Wavelength of peak with maximum intensity	Approximate Number of Aromatic Rings
270 nm	1 ring	390 nm	5 ring
300 nm	2 ring	420 nm	6 ring
330 nm	3 ring	450 nm	7 ring
360 nm	4 ring	≥480 nm	≥8 ring

S3.7; PC fractions SEC, LD-MS and UV-F results

In this section a detailed account of the SEC, UV-F and LD-MS results from the analysis of the PC mobility-fractions is given. The PC fractions that were *not* observed in all the samples are discussed first followed by those common to all the samples. This is beneficial because the fractions that were *not* observed in all the samples are of greatest interest as they are the materials that have reacted or are the products of reactions.

Fluorescent material, PC fraction F3a (SI Section S9, Figures S9.1a-c)

This material was only observed in $T_{N2\text{-}0h}$. It contains some material with molecular masses approaching 1000 u, and also contains significant amounts of smaller molecules (~200 u). UV-F shows 5-9 aromatic rings equivalent chromophores, on average (Table S7.1). It is not surprising that the material in F3a was not found in the aged samples considering previous studies [3, 14, 16]. Where it has been found that the PAH molecules containing the most highly-conjugated chromophores (largest poly nuclear aromatic groups) are the most reactive, described further in the manuscript. PC fraction F3a contains aromatic molecules with some of the most highly-conjugated chromophores

that were observed for the fresh tar; therefore it is not surprising these molecules have reacted, probably to produce larger, higher mass molecules with different mobility on the PC plate after ageing the tar (or have precipitated). Hence, PC fraction F3a was not observed in the aged samples.

Table S7.1, Summary of SEC and LD-MS mass estimates, and UV-F results for PC fraction F3a from $T_{N2\text{-}0h}$

F3a	Definition	Units	$T_{N2\text{-}0h}$
LD-MS	Peak Max. / m/z	m/z	<200
	Upper mass		800
SEC	Peak Max.	u	220
	2nd Peak		900
UV-F	Peak Max., (Ar. Rings+)	nm (rings)	390 (5)
	2nd Peak, (Ar. Rings+)		440 (7)
	3rd Peak, (Ar. Rings+)		470 (8)

+ Ar. Rings refers to the equivalent number of conjugated aromatic rings that would fluoresce at the same wavelength, as described in SI Section S6.

Fluorescent material, PC fraction F4b: (Figures S8.1a-c, SI Section S8).

$T_{N2\text{-}0h}$ and $T_{5C\text{-}6m}$ were the only samples to noticeably contain this PC fraction. The results indicate that it was roughly the same material in both samples. UV-F shows the spectra from $T_{N2\text{-}0h}$ and $T_{5C\text{-}6m}$ were very similar (Table S7.2, Figure S8.1c). There was one significant difference however; $T_{N2\text{-}0h}$ contained a chromophore that fluoresced strongly at 360 nm (~4 rings eq.) that was not present in $T_{5C\text{-}6m}$. In addition, the fresh tar contains a greater abundance of the least-conjugated chromophores (3-4 rings) and fewer 5 ring

species, relatively. The ring sizes predicted from UV-F correspond with the mass estimates from LD-MS and SEC.

Despite the low average mass of this fraction it was still possible to obtain reasonably strong ions counts, and repeatable spectra, during LD-MS analysis. This was not the case for fraction F3b (discussed next).

Table S7.2, Summary of SEC and LD-MS mass estimates, and UV-F results for PC fraction F4b from $T_{N2\text{-}0h}$ and $T_{5C\text{-}6m}$

F4b	Definition	Units	$T_{N2\text{-}0h}$	$T_{5C\text{-}6m}$
LD-MS	Peak Max.	m/z	210	200
	Upper mass		400	300
SEC	Peak Max.	u	150	140
UV-F	Peak Max., (Ar. Rings^{+})	nm (rings)	390 (5)	390 (5)
	2nd Peak, (Ar. Rings^{+})		355 (4)	355 (4)
	3rd Peak, (Ar. Rings^{+})		360 (4)	345 (3)
	4th Peak, (Ar. Rings^{+})		345 (3)	-

$^{+}$ Ar. Rings refers to the equivalent number of conjugated aromatic rings that would fluoresce at the same wavelength, as described in SI Section S6.

Fluorescent material, PC fraction F3b: (Figures S8.4a-c, SI Section S8).

PC fraction F3b was only observed for $T_{N2\text{-}0h}$ and $T_{20C\text{-}6m\text{-}L}$. The combined information from SEC, LD-MS and UV-F reveals that fraction F3b from the two samples is *not* composed of the same materials (Table S7.3). $T_{N2\text{-}0h}$ contains molecules of lower

molecular weight (~300 u) and with less-conjugated aromatic systems (4-5 rings equivalent), on average, than $T_{20C\text{-}6m\text{-}L}$ which has an average mass of ~450 u from SEC. However, LD-MS analysis resulted in mainly fragment ions being observed with few ions detected above m/z 450. UV-F confirmed that $T_{20C\text{-}6m\text{-}L}$ is likely to contain more, higher mass molecules than $T_{N2\text{-}0h}$ as it provides evidence for larger-sizes of conjugated systems (5-8 rings equivalent in $T_{20C\text{-}6m\text{-}L}$ compared to 4-5 rings in $T_{N2\text{-}0h}$). Fraction 3b was not observed in $T_{5C\text{-}6m}$.

UV-F reveals marked differences in the extents of conjugation of the chromophores in the F3b fractions. The fresh tar ($T_{N2\text{-}0h}$) mainly contains chromophores equivalent to 4-5 fused aromatic rings, while the aged sample ($T_{20C\text{-}6m\text{-}L}$) contain mainly 5-8 fused rings equivalents. It should be relatively easy to observe these materials via LD-MS; however, for $T_{20C\text{-}6m\text{-}L}$ there was little evidence of molecules large enough to contain the number of rings suggested by UV-F. It is likely that the molecules in $T_{20C\text{-}6m\text{-}L}$ fraction F3b contain bridges between 3-4 ring aromatic units in a way that maintains conjugation; this is possibly related to the incorporation of oxygen into the samples (Table 4). Moreover, this may also explain why the UV-F and SEC results indicate the presence of larger molecules than could be observed by LD-MS, and why fragment ions were mainly observed. In addition, as $T_{20C\text{-}6m\text{-}L}$ was exposed to indirect sunlight the sample has probably undergone photo-oxidation reactions during ageing; this could be related to the observation outlined above.

Of the three techniques UV-F provided the clearest evidence for their being different molecules present in the F3b PC fraction of $T_{N2\text{-}0h}$ and $T_{20C\text{-}6m\text{-}L}$ (not present in $T_{5C\text{-}6m}$). There was a surprising range of diversity in extents of conjugation and mass range for the two samples. It is possible that the bright green fluorescence observed from this material, when observed under UV for both $T_{N2\text{-}0h}$ and $T_{20C\text{-}6m\text{-}L}$, was from a single type of chromophore that is common to different molecules in the two samples.

Comparing fractions F3b and F4b shows that F3b appears to contain higher mass materials, on average; however, the higher mass molecules were not stable toward laser ionisation. Both fractions F3b and F4b predominantly contain 5 aromatic ring equivalent

chromophores however, F3b contains chromophores that were more conjugated, on average.

Table S7.3, Summary of SEC and LD-MS mass estimates, and UV-F results for PC fraction F3b from $T_{N2\text{-}0h}$ and $T_{20C\text{-}6m\text{-}L}$

F3b	Definition	Units	$T_{N2\text{-}0h}$	$T_{20C\text{-}6m\text{-}L}$
LD-MS	Peak Max. Upper mass	m/z	<200 400	<200 750
SEC	Peak Max.	u	275	460
UV-F	Peak Max., (Ar. Rings[+]) 2nd Peak, (Ar. Rings[+]) 3rd Peak, (Ar. Rings[+])	nm (rings)	400 (5) 370 (4) -	415 (5) 445 (7) 490 (8)

[+] Ar. Rings refers to the equivalent number of conjugated aromatic rings that would fluoresce at the same wavelength, as described in SI Section S6.

PC fractions common to all the samples:

PC fraction F4a (Figures S8.2a-c, SI Section S8)

The analysis of the F4a PC fractions from the three tar samples reveals some common features (Table S7.4). The SEC results were almost identical as were the UV-F spectra; however, LD-MS revealed differences. $T_{N2\text{-}0h}$ and $T_{5C\text{-}6m}$ have similar ion distributions, centred around m/z 250; however, $T_{5C\text{-}6m}$ also contains a significant amount of higher m/z ions, ~650, tailing to m/z ~1500. $T_{20C\text{-}6m\text{-}L}$ shows a main band of ions around m/z

325 and a second band at m/z ~650; these higher mass (m/z) ions were present in lower abundance than seen for $T_{5C\text{-}6m}$.

The highest mass material predicted in $T_{N2\text{-}0h}$ from SEC appears to fragment during LD-MS as few ions were observed with m/z >500. Whereas, in the aged samples a new group of higher mass molecules were detected that were more amenable to LD-MS analysis. UV-F showed that $T_{N2\text{-}0h}$ and $T_{5C\text{-}6m}$ contain molecules with very similar extents of conjugation (5-7 rings); $T_{20C\text{-}6m\text{-}L}$ shows a slight increase in 4 ring chromophores and a decrease in 7 ring equivalents.

The combined information suggests a subtle change in the materials present in PC fraction F4a depending on the storage conditions. This could be interpreted as evidence for changes in structure rather than just a change in mass distribution. The sample stored at room temperature has lost the material that contained the aromatic molecules with the highest degrees of conjugation and the highest mass species as seen in $T_{N2\text{-}0h}$. It is possible that material has reacted with oxygen and/or other tar molecules resulting in it becoming part of another PC fraction or formed precipitate. The lack of oxygen in $T_{5C\text{-}6m}$ (compared to $T_{20C\text{-}6m\text{-}L}$, Table 4) could be related to it containing more low-mass molecules that are not stable towards laser ionization.

Table S7.4, Summary of SEC and LD-MS mass estimates, and UV-F results for PC fraction F4a from $T_{N2\text{-}0h}$, $T_{5C\text{-}6m}$ and $T_{20C\text{-}6m\text{-}L}$

F4a	Definition	Units	$T_{N2\text{-}0h}$	$T_{5C\text{-}6m}$	$T_{20C\text{-}6m\text{-}L}$
LD-MS	Peak Max. Upper mass	m/z	260 500	250 1500	325 1250
SEC	Peak Max. 2nd Peak	u	190 1100	180& 1000&	160 1000
UV-F	Peak Max., (Ar. Rings+) 2nd Peak, (Ar. Rings+) 3rd Peak, (Ar.	nm (rings)	390 (5) 420 (6) 440 (7)	390 (5)& 420 (6)& 440 (7)&	390 (5) 420 (6) 370 (4)

	Rings[+])				

[+] Ar. Rings refers to the equivalent number of conjugated aromatic rings that would fluoresce at the same wavelength, as described in SI Section S6.

[&]Fractions F4a and F3c combined; the samples could not be recovered separately.

PC fraction F3c (Figures S8.3a-c, SI Section S8)

SEC shows all three samples contain molecules with a similar size distribution which is composed mainly of small molecules (~200 u) and a low intensity shoulder, relating to larger molecules (~1000 u). LD-MS reveals a trend towards higher masses (m/z) from $T_{N2\text{-}0h} < T_{5C\text{-}6m} < T_{20C\text{-}6m\text{-}L}$.

UV-F reveals a dramatic difference in the extents of conjugation between the F3c fractions. $T_{N2\text{-}0h}$ contains mainly 7-8 ring equivalent chromophores whereas $T_{5C\text{-}6m}$ and $T_{20C\text{-}6m\text{-}L}$ contain 5-6 ring chromophores (almost identical spectra).

The results reveal that the material present in PC fraction F3c in the aged samples is very different when compared to $T_{N2\text{-}0h}$ (Table S7.5). It seems that in $T_{N2\text{-}0h}$ this PC fraction comprises of small- to medium-sized molecules (200-500 u) that contain highly-conjugated aromatic chromophores (7-8 rings eq.). Upon storage the majority of this material disappears, presumable due to reactions to produce larger-sized molecules with different mobility on the PC plate, or forms precipitate. The material observed in this fraction in the aged samples appears to contain molecules of greater mass and less conjugated chromophores than were present in $T_{N2\text{-}0h}$.

Table S7.5, Summary of SEC and LD-MS mass estimates, and UV-F results for PC fraction F3c from $T_{N2\text{-}0h}$, $T_{5C\text{-}6m}$ and $T_{20C\text{-}6m\text{-}L}$

F3c	Definition	Units	$T_{N2\text{-}0h}$	$T_{5C\text{-}6m}$	$T_{20C\text{-}6m\text{-}L}$
LD-MS	Peak Max.	m/z	275	330	350
	Upper mass		550	1100	1100
SEC	Peak Max.	u	220	180[&]	180
	2nd Peak		900	1000[&]	1000
UV-F	Peak Max., (Ar. Rings[+])	nm (rings)	440 (7)	390 (5)[&]	390 (5)
	2nd Peak, (Ar. Rings[+])		460 (8)	420 (6)[&]	420 (6)
	3rd Peak, (Ar. Rings[+])		410 (6)	440 (7)[&]	440 (7)

[+] Ar. Rings refers to the equivalent number of conjugated aromatic rings that would fluoresce at the same wavelength, as described in SI Section S6.

[&]Fractions F4a and F3c combined; the samples could not be recovered separately.

PC fraction F2 (Figures S8.5a-c, SI Section S8)

SEC results show that PC fraction F2 from $T_{N2\text{-}0h}$ and $T_{5C\text{-}6m}$ have a similar size distribution with a peak maximum at ~200 u and a significant shoulder at ~600 u. In contrast $T_{20C\text{-}6m\text{-}L}$ has a peak max. at ~600 u and more material eluting in the excluded SEC region. Material eluting in the excluded SEC region has previously been shown to be of average mass ~2500 u or greater for similar material [5]; cf. SI S4 for details.

The LD-MS results show a mono distribution for all the tars. $T_{N2\text{-}0h}$ had the lowest average mass (m/z) ~550; the aged samples had roughly the same distribution as one another, with an average m/z of 600-700 and ions tailing off to m/z ~1100. The low mass material (200 u) predicted by SEC for $T_{N2\text{-}0h}$ and $T_{5C\text{-}6m}$ was not observed; this was

probably due to it being lost in the high vacuum of the MS sample chamber. The contradiction between the SEC and LD-MS results for $T_{5C\text{-}6m}$ and $T_{20C\text{-}6m\text{-}L}$ could be evidence of $T_{20C\text{-}6m\text{-}L}$ contain more larger-sized molecules than $T_{5C\text{-}6m}$ but they fragment during LD-MS, hence their mass spectra appear similar.

UV-F shows $T_{N2\text{-}0h}$ contains less-conjugated chromophores (4-5 rings) than $T_{5C\text{-}6m}$ or $T_{20C\text{-}6m\text{-}L}$ which gave identical spectra to one another (5-6 rings).

These results show that the molecules in PC fraction F2 of $T_{N2\text{-}0h}$ are of lower average mass and contain less-conjugated chromophores than the aged samples (Table S7.6). $T_{5C\text{-}6m}$ contains more, low mass molecules than $T_{20C\text{-}6m\text{-}L}$; although, the extents of conjugation were almost identical. This suggests that on going from $T_{N2\text{-}0h}$ to $T_{5C\text{-}6m}$ or $T_{20C\text{-}6m\text{-}L}$ there is a common mechanism which results in chromophores of similar extents of conjugation remaining in F2 (or being formed). For $T_{20C\text{-}6m\text{-}L}$ there appears to be a second process which results in higher molecular mass molecules remaining in F2 (or being produced) which were not stable towards LD-MS analysis, with no additional change in the extent of conjugation. This could be related to the greater abundance of oxygen in $T_{20C\text{-}6m\text{-}L}$ and may be evidence for oxygen bridges between tar molecules resulting in no change in the extent of conjugation which are cleaved relatively easily during LD-MS analysis. This may be related to the possibility of photo-oxidation reactions occurring during storage of tar $T_{20C\text{-}6m\text{-}L}$. However, further work is needed to understand these aspects.

Table S7.6, Summary of SEC and LD-MS mass estimates, and UV-F results for PC fraction F2 from $T_{N2\text{-}0h}$, $T_{5C\text{-}6m}$ and $T_{20C\text{-}6m\text{-}L}$

F2	Definition	Units	$T_{N2\text{-}0h}$	$T_{5C\text{-}6m}$	$T_{20C\text{-}6m\text{-}L}$
LD-MS	Peak Max.	m/z	550	700	600
	Upper mass		1300	1500	1500
SEC	Peak Max.	u	210	200	650
	2nd Peak		650	600	>2000

UV-F	Peak Max., (Ar. Rings+) 2nd Peak, (Ar. Rings+) 3rd Peak, (Ar. Rings+)	nm (rings)	390 (5) 350 (4) 445 (7)	415 (6) 395 (5) 470 (8)	415 (6) 395 (5) 470 (8)

+ Ar. Rings refers to the equivalent number of conjugated aromatic rings that would fluoresce at the same wavelength, as described in SI Section S6.

PC fraction F1 (Figures S8.6a-c, SI Section S8)

The SEC and LD-MS results for PC fraction F1 were generally similar from all the samples. The most significant difference was seen for $T_{N2\text{-}0h}$ which gave very weak signal when analysed by SEC and UV-F. However; this was mainly due to the low abundance of fraction F1 in $T_{N2\text{-}0h}$. It was possible to obtain satisfactory LD-MS results from all the samples. All the F1 samples had similar mass distributions with a peak maximum between m/z 600-750, and ions tailing off to around m/z 2000, with a shift towards higher masses in the aged tars. All the samples showed a SEC chromatogram with a peak max. in the excluded region (<15 minutes, >2500 average mass) with some material also eluting in the retained region (15-25 minutes). Considering the limitations of SEC and LD-MS derived mass estimates (cf. SI S4 and S5) these results show good consistency.

UV-F revealed the largest differences between the F1 samples. $T_{N2\text{-}0h}$ gave a very low intensity spectrum; however, the signal that could be detected had a similar profile as $T_{20C\text{-}6m\text{-}L}$ (4-6 ring eq.). On the other hand, $T_{5C\text{-}6m}$ showed a very different spectrum with chromophores of 6-10 aromatic rings equivalent, on average.

The results from the immobile fraction (F1) show there was a low abundance of this material in the fresh tar and it was composed of high mass molecules (>500 u average mass) with chromophores equivalent to 4-6 rings. $T_{5C\text{-}6m}$ had a much greater abundance of this material; it was also structurally very different to the equivalent from $T_{N2\text{-}0h}$, or $T_{20C\text{-}6m\text{-}L}$, despite having a similar molecular size and mass distribution. The molecules in

$T_{5C\text{-}6m}$ contain aromatic molecules with significantly higher degrees of conjugation than any of the other tars or PC fractions (Table S7.7, Figures S9.1c, S9.2c and S9.3C).

The differences outlined above are possibly related to the different oxygen contents of the samples, where $T_{5C\text{-}6m}$ had less than the fresh tar or $T_{20C\text{-}6m\text{-}L}$ (Table 4). The implications of these findings are discussed further in the manuscript (Section 3.5).

Table S7.7, Summary of SEC and LD-MS mass estimates, and UV-F results for PC fraction F1 from $T_{N2\text{-}0h}$, $T_{5C\text{-}6m}$, and $T_{20C\text{-}6m\text{-}L}$

F1	Definition	Units	$T_{N2\text{-}0h}$	$T_{5C\text{-}6m}$	$T_{20C\text{-}6m\text{-}L}$
LD-MS	Peak Max.	m/z	650	725	725
	Upper mass		2000	2000	1900
SEC	Peak Max.	u	>2500*	>2500	>2500
	2nd Peak		1000*	1300	1100
UV-F	Peak Max., (Ar. Rings+)	nm (rings)	400* (5)	475 (8)	400 (5)
	2nd Peak, (Ar. Rings+)		470* (8)	410 (5-6)	410 (5-6)
	3rd Peak, (Ar. Rings+)		-	535 (10)	460 (7)

+ Ar. Rings refers to the equivalent number of conjugated aromatic rings that would fluoresce at the same wavelength, as described in SI Section S6.

* Very weak signal.

3.8; Figures, by PC fraction (SEC, LD-MS and UV-F)

PC fraction F4b

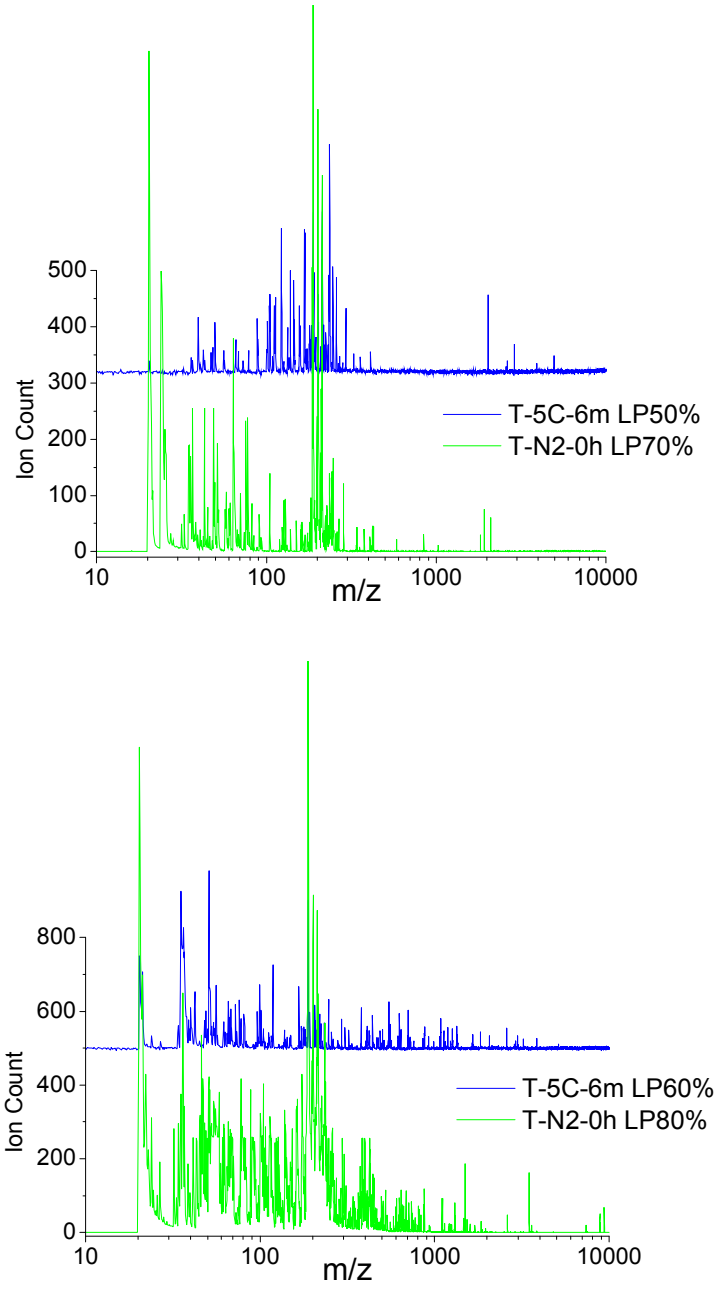

Figure S8.1a, LD-MS spectra of PC fraction F4b at low and high laser power (top and bottom respectively), no DIE, HMA voltage was 10 kV.

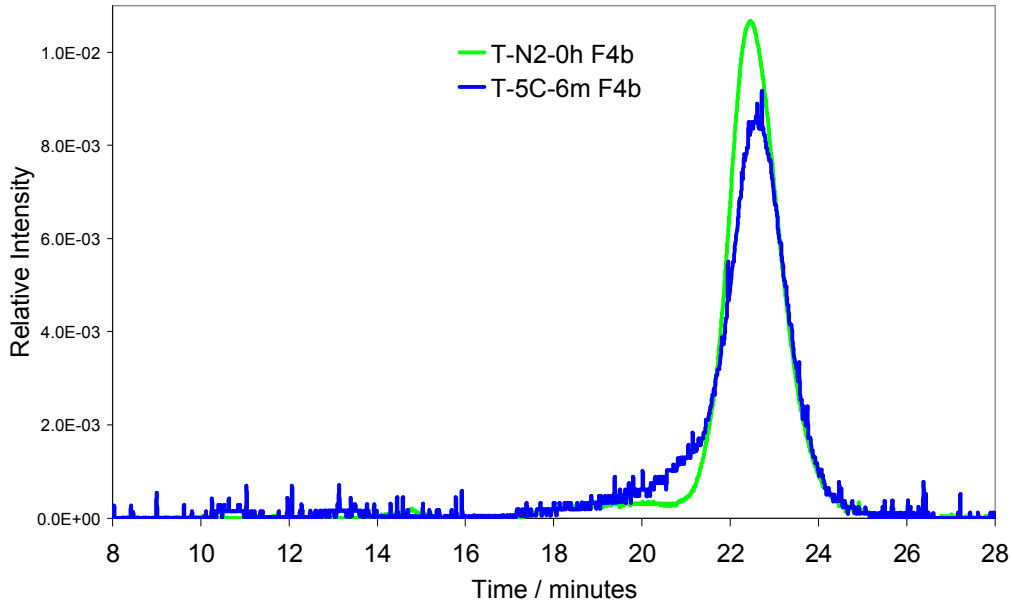

Figure S8.1b, SEC chromatograms (area normalised) of PC fraction F4b at 300 nm.

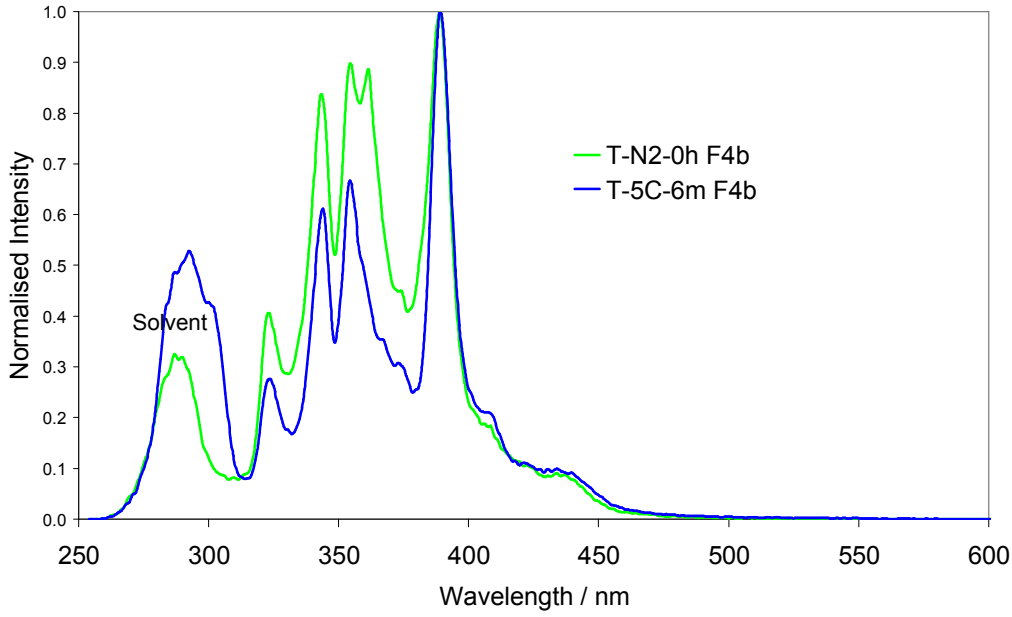

Figure S8.1c, Synchronous UV-F spectra (peak normalised) of PC fraction F4b.

PC fraction F4a

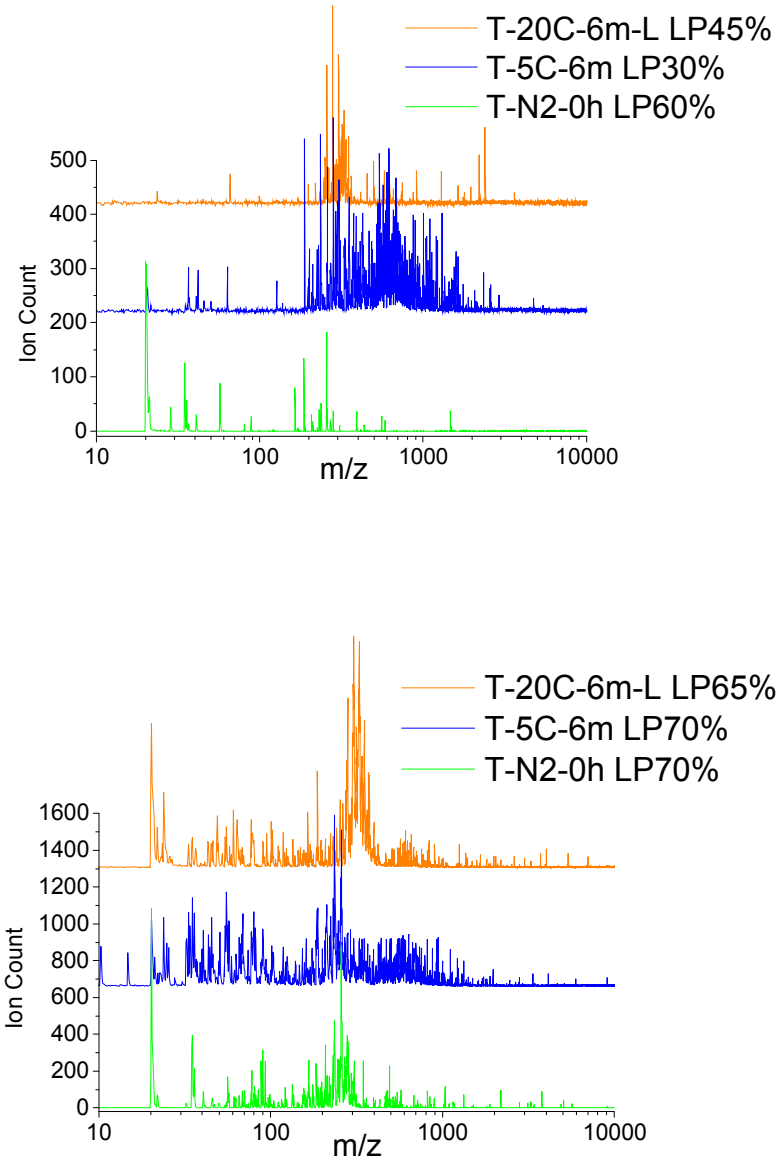

Figure S8.2a, LD-MS spectra of PC fraction F4a at low and high laser power (top and bottom and right respectively), no DIE, HMA voltage 10 kV.

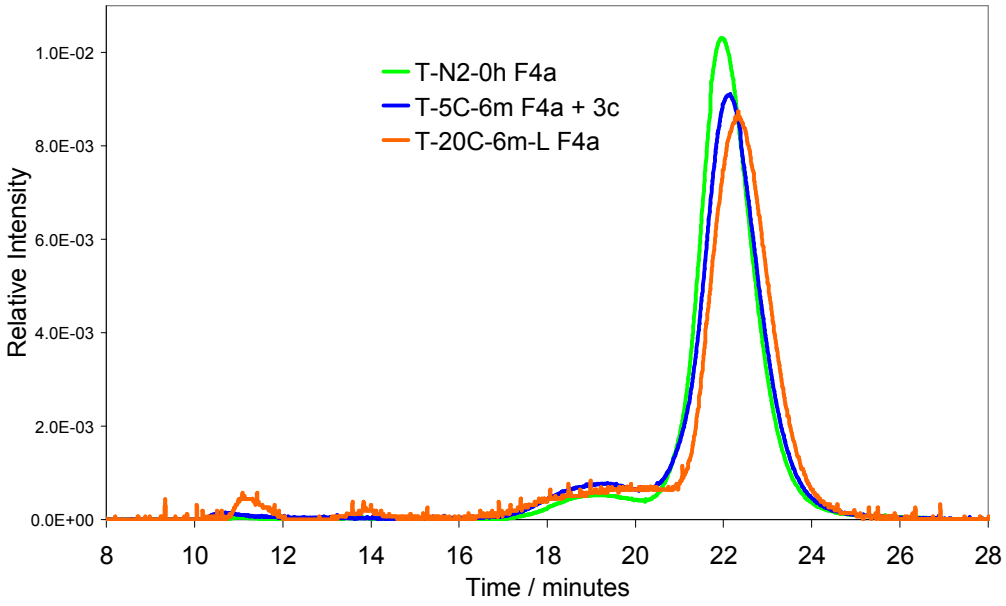

Figure S8.2b, SEC chromatograms (area normalised) of PC fraction F4a at 300 nm.

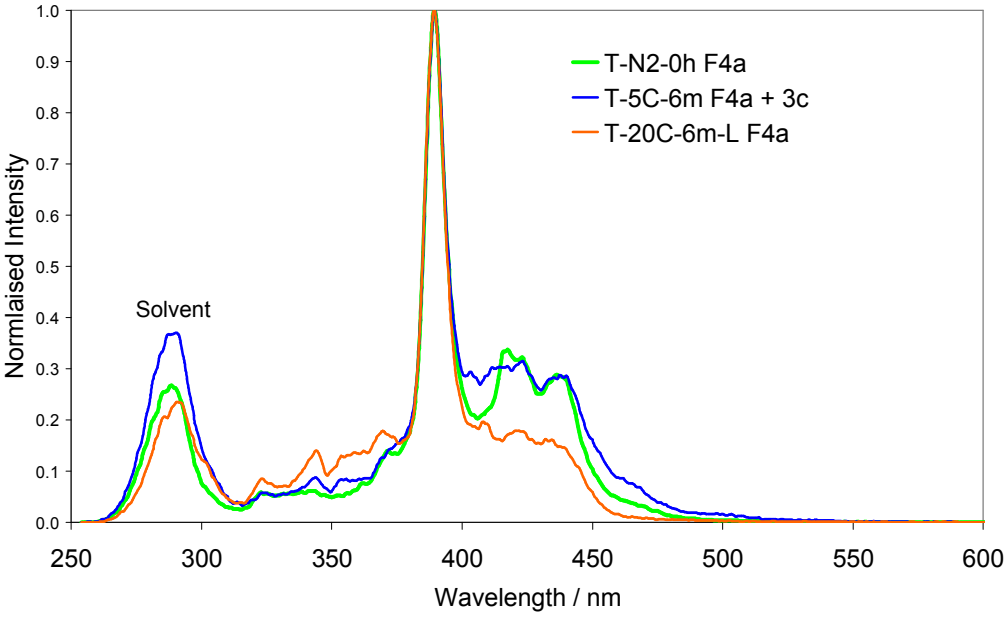

Figure S8.2c, Synchronous UV-F spectra (peak normalised) of PC fraction F4a.

PC fraction F3c

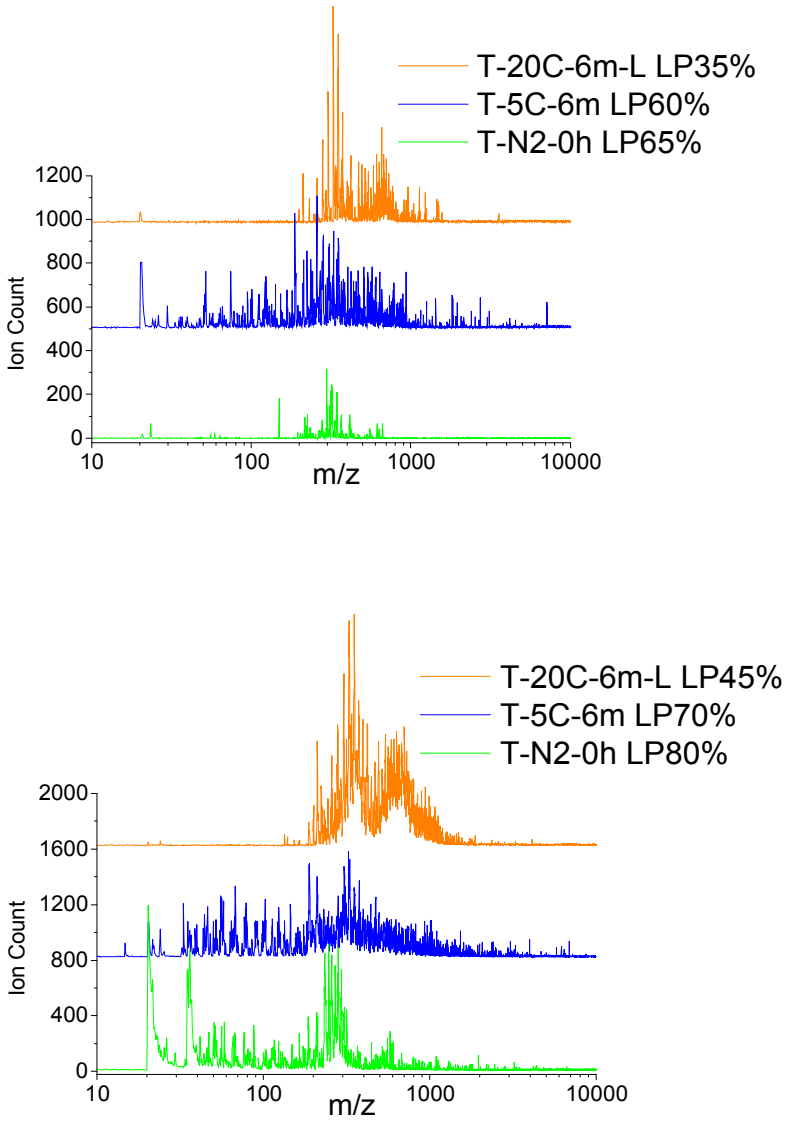

Figure S8.3a, LD-MS spectra of PC fraction F3c at low and high laser power (top and bottom respectively), no DIE, HMA voltage was 10 kV.

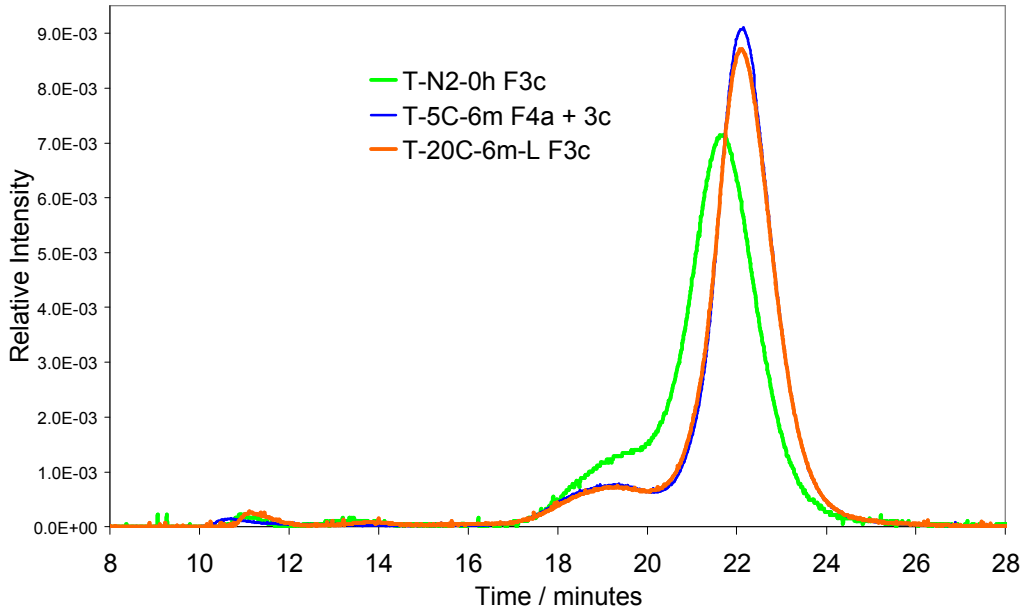

Figure S8.3b, SEC chromatograms (area normalised) of PC fraction F3c at 300 nm.

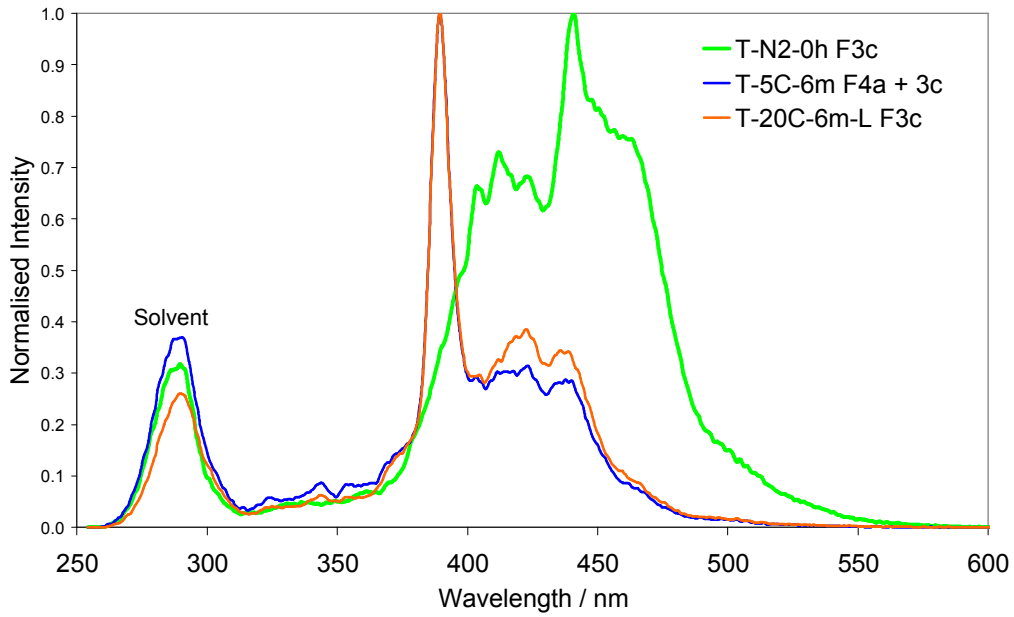

Figure S8.3c, Synchronous UV-F spectra (peak normalised) of PC fraction F3c.

PC fraction F3b

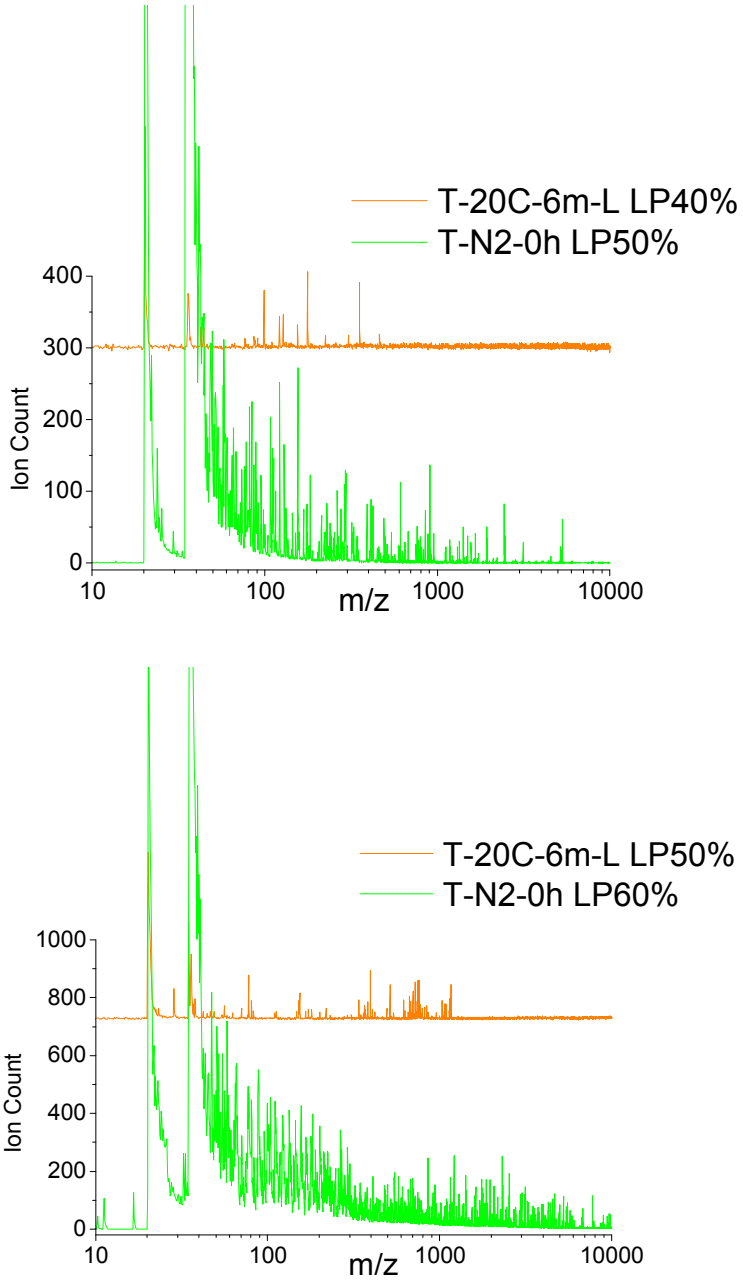

Figure S8.4a, LD-MS spectra of PC fraction F3b at low and high laser power (top and bottom respectively), no DIE, HMA voltage was 10 kV.

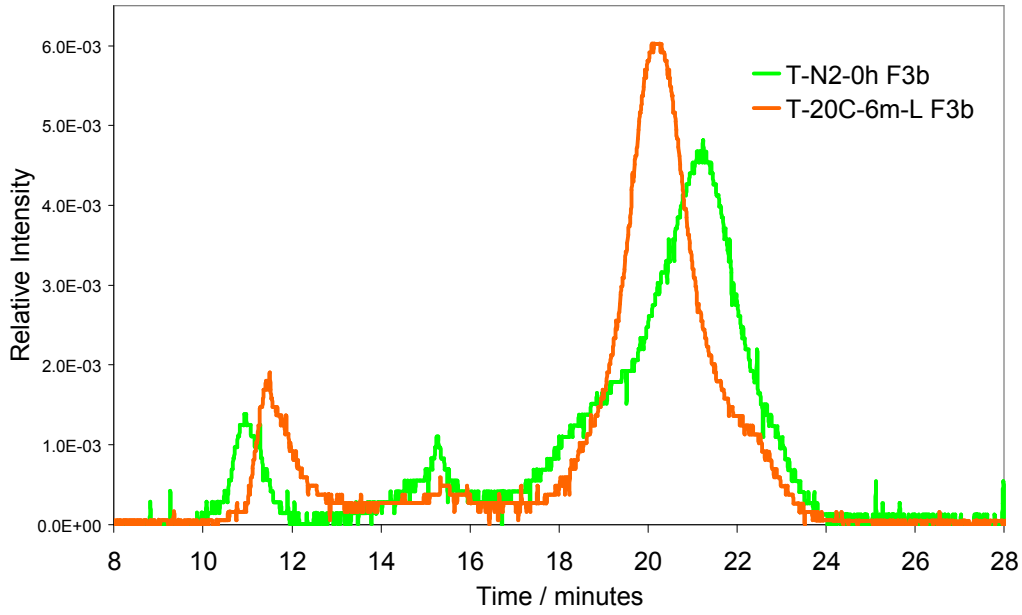

Figure S8.4b, SEC chromatograms (area normalised) of PC fraction F3b at 300 nm.

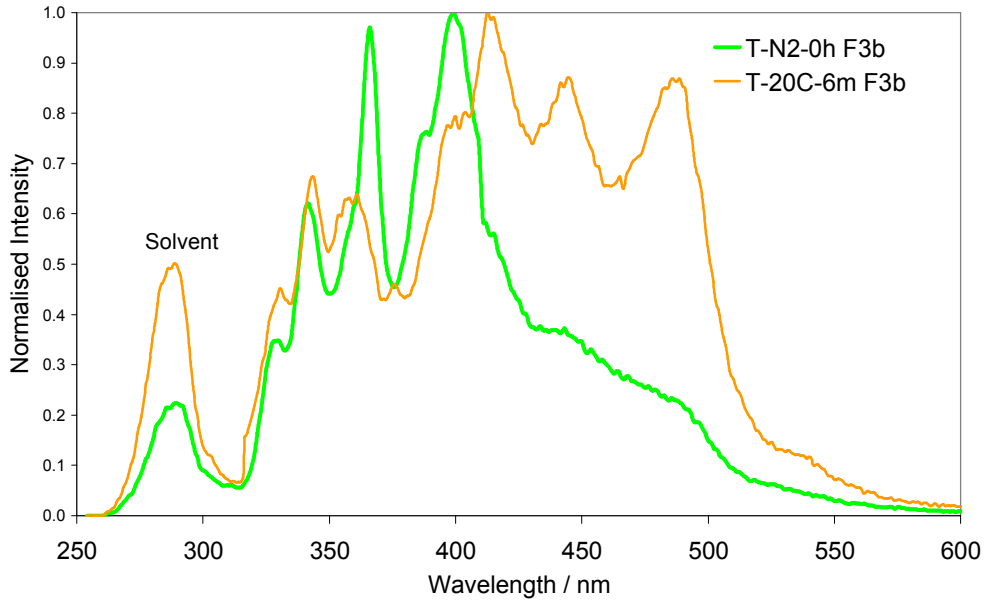

Figure S8.4c, Synchronous UV-F spectra (peak normalised) of PC fraction F3b.

PC fraction F3a (not shown as only present in $T_{N2\text{-}0h}$, see Figures S9.1a-c)

PC fraction F2

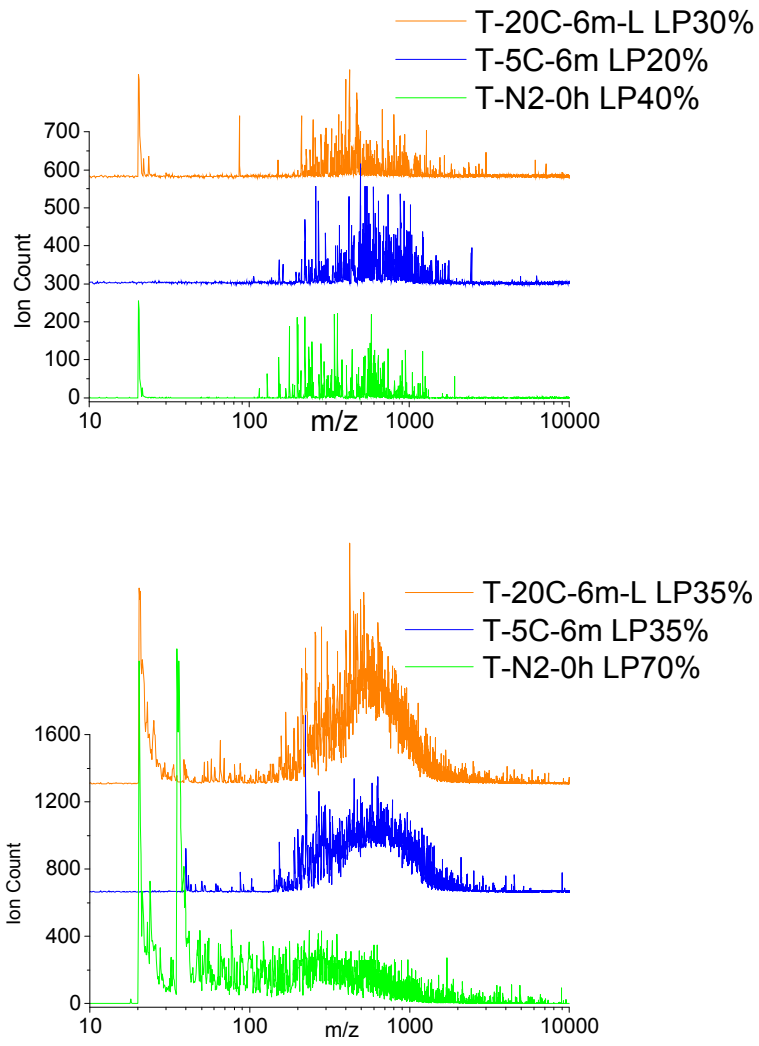

Figure S8.5a, LD-MS spectra of PC fraction F2 at low and high laser power (top and bottom respectively), no DIE, HMA voltage was 10 kV.

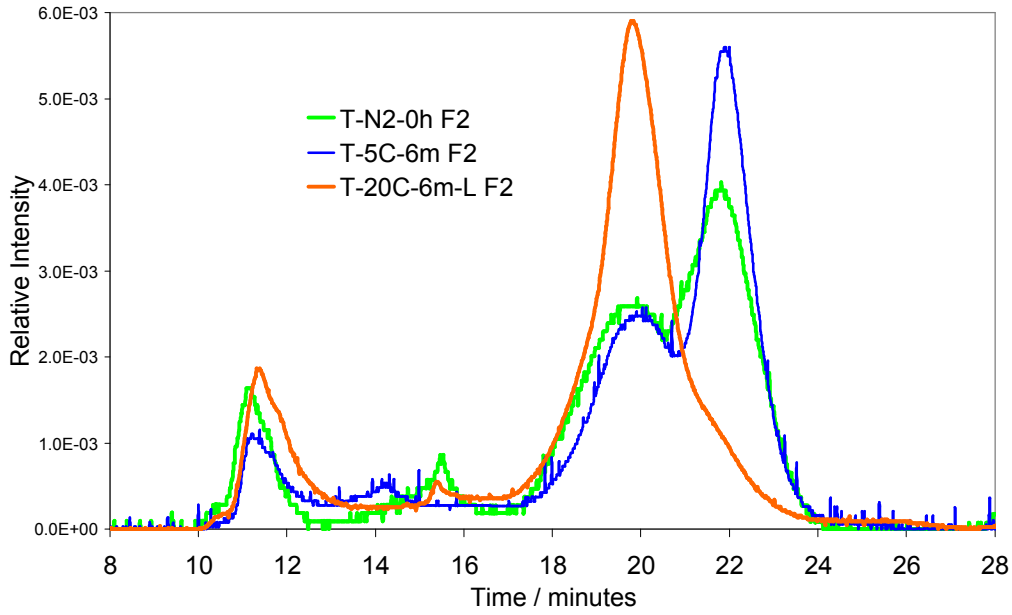

Figure S8.5b, SEC chromatograms (area normalised) of PC fraction F2 at 300 nm.

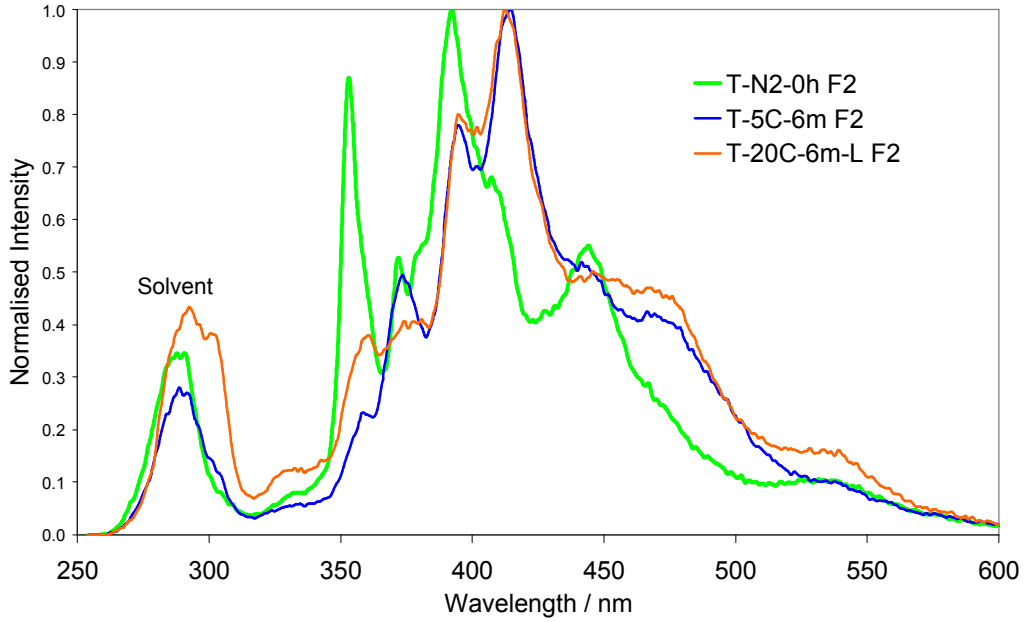

Figure S8.5c, Synchronous UV-F spectra (peak normalised) of PC fraction F2.

PC fraction F1

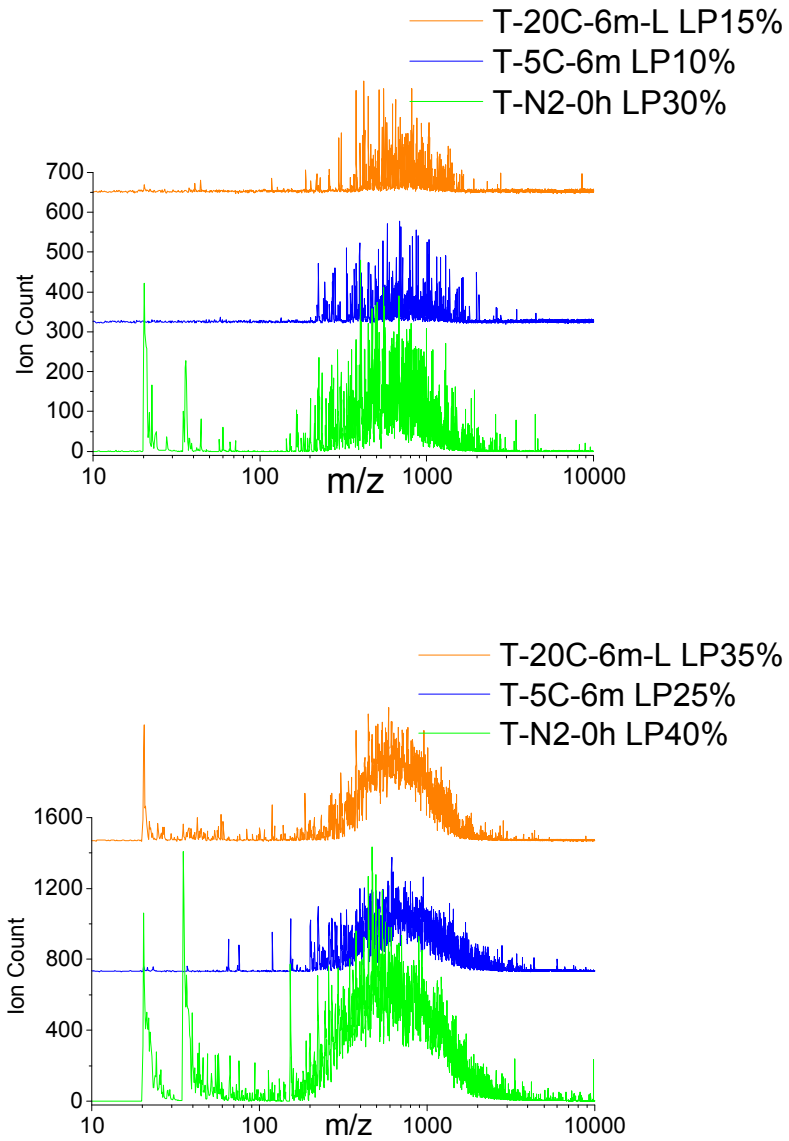

Figure S8.6a, LD-MS spectra of PC fraction F1 at low and high laser power (left and right respectively), no DIE, HMA voltage was 10 kV.

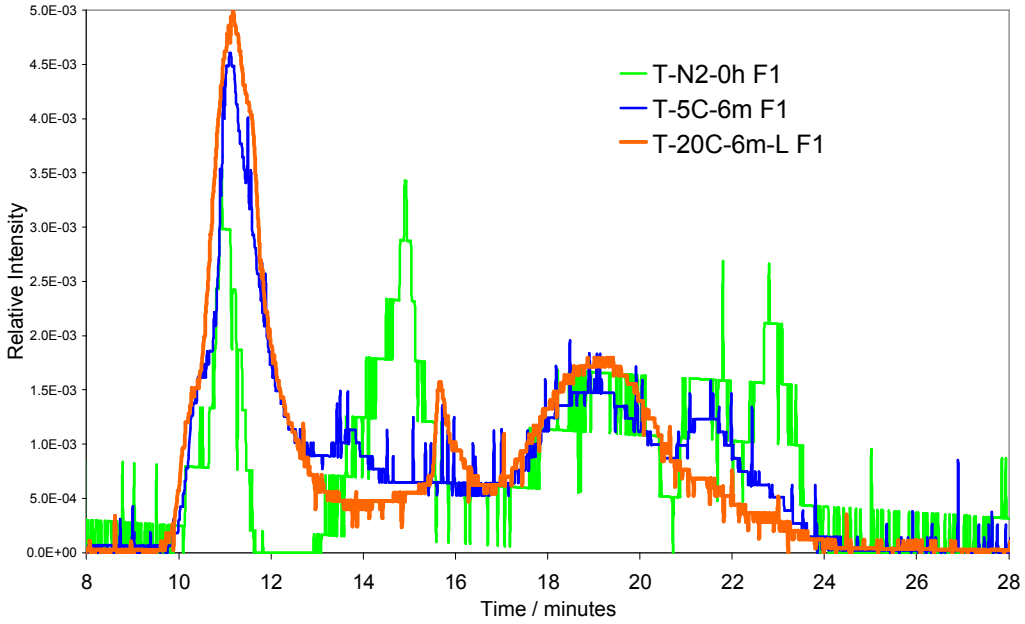

Figure S8.6b, SEC chromatograms (area normalised) of PC fraction F1 at 300 nm; for $T_{N2\text{-}0h}$ there was weak signal due to low abundance.

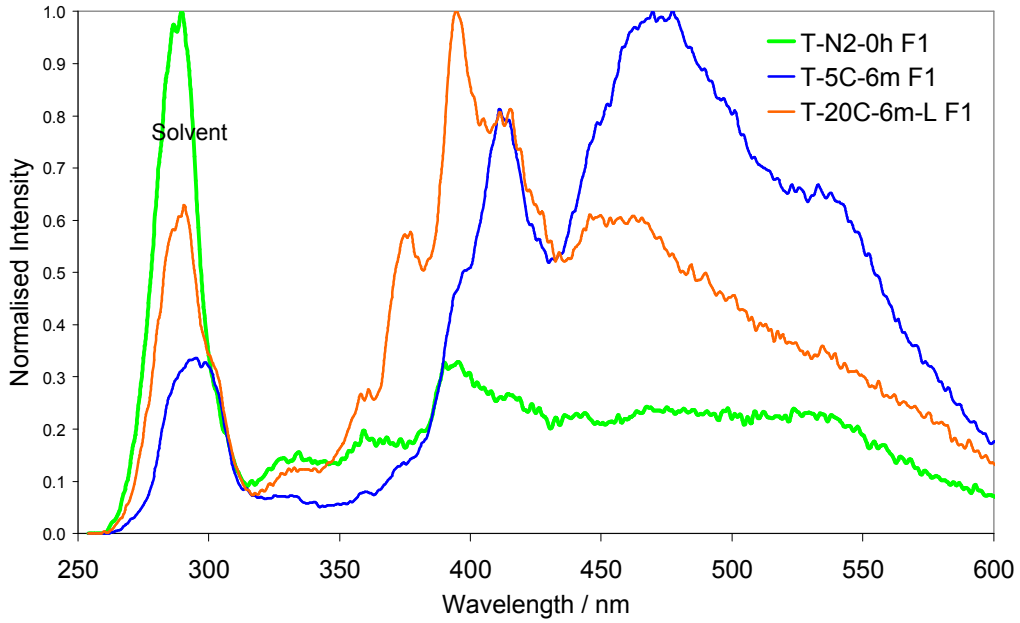

Figure S8.6c, Synchronous UV-F spectra (peak normalised) of PC fraction F1; for $T_{N2\text{-}0h}$ there was weak signal due to sample low abundance

S3.9; Figures, by sample (SEC, LD-MS and UV-F of the PC fractions)

Tar Sample $T_{N2\text{-}0h}$

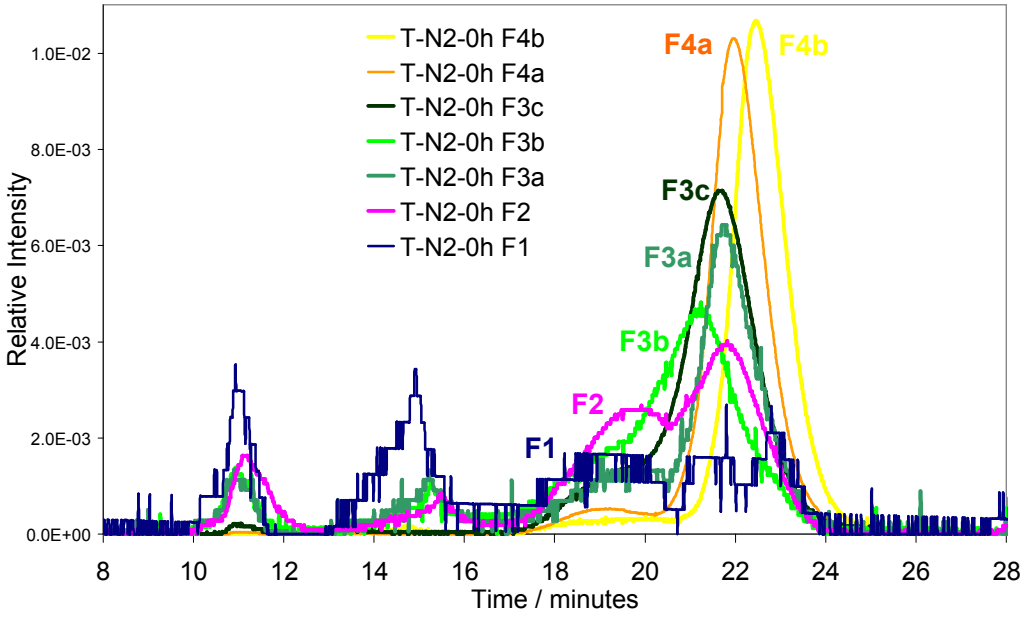

Figure S9.1a, SEC chromatograms (area normalised) of PC fractions from $T_{N2\text{-}0h}$, at 300nm.

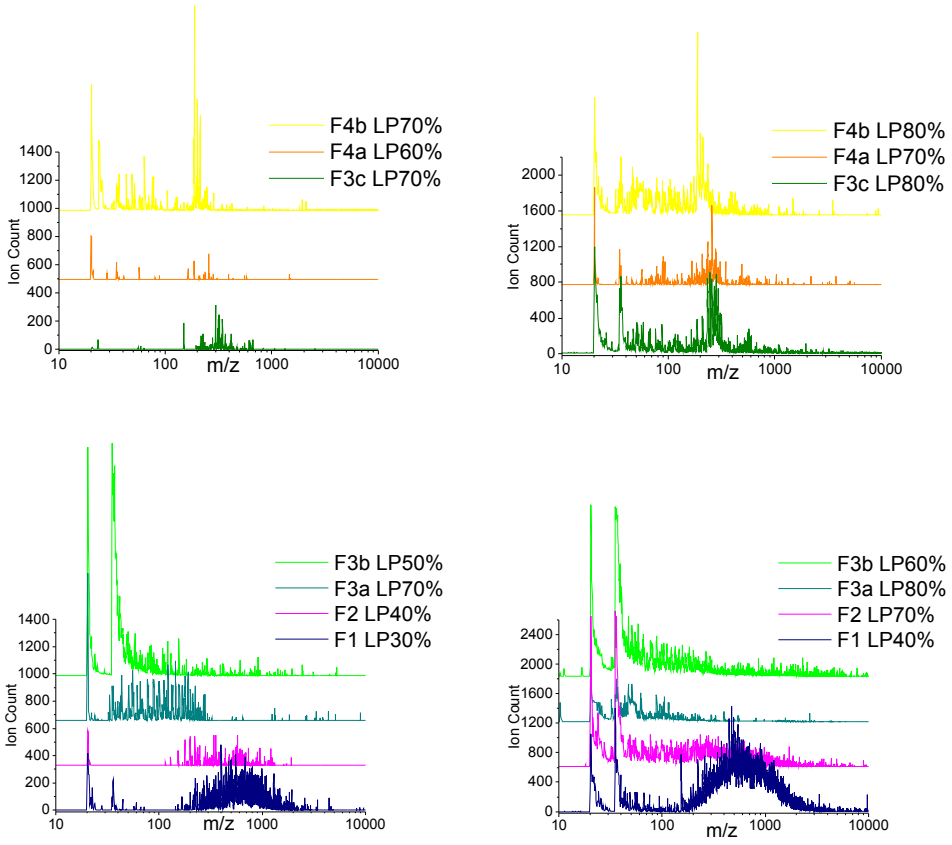

Figure S9.1b, LD-MS spectra of the PC fractions from $T_{N2\text{-}0h}$ when low and high laser power was used (left and right respectively), no DIE, HMA voltage was 10 kV.

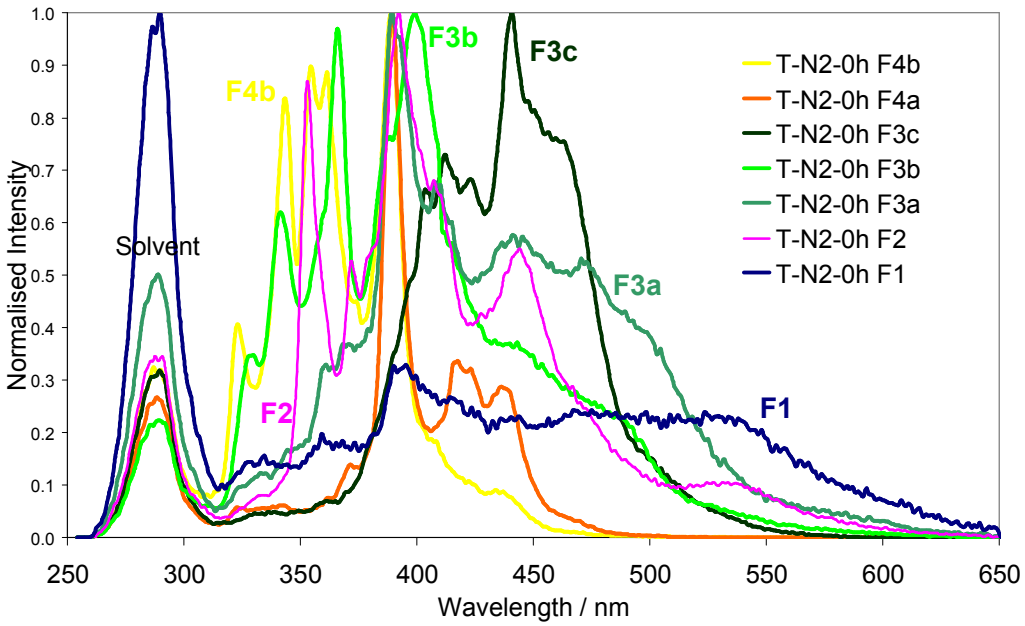

Figure S9.1c, Synchronous UV-F spectra (peak normalised) of the PC fractions from $T_{N2\text{-}0h}$.

Tar Sample $T_{5C\text{-}6m}$

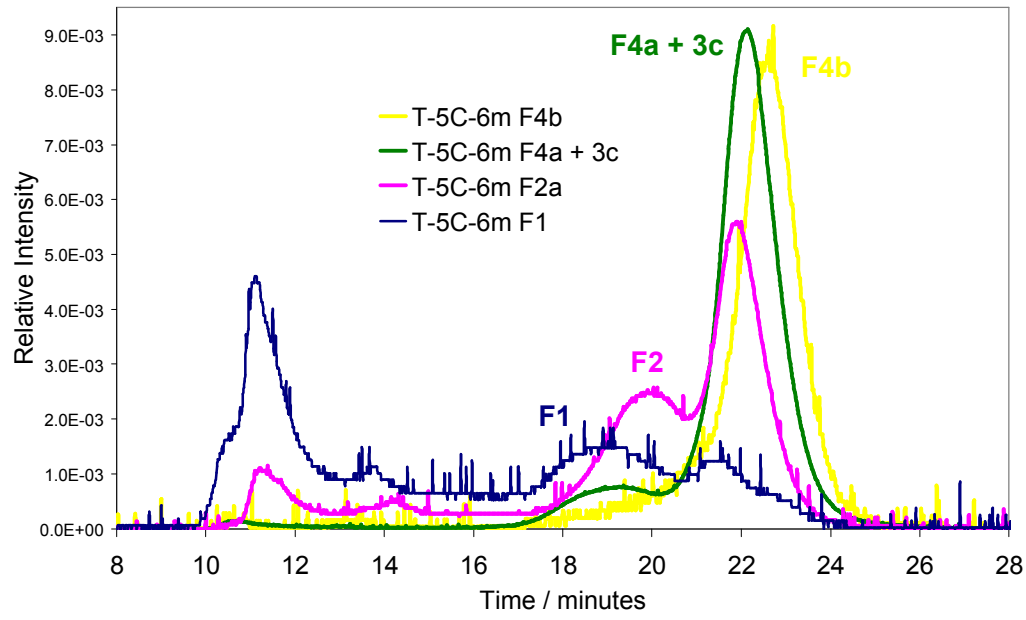

Figure S9.2a, SEC chromatograms (area normalised) of PC fractions from $T_{5C\text{-}6m}$, at 300nm.

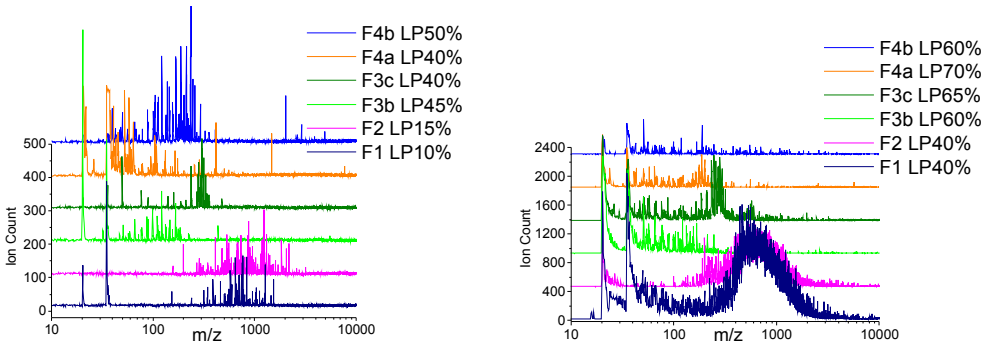

Figure S9.2b, LD-MS spectra of the PC fractions from $T_{5C\text{-}6m}$ when low and high laser power was used (left and right respectively), no DIE, HMA voltage was 10 kV.

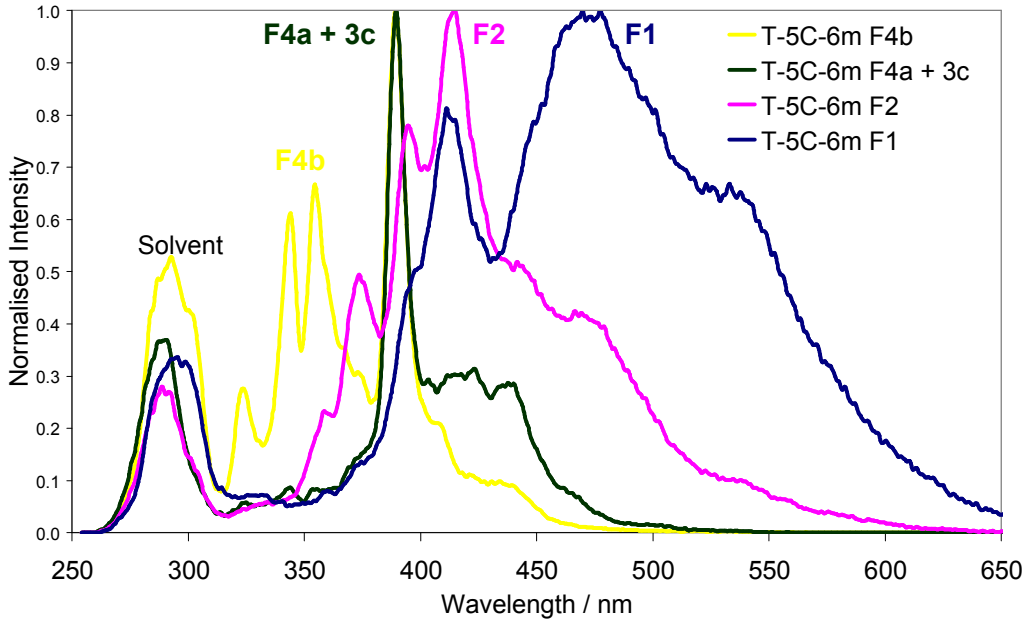

Figure S9.2c, Synchronous UV-F spectra (peak normalised) of the PC fractions from $T_{5C\text{-}6m}$.

Tar Sample $T_{20C\text{-}6m\text{-}L}$

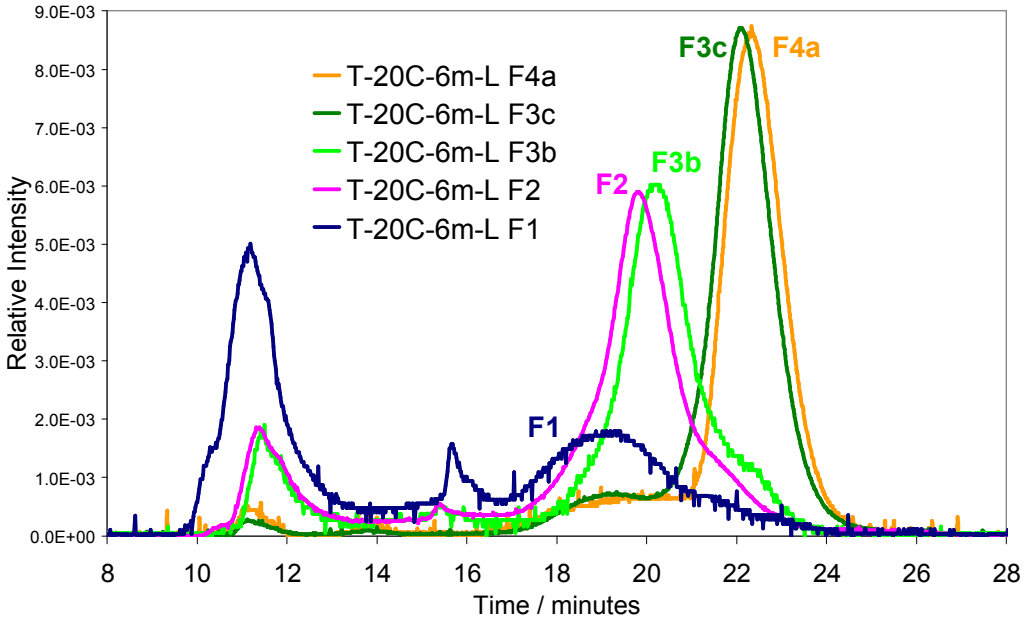

Figure S9.3a, SEC chromatograms (area normalised) of PC fractions from $T_{20C\text{-}6m\text{-}L}$, at 300nm.

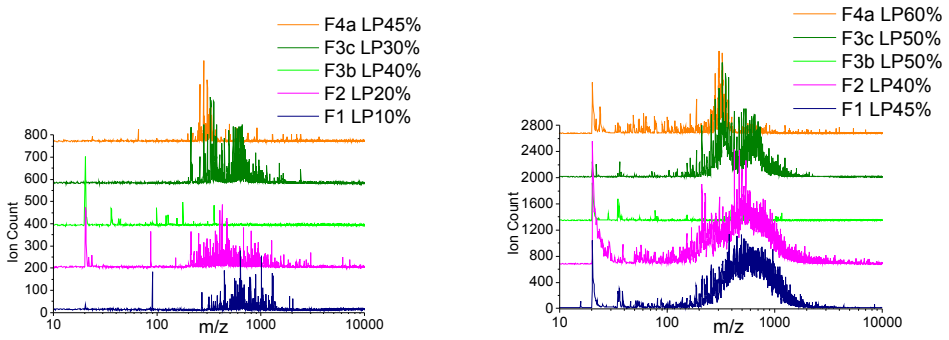

Figure S9.3b, LD-MS spectra of the PC fractions from $T_{20C\text{-}6m\text{-}L}$ when low and high laser power was used (left and right respectively), no DIE, HMA voltage was 10 kV. Note, it was very difficult to obtain a spectrum from F3.

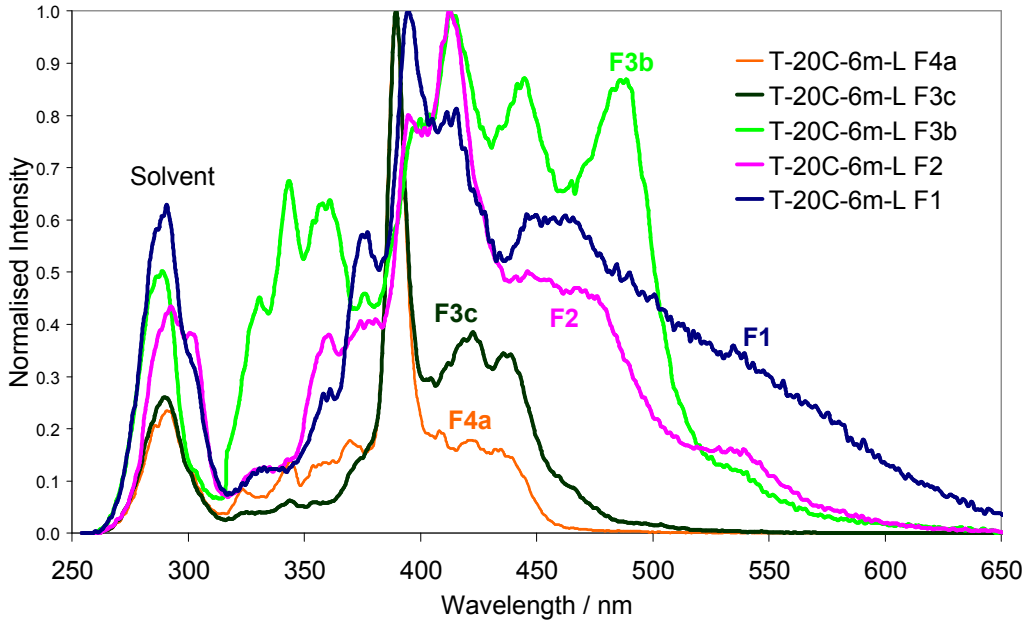

Figure S9.3c, Synchronous UV-F spectra (peak normalised) of the PC fractions from $T_{20C\text{-}6m\text{-}L}$.

S3.10; Figures, LD-MS of the bulk tars

Examples of the influence of the laser power strength and use of different DIE times, on the LD-MS spectra obtained from the bulk tar T5C-6 m are shown in Figures S10.1 – S10.2.

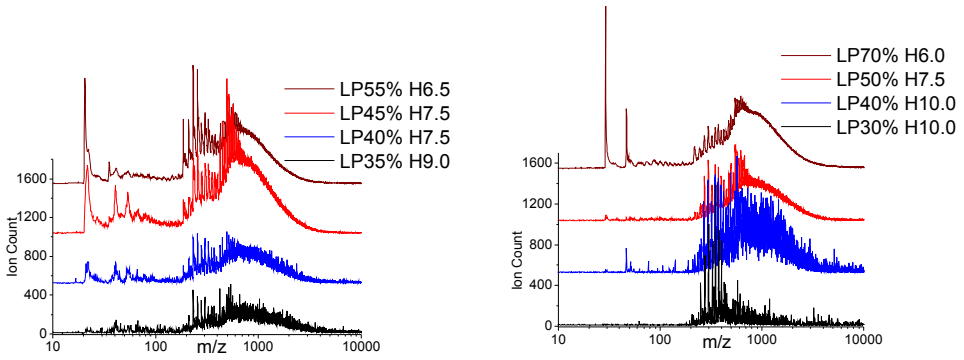

Figure S10.1, LD-MS spectra of the bulk $T_{5C\text{-}6m}$ when zero and 600 ns DIE time were used (left and right respectively); laser power strength and HMA voltage (kV) are given in the legend.

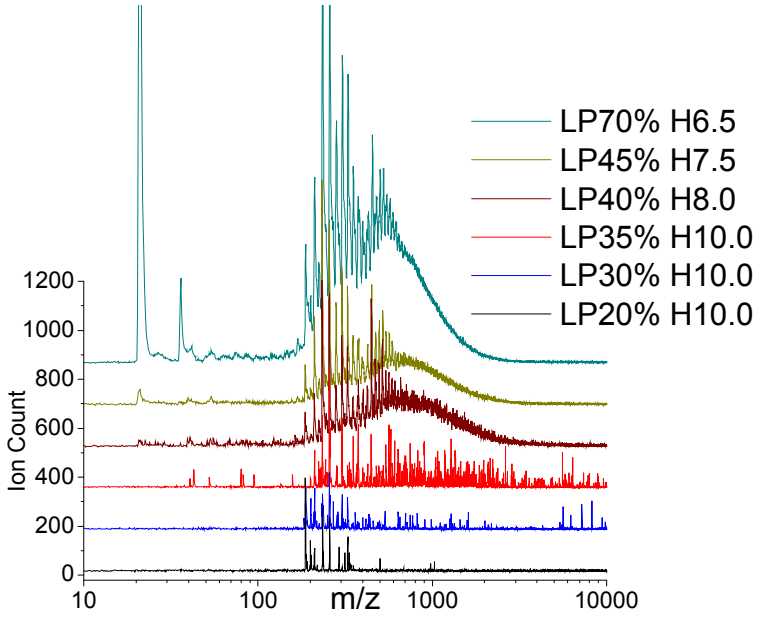

Figure S10.2, LD-MS spectra of the bulk tar $T_{20C\text{-}6m\text{-}L}$ when zero DIE time was used, showing the influence of laser power strength and HMA voltage (kV) on the spectrum; laser power and HMA are given in the legend.

4.0 Pyrolysis of biomass residues from transgenic plant material

In models of future bio-refineries it is deemed that use of genetically modified plants that are easier to degrade by enzymes will be beneficial. The residues from these bio refineries will need to be utilized and thermochemical conversion is considered one of the most technically advanced methods by which to achieve valorization of these residues. Recently significant advances have been made in modifying biomass composition in planta. This includes manipulating the type, amount and degree of polymerization of lignin, which causes many of the pyrolysis problems associated with the thermochemical conversion of biomass. The possibility exists to remove some or all of these R&D challenges by conducting pyrolysis experiments on the genetically modified plants and understanding how these modifications affect pyrolysis behavior. Theoretically, for example, reducing the lignin content in plants should reduce the final char content and quality, and enhance the yields of the lighter components in the bio-oil. Investigations need to be carried out to ascertain the effects of altering the biomass composition in the lignin.

The Joint BioEnergy Institute (JBEI) has developed plants which contain less lignin and lignin of a smaller degree of polymerization as well as lignin of a different composition. We propose to conduct pyrolysis on these plants and ascertain how modifications in the plant affect fundamental pyrolysis behavior. In this part of the study we aimed to understand the differences in the proportion of char, tar and gas produced by the genetically modified plants versus the wild type, and also to understand differences in the composition of the bio-oil, and char reactivity as a function of the genetic modification.

4.1 Transgenic lignin samples

Two samples sets have thus far been investigated, from plants engineered at JBEI. The first set used an alternative strategy to reduce lignin recalcitrance. A dominant approach was developed that diverts precursors from the lignin pathway and enhances production of C_6C_1 aromatics that are known as non-conventional lignin monomers after export to the apoplast. Compared with regular C_6C_3 monolignols, these C_6C_1 monomers have reduced polymerization properties as they lack propanoid side-chain and its conjugated double bond, disabling them from undergoing condensation at their b-

position. We also demonstrated that C_6C_1 monomers accumulate as end-groups in the lignin of FCA transgenics, resulting in reduced lignin DP and cell walls less recalcitrant to enzymatic hydrolysis. The reduced degree of polymerization is shown for the cellulolytic enzymatic lignin (CEL) of Arabidopsis plants in Figure 4.1a and b below. Due to the lack of calibrations standards for lignin and difficulty in understanding precise lignin structure polydispersity values are always relative rather than absolute. Nevertheless a reduced degree of polymerization was shown in the samples below.

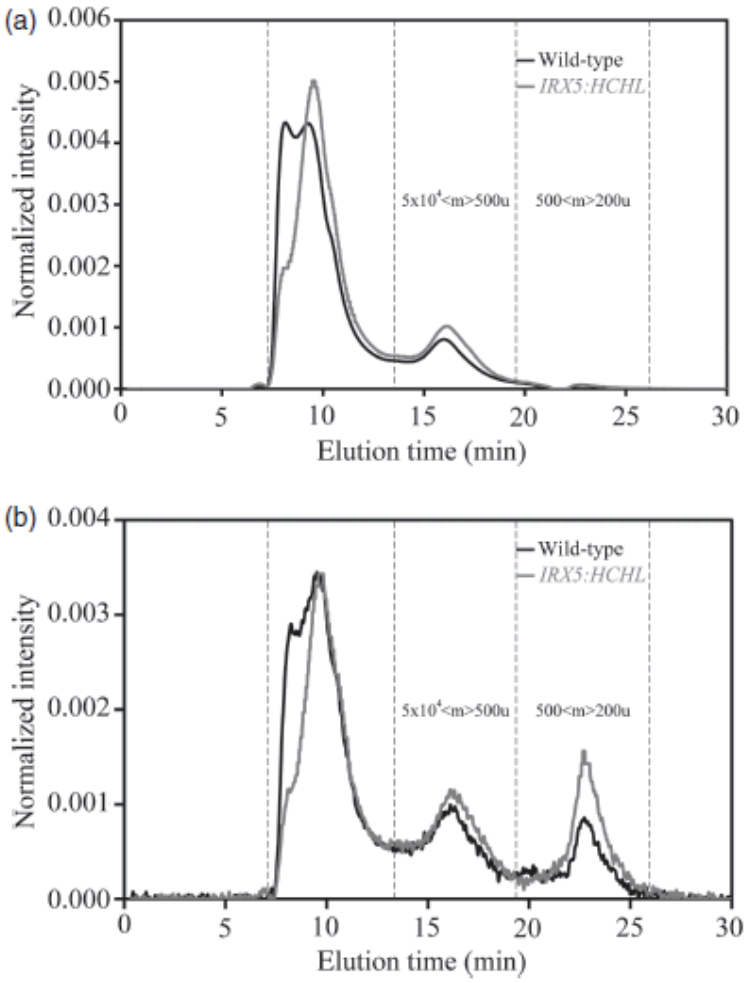

Figure 4. Polydispersity of cellulolytic enzymatic lignin (CEL) in the wild type (solid black line) FCA transgenics (grey line) as analysed by size exclusion chromatography using UV absorbance detection (Figure 4a) and UV fluorescence detection (b).

The second set of samples, so called Qsub samples, were developed to have a reduced lignin content, rather than a reduced degree of polymerization. Two new samples were created to have 11% and 7% lignin compared to 19% lignin in the wild type.

4.2 Reactor configuration for pyrolysis of transgenic lignin plants

Transgenic plants were available in very small quantities (100's mg), therefore it was deemed the most appropriate reactor to analyses these samples was the atmospheric pressure wire-mess, available at the laboratories of our collaborators at Imperial College London. The reactor is shown in Figure 4.2. The design and principle of wire-mesh reactors is described in detail elsewhere. The basic design concept of these instruments is straightforward. Milligram quantities of sample particles are placed between two layers of folded wire-mesh. This assembly is weighed and stretched between two electrodes. Fine wire thermocouples are attached. A controlled current is then passed through the mesh, which also serves as a resistance heater. After the sample has been exposed to a pre-programmed time-temperature profile, the weight change of the assembly is determined. Depending on the purpose of the experiment, volatiles and/or tars may be recovered and characterised. This reactor configuration allows experiments to be carried out using wide ranges of heating rates (1 – 20,000 °C s-1), temperatures (to 2,000 °C) and pressures (to 160 bar). This reactor configuration provides the currently most optimized method by which to pyrolyse small quantities of transgenic plants and their lignin to understand small changes in pyrolysis behavior which might occur.

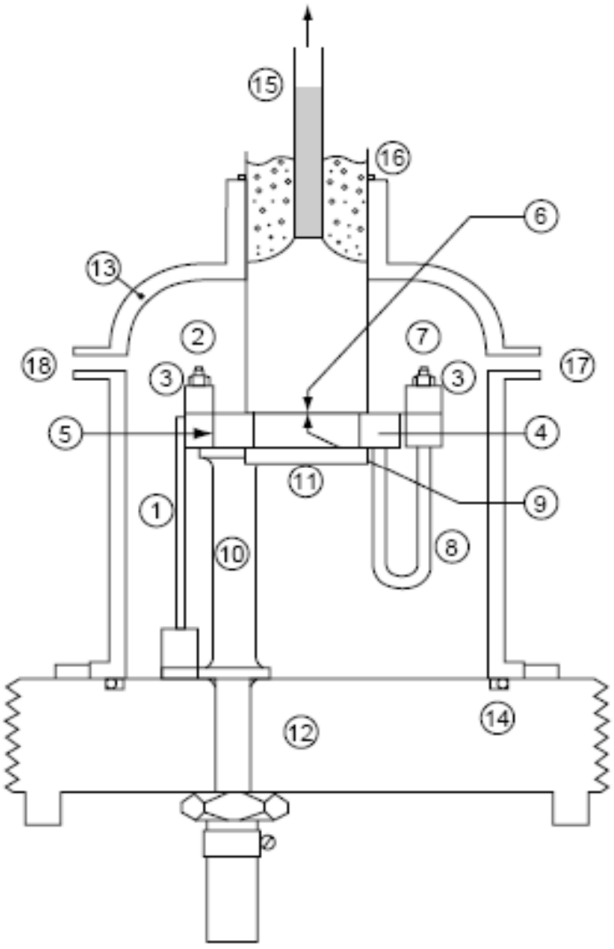

Figure 4.1 The atmospheric pressure wire-mesh reactor with tar trap, maximum heating rate 10,000 °Cs^{-1}, batch. Legend: [1] Copper Current Carrier; [2] Live Electrode; [3] Brass Clamping Bar; [4] Sample Holder Support Plate; [5] Mica Strip; [6] Wire-mesh Sample Holder; [7] Electrode; [8] Stainless Steel Tubes; [9] Mica Layer; [10] Brass Pillars; [11] Sintered Pyrex Glass Disk; [12] Base Plate; [13] Pyrex Bell; [14] O-ring Seal; [15] Off-take Column; [16] O-ring; [17] Carrier Gas Entry Port; [18] Connection for Vacuum Pump.

4.3 Pyrolysis of Arabidopsis samples with reduced degree of polymerization (FCA)

The pyrolysis of two samples FCA and the corresponding wild type (WT) was carried out in the atmospheric wire mesh reactor at a peak temperature of 400 °C, 5s of holding time and a heating rate of 1000 °C/s. These operating conditions were selected with the aim of observing clear differences between the samples due to incomplete pyrolysis. Before being used, the two samples were crushed and sieved between 106 and 150 μm and

dried overnight. The nomenclature FCA3 and WT3 is given as three separate samples were used.

Table 2 shows the product yields obtained from the pyrolysis of both samples. Duplicate experiments were carried out for each data point. FCA3 yielded slightly larger amount of char than WT3. FCA3 has an increased level of condensation (C-C bonds) which explains the increased char yield. On the other hand, FCA3 gave rise to less tar yield than WT3. Tar proportion in within the total volatile fraction also diminished in the case of FCA3 compared to that in the case of WT3.

Table 4.1. Experimental conditions and product yields from Wire Mesh Reactor experiments of biomass with reduced degree of polymerization and its corresponding wildtype. Heating rate – 1,000 ^{o}C/s, Pressure – 1 bar, Atmosphere - He

Sample	Peak Temperature (^{o}C)	Holding time (s)	Char (wt.%)	Tar (wt.%)	Gas (wt.%)
WT3	400	5	27.8±0.6	37.4±0.2	34.9±0.8
FCA3	400	5	27.1±0.4	34.9±0.1	38.1±0.5

Tars from pyrolysis of WT3 and FCA3 were analysed by gas chromatography (GC) and size exclusion chromatography (SEC).

GC analyses were performed in a Perkin Elmer "Clarus 500" chromatograph with flame ionization detector (FID). The GC was equipped with a non-polar capillary column HT5 (25 m x 0.32 mm and 0.1 μm film thickness). A flow rate of 10 mL/min of He was used as carrier gas with a split ratio of 5.4:1. The initial oven temperature was 40 ^{o}C, which was held for 1.0 min. It was then programmed to rise to 380 ^{o}C at 10 ^{o}C/min with an isotherm held for 10 min. The programmed temperature injector was ramped from 80 ^{o}C (held for 0.5 min) to 380 ^{o}C at 100 ^{o}C/min. The flame was maintained with H_2 flow rate of 45 mL/min and air flow rate of 450 mL/min. Calibrations with a set of n-alkanes (C8 to C30) and a standard PAH were used to evaluate the percentage of elution of the material.

Figure 1 shows the chromatograms obtained for the analyses of tars from FCA3 and WT3. As can be seen, no significant differences are observed between the two tar samples.

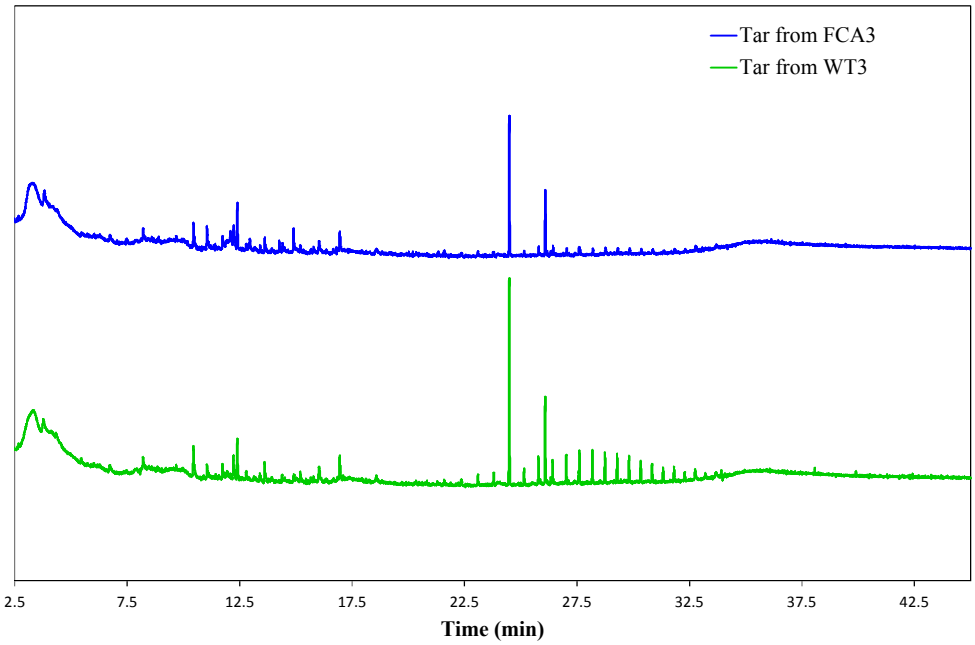

Figure 4.2. GC chromatograms of tars obtained from the pyrolysis of FCA3 and WT3. WMR at 400°C, 5s and 1000°C/s.

In addition, Table 4.2 summarizes the data calculated from the n-alkanes and PAH calibrations. Approximately 80% of the area under the evolved peaks was identified based on the n-alkanes and PAH calibrations. However, the area identified only corresponds to around 1 % of the area expected based on the calibration. In other words, 99% of the injected samples did not evolve through the GC column (material with boiling point higher than 550 °C). This is being investigated futhre.

Table 4.2. Results from GC analyses of tars obtained from the pyrolysis of FCA3 and WT3. WMR at 400°C, 5s and 1000°C/s

Compound	Boiling point (°C)	Tar from WT3 (wt. %)	Tar from FCA3 (wt. %)
Acenaphthylene	280	0.12	0.14
C29	441	0.63	0.47
Benzo(A)Pyrene	496	0.30	0.24
Indeno(1,2,3,CD) Pyrene & Dibenz(A,H)Anthracene	524 & 536	0.09	0.00

Benzo(G,H,I)Perylene	550	0.07	0.00
Percentage identified from the area obtained		74.65	84.58

A 300 mm long, 7.5 mm i.d. polystyrene/polydivinylbenzene-packed Mixed-D column with 5µm particles was used for SEC analyses. The column was operated at 80 °C and a flow rate of 0.5 mL/min. NMP was used as the mobile phase. Detection was carried out using a Knauer Smartline diode array UV-absorbance detector. As NMP is opaque at 254 nm, detection of standard compounds and samples was performed at 300 nm, where NMP is partially transparent.

A calibration of the Mixed-D column was carried out using two sets of standards, polystyrene (PS) and polyaromatic hydrocarbons (PAH). The PS-based calibration is applied to the 11- 20 min time range, while the PAH-based calibration is used in 20-24 min region, resulting in the following calibration equations:

11-20 min region: log10 [MM] = 10.6320 – 0.4038 [elution time (min)]

20-24 min region: log10 [MM] = 6.8495 – 0.2095 [elution time (min)]

Figure 4.3 shows molecular weight distribution by size exclusion chromatography of the tars from the pyrolysis of FCA3 and WT3. In both cases, bimodal distributions of signal are observed. The early eluting peak corresponds to material of molecular size unable to penetrate the porosity of the column packing, and is referred to as “excluded” from the column porosity. The exclusion limit of the column, defined according to the behaviour of polystyrene standards, is about 200,000 u (although molecular conformation is considered to be the factor that causes molecules to become excluded from the column porosity rather than molecular weight). The second eluting peak corresponds to the material able to penetrate the porosity of the column packing.

The two tars show similar molecular weight distributions, with no significant differences between them. Both chromatograms show a lift-off in the baseline around 16.7 min, which corresponds to a polystyrene mass of about 7,740 u. This is considered the upper limit in the molecular weight distribution of these samples. Both tars present a maximum peak at 19.7 min, which corresponds to a polystyrene mass of about 475 u.

Tar from WT3 seems to have a molecular weight distribution slightly shifted to lower values than the tar from FCA3. However, this difference is not significant.

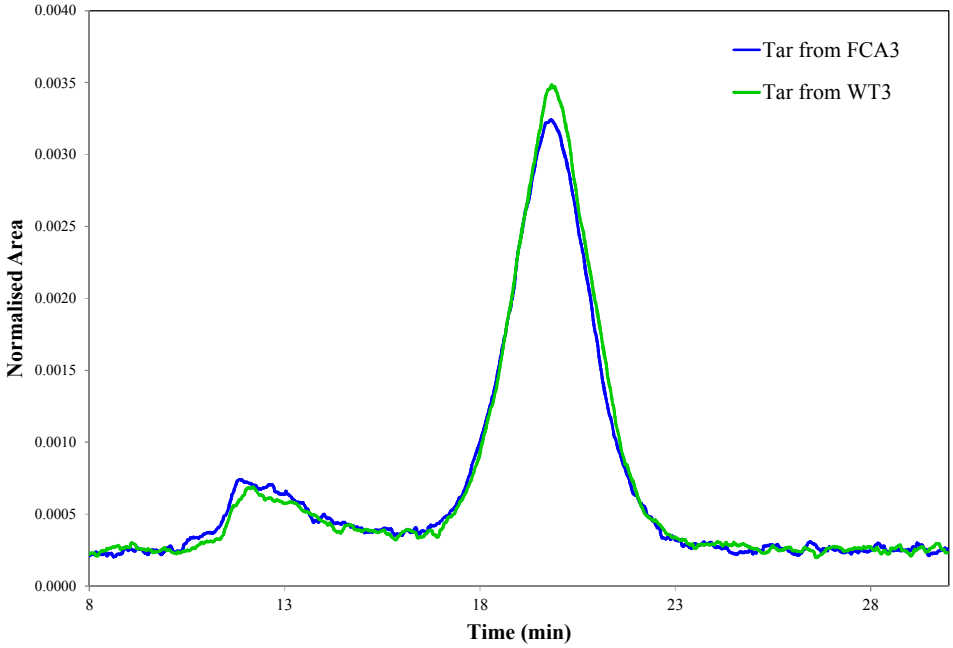

Figure 4.3. SEC chromatograms of tars obtained from the pyrolysis of FCA3 and WT3. WMR at 400°C, 5s and 1000°C/s.

A Perkin-Elmer LS50 luminescence spectrometer was used for UV-F analyses. The device was set with a slit width of 5 nm, to scan at 240 nm min-1; synchronous spectra were acquired at a constant wavelength difference of 20 nm. A quartz cell with 1 cm path length was used. The spectrometer featured automatic correction for changes in source intensity as a function of wavelength. Synchronous spectra of the samples were obtained in NMP. Solutions were diluted with NMP to avoid self-absorption effects: dilution was increased until the fluorescence signal intensity began to decrease. All shown spectra have been peak-normalized to account for the different fluorescence yields of the different samples and highlight the shifts in the peak maximum.

Figure 4.4 shows the UV-F spectra of the tars from the pyrolysis of FCA3 and WT3. The two tars exhibit similar fluorescence. The most intense fluorescence for both samples was centered around 315 nm. Additionally, both tars presented a second peak at the longer wavelength of 350 nm, the tar from WT3 showing a slightly more intense signal.

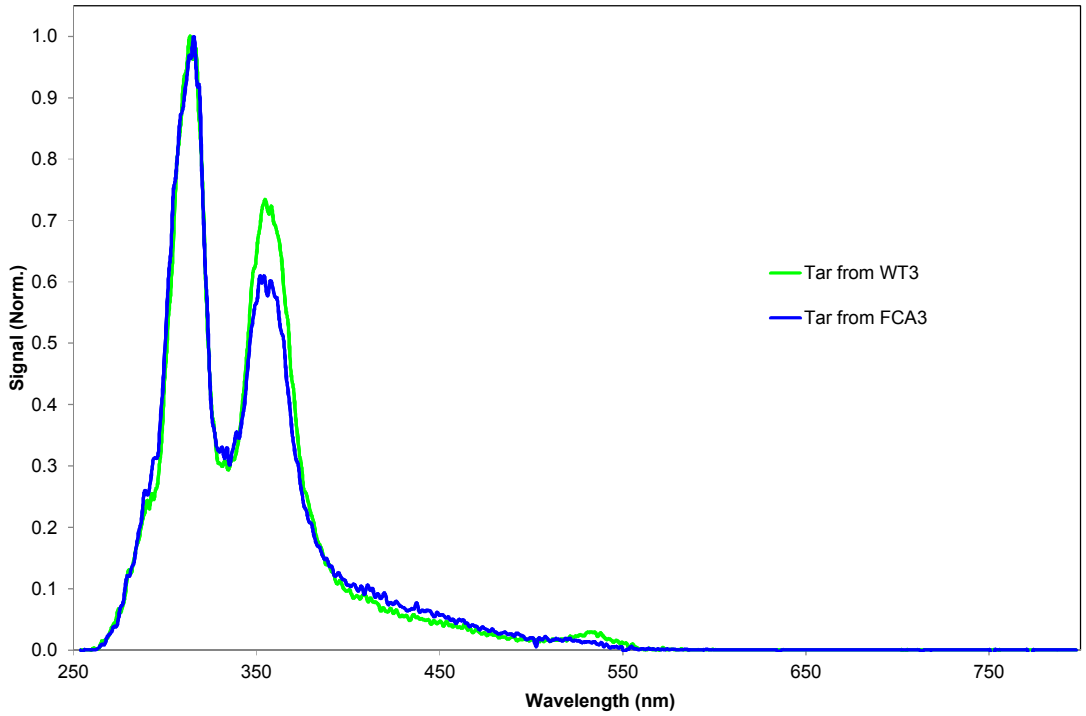

Figure 4.4. UV-F spectra of tars obtained from the pyrolysis of FCA3 and WT3. WMR at 400°C, 5s and 1000°C/s.

The main conclusions obtained from the pyrolysis of WT3 and FCA3 thus far are:

- Char yield from FCA3 was higher than that from WT3. On the contrary, FCA3 gave rise to less tar yield than WT3.
- Based on GC, SEC and UV-F analyses, there are no significant differences between the tars obtained from FCA3 and WT3.
- The change in the degree of polymerization of the samples seems to affect the pyrolysis product yields but not the composition of the tars produced. More experiments are needed to prove this statement.
- Since pyrolysis of the biomass samples is incomplete under the operating conditions studied, clearer differences were expected. As further conditions need to be evaluate.

4.4 Pyrolysis of Arabidopsis samples with reduced amount of lignin (Qsub2)

The pyrolysis of two samples from Set 3 (WT2 and Qsub2) was carried out in the atmospheric wire mesh reactor at different peak temperatures and holding times, and at

a heating rate of 1000 °C/s. Before being used, the two samples were crushed and sieved between 106 and 150 μm and dried overnight.

Table 4.3 shows the product yields obtained from the pyrolysis of both samples. Duplicate experiments were carried out for each data point. Qsub2 yielded slightly larger amount of char than the corresponding wildtype WT2 at 400 °C and 5 s of holding time. On the other hand, Qsub2 gave rise to less amount of tar fraction than WT2. Therefore, tar proportion in within the total volatile fraction also diminished in the case of the modified biomass Qsub2 compared to that in the case of WT2. On the other hand, the increase in temperature from 400 to 550 °C gave rise to a slight higher yield of total volatiles. Nevertheless, change in tar yield was negligible. Additionally, product yields were not affected by the increase in holding time from 5 to 30 s.

Table 4.3. Experimental conditions and product yields from Wire Mesh Reactor experiments of biomass with less lignin content and its corresponding wildtype. Heating rate – 1,000 °C/s, Pressure – 1 bar, Atmosphere – He

Sample	Peak Temperature (°C)	Holding time (s)	Char (wt.%)	Tar (wt.%)	Gas (wt.%)
WT2 (S3)	400	5	18.3±0.5	41.7±0.4	40.1±0.1
Qsub2 (S3)	400	5	18.8±1.2	39.6±0.1	41.6±1.3
Qsub2 (S3)	550	5	17.1±0.4	39.9±0.2	43.1±0.6
Qsub2* (S3)	550	30	16.6	40.0	43.4

*further replicates required

Tars from pyrolysis of WT2 and Qsub2 were analysed by GC, SEC and UV-F.

- **GC analyses**

GC analyses were performed in a Perkin Elmer "Clarus 500" chromatograph with flame ionization detector (FID). The GC was equipped with a non-polar capillary column HT5 (25 m x 0.32 mm and 0.1 μm film thickness). A flow rate of 10 mL/min of He was used as carrier gas with a split ratio of 5.4:1. The initial oven temperature was 40 °C, which was held for 1.0 min. It was then programmed to rise to 380 °C at 10 °C/min with an isotherm held for 10 min. The programmed temperature injector was ramped from 80 °C (held for 0.5 min) to 380 °C at 100 °C/min. The flame was maintained with H_2 flow

rate of 45 mL/min and air flow rate of 450 mL/min. Calibrations with a set of n-alkanes (C8 to C30) and a standard PAH were used to evaluate the percentage of elution of the material.

Figure 4.5 shows the chromatograms obtained for the analyses of tars from WT2 and Qsub2. As can be seen, no remarkable results were obtained from these analyses. Almost no peak was detected for the tar from Qsub2. Some peaks were observed in the case of tar from WT2, which shows the presence of some compound eluting within the temperature range relative to GC analyses. In general, it can be said that most of the components in the tars from WT2 and Qsub2 present a MW distribution that exceed the operating window of the GC (material with boiling point lower than 570 ^{o}C). Thus, the area identified corresponds to less than 0.1 % of the area expected based on the PAH calibration.

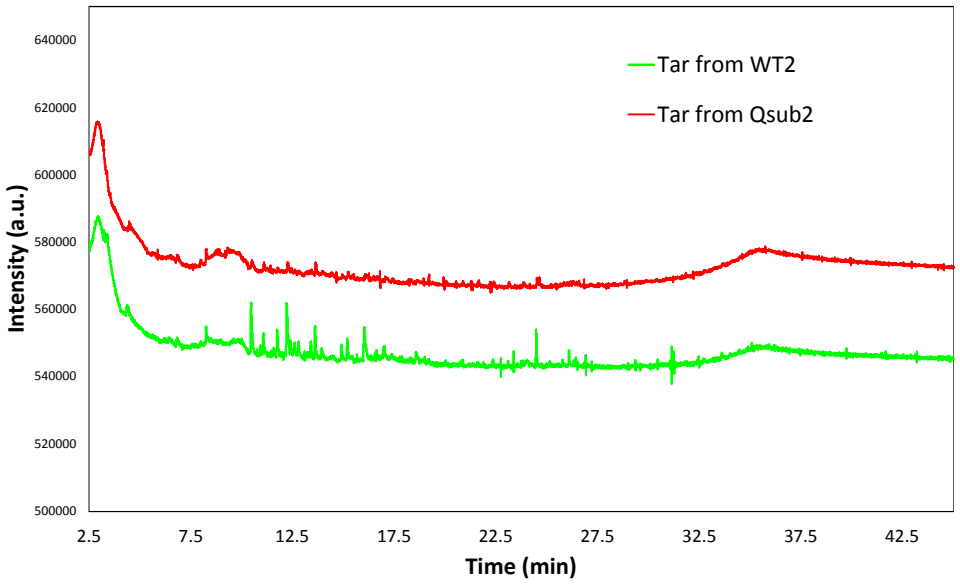

Figure 4.5. GC chromatograms of tars obtained from the pyrolysis of WT2 and Qsub2. WMR at 400^{o}C, 5s and 1000^{o}C/s.

Table 2 shows the results obtained from the GC analyses of WT2 and Qsub2 biomass. Results are given as the ratio of the mass obtained in different boiling point ranges with the initial mass of biomass charged on the WMR. Results of tars from Series 1 biomass are included for comparison.

Table 4.4. Results from GC analyses of tars obtained from the pyrolysis of FCA3 and WT3 (Series 1) and WT2 and Qsub2 (Series 2)

	Mass in the BP range/Initial Mass of Biomass (µg/µg)					
Boiling point range (^{o}C)	Tar from WT3 (S1)	Tar from FCA3 (S1)	Tar from WT2 (S3)	Tar from Qsub2 (S3)	Tar from Qsub2 @550^{o}C, 5s	Tar from Qsub2 @550^{o}C, 30s
147 - 266	0.027	0.041	0.037	0.005	0.046	0.027
267 - 339	0.080	0.090	0.034	0.010	0.011	0.005
340 - 399	0	0.002	0.020	0.005	0.003	0
400 - 449	0.202	0.152	0.017	0.002	0.033	0.001
450 - 491	0.197	0.078	0.002	0.002	0.016	0
592 - 572	0.050	0	0.004	0.001	0	0.001
573 - 587	0	0	0	0	0	0.021
Total amount analysed (wt.%)	1.53	1.11	0.28	0.07	0.36	0.15

As can be seen, the amount analysed by GC respect to the initial mass of biomass charge on the WMR was slightly larger in the case of the samples from Series 1. The amount evolved in the case of Qsub2 at 400 ^{o}C and 5 s was negligible. Regarding tars from Series 1, most of the detected compounds evolved in the range of equivalent boiling point of 400-490 ^{o}C. In the case of tar from WT2 (Series 2), the small amount of detected material eluted in the range between 150 and 400 ^{o}C. In the case of tar from Qsub2 (Series 2) at 550 ^{o}C and 5s, the small amount of detected material eluted in the ranges between 150 and 340 ^{o}C and 400 and 491 ^{o}C. Regarding the tar from Qsub2 (Series 2) at 550 ^{o}C and 30s, the small amount of detected material eluted in the ranges between 150 and 270 ^{o}C and 575 and 590 ^{o}C.

- **SEC analyses**

A 300 mm long, 7.5 mm i.d. polystyrene/polydivinylbenzene-packed Mixed-D column with 5μm particles was used for SEC analyses. The column was operated at 80 °C and a flow rate of 0.5 mL/min. NMP was used as the mobile phase. Detection was carried out using a Knauer Smartline diode array UV-absorbance detector. As NMP is opaque at 254 nm, detection of standard compounds and samples was performed at 300 nm, where NMP is partially transparent.

A calibration of the Mixed-D column was carried out using two sets of standards, polystyrene (PS) and polyaromatic hydrocarbons (PAH). The PS-based calibration is applied to the 11- 20 min time range, while the PAH-based calibration is used in 20-24 min region, resulting in the following calibration equations:

11-20 min region: log10 [MM] = 10.6320 – 0.4038 [elution time (min)]

20-24 min region: log10 [MM] = 6.8495 – 0.2095 [elution time (min)]

Figures 4.6 and 4.7 show molecular weight distribution by size exclusion chromatography of the tars from the pyrolysis of WT2 and Qsub2. In all cases, bimodal distributions of signal are observed. The early eluting peak corresponds to material of molecular size unable to penetrate the porosity of the column packing, and is referred to as “excluded” from the column porosity. The exclusion limit of the column, defined according to the behaviour of polystyrene standards, is about 200,000 u (although molecular conformation is considered

to be the factor that causes molecules to become excluded from the column porosity rather than molecular weight). The second eluting peak corresponds to the material able to penetrate the porosity of the column packing.

Figure 4.6 shows molecular weight distribution by size exclusion chromatography of the tars from the pyrolysis of WT2 and Qsub2 at 400 ºC and 5 s. The two tars show similar molecular weight distributions. Both chromatograms show a lift-off in the baseline around 16.7 min, which corresponds to a polystyrene mass of about 7,740 u. This is considered the upper limit in the molecular weight distribution of these samples. Both tars present a maximum peak around 19.65 min, which corresponds to a polystyrene mass of about 475 u. Tar from Qsub2 seems to have a slightly narrower molecular weight distribution than the tar from WT2, which is shifted to lower MW values.

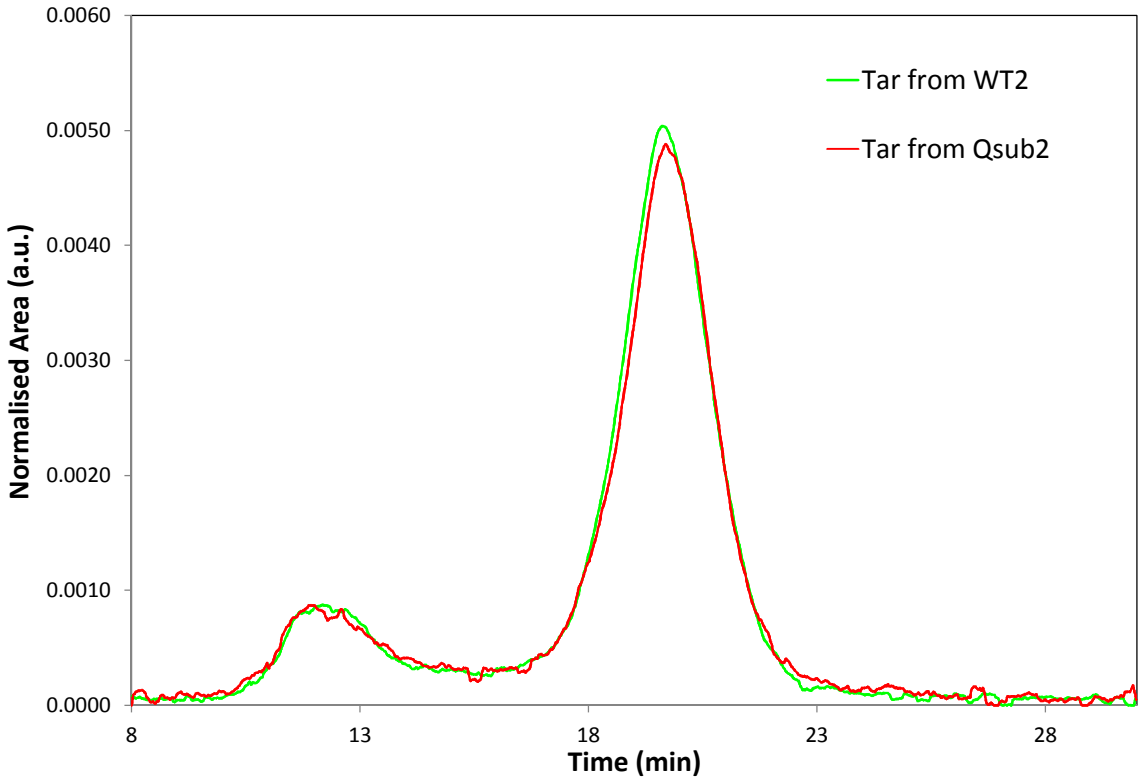

Figure 4.6. SEC chromatograms of tars obtained from the pyrolysis of WT2 and Qsub2. WMR at 400ºC, 5s and 1000ºC/s.

Figure 4.7 shows molecular weight distribution by size exclusion chromatography of the tars from the pyrolysis of Qsub2 at different final temperatures and holding times. The three tars show similar molecular weight distributions. Thus, the three chromatograms show a lift-off in the baseline around 16.7 min, which corresponds to a polystyrene mass of about 7,740 u. This is considered the upper limit in the molecular weight distribution of these samples. Tar from pyrolysis at 550 ^{o}C and 5 s presents a maximum peak around 19.78 min, which corresponds to a polystyrene mass of about 440 u. Although the maximum peak was slightly displaced towards longer retention time than that of tar from pyrolysis at 400 ^{o}C and 5 s, tar from 550 ^{o}C and 5 s exhibits a broader MW distribution. Thus, the chromatogram covers both lighter and heavier MW. Tar from pyrolysis at 550 ^{o}C and 30 s presents a MW distribution clearly displaced towards lighter values. It has a maximum peak around 19.97 min, which corresponds to a polystyrene mass of about 370 u. Therefore, the increase in in holding time seems to give rise to lighter molecular weight distribution.

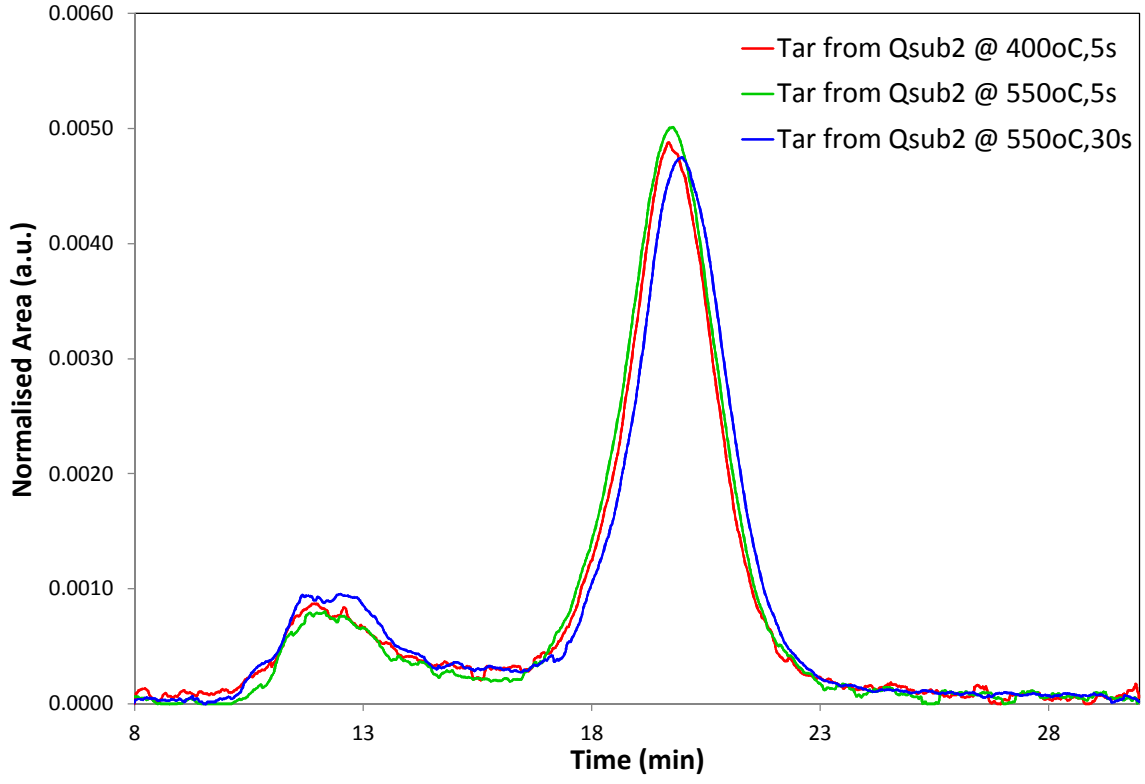

Figure 4.7. SEC chromatograms of tars obtained from the pyrolysis of Qsub2 at different temperatures and holding times.

- **UV-F spectra**

A Perkin-Elmer LS50 luminescence spectrometer was used for UV-F analyses. The device was set with a slit width of 5 nm, to scan at 240 nm min-1; synchronous spectra were acquired at a constant wavelength difference of 20 nm. A quartz cell with 1 cm path length was used. The spectrometer featured automatic correction for changes in source intensity as a function of wavelength. Synchronous spectra of the samples were obtained in NMP. Solutions were diluted with NMP to avoid self-absorption effects: dilution was increased until the fluorescence signal intensity began to decrease. All shown spectra have been peak-normalized to account for the different fluorescence yields of the different samples and highlight the shifts in the peak maximum.

Figure 4.8 shows the UV-F spectra of the tars from the pyrolysis of WT2 and Qsub2 at 400 ^{o}C and 5 s. The two tars exhibit fluorescence in the same region of the spectra. Similar profiles are observed; however, Qsub2 present a spectrum slightly displaced towards shorter wavelengths compared to that from WT2. This result points to the presence of smaller polynuclear aromatic groups in the case of Qsub2. Thus, the most intense fluorescence was centred around 314 nm for WT2 and 307 nm for Qsub2. Additionally, both tars presented a second peak at longer wavelength. WT2 showed a more intense signal at this longest wavelength, with a peak at 360 nm. The second peak was around 355 nm in the case of Qsub2. The less intense florescence at shorter wavelength suggests the presence of smaller conjugated aromatic systems in the tar obtained from the modified biomass Qsub2, with reduced amount of lignin. These results are consistent with earlier findings from SEC, both of which point toward higher concentrations of larger MW groups being produced in the tar obtained from the wildtype biomass.

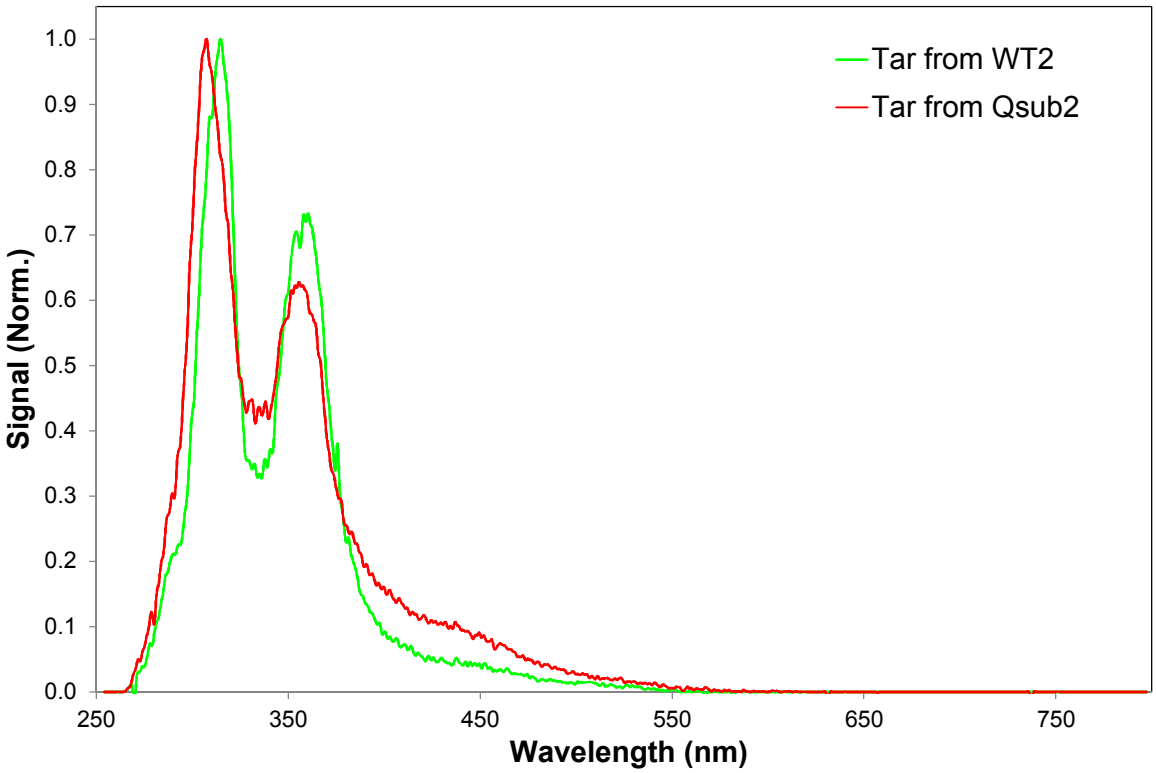

Figure 4.8 UV-F spectra of tars obtained from the pyrolysis of WT2 and Qsub2. WMR at 400°C, 5s and 1000°C/s.

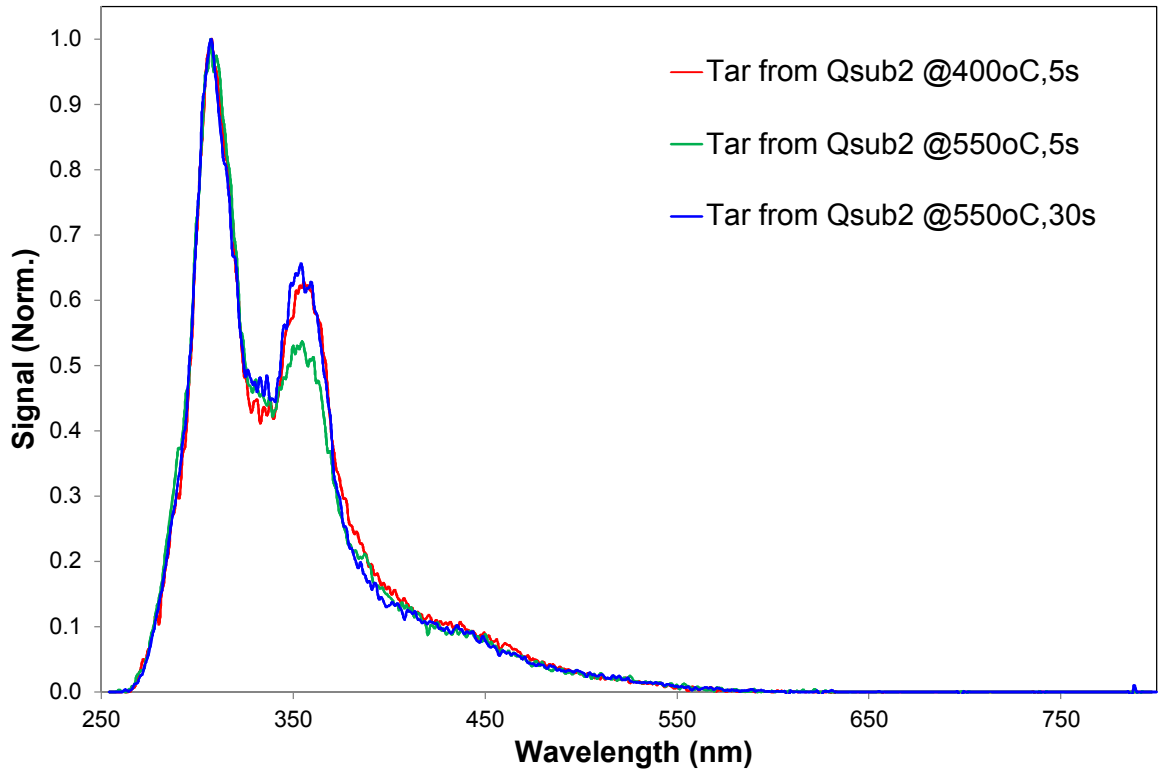

Figure 4.9. UV-F spectra of tars obtained from the pyrolysis Qsub2 at different temperatures and holding times.

Figure 4.9 shows the UV-F spectra of the tars from the pyrolysis of Qsub2 at different peak temperatures (400 and 550 ^{o}C) and holding times (5 and 30 s). The three tars exhibit similar fluorescence profiles. Thus, the most intense fluorescence was centred around 307 nm for all the cases. Additionally, the three tars presented a second peak around 354 nm.

Conclusions

The main conclusions obtained from the pyrolysis of WT2 and Qsub2 in Series 3 are:

- Tar yield from Qsub2 at 400 ^{o}C and 5 s was smaller than that from WT2. On the contrary, Qsub2 gave rise to more char yield than WT2.
- GC did not gave rise to significant results, since less than 0.3 wt.% of the injected material seems to have eluted from the column. This needs to be revisited.

- SEC and UV-F results showed slight differences between the tars obtained from WT2 and Qsub2. Findings from SEC and UV-F point toward higher concentrations of smaller aromatic groups in the tar obtained from the modified biomass Qsub2.
- Increasing final temperature and holding time had a slight influence on the products yields.
- SEC results showed differences in the MW distribution of the tars obtained.

5.0 References

1. Huber, G.W., S. Iborra, and A. Corma, *Synthesis of Transportation Fuels from Biomass: Chemistry, Catalysts, and Engineering.* Chem. Rev. (Washington, DC, U. S.), 2006. **106**(9): p. 4044-4098.

2. Koppatz, S., et al., *H2 rich product gas by steam gasification of biomass with in situ CO2 absorption in a dual fluidized bed system of 8 MW fuel input.* Fuel Process. Technol., 2009. **90**(7–8): p. 914-921.

3. Pan, Y.G., et al., *Fluidized-bed co-gasification of residual biomass/poor coal blends for fuel gas production.* Fuel, 2000. **79**(11): p. 1317-1326.

4. Vélez, J.F., et al., *Co-gasification of Colombian coal and biomass in fluidized bed: An experimental study.* Fuel, 2009. **88**(3): p. 424-430.

5. Pinto, F., et al., *Effect of catalysts in the quality of syngas and by-products obtained by co-gasification of coal and wastes. 1. Tars and nitrogen compounds abatement.* Fuel, 2007. **86**(14): p. 2052-2063.

6. Brage, C., et al., *Tar evolution profiles obtained from gasification of biomass and coal.* Biomass Bioenergy, 2000. **18**(1): p. 87-91.

7. Abu El-Rub, Z., E.A. Bramer, and G. Brem, *Review of Catalysts for Tar Elimination in Biomass Gasification Processes.* Industrial & Engineering Chemistry Research, 2004. **43**(22): p. 6911-6919.

8. Rabou, L.P.L.M., et al., *Tar in Biomass Producer Gas, the Energy research Centre of The Netherlands (ECN) Experience: An Enduring Challenge.* Energy Fuels, 2009. **23**(Copyright (C) 2012 American Chemical Society (ACS). All Rights Reserved.): p. 6189-6198.

9. Pfeifer, C. and H. Hofbauer, *Development of catalytic tar decomposition downstream from a dual fluidized bed biomass steam gasifier.* Powder Technology, 2008. **180**(1–2): p. 9-16.

10. Wolfesberger-Schwabl, U., I. Aigner, and H. Hofbauer, *Mechanism of Tar Generation during Fluidized Bed Gasification and Low Temperature Pyrolysis.* Industrial & Engineering Chemistry Research, 2012. **51**(40): p. 13001-13007.

11. EPA. *http://www.epa.gov/region9/waste/solid/projects/pdf/ColumbiaFinal-reportJune20.pdf*. 2012 [cited 2012 Sept].

12. Herod, A.A., K.D. Bartle, and R. Kandiyoti, *Characterization of Heavy Hydrocarbons by Chromatographic and Mass Spectrometric Methods: An Overview.* Energy & Fuels, 2007. **21**(4): p. 2176-2203.

13. Kandiyoti, R., Herod, A.A., Bartle, K.D., *Solid Fuels and Heavy Hydrocarbon Liquids: Thermal Characterisation and Analysis*2006: Elsevier.

14. Diebold, J.P., *A Review of the Chemical and Physical Mechanisms of the Storage Stability of Fast Pyrolysis Bio-Oils.*, 2000, National Renewable Energy Laboratory: Golden, Colorado.

15. Oasmaa, A. and S. Czernik, *Fuel Oil Quality of Biomass Pyrolysis OilsState of the Art for the End Users.* Energy & Fuels, 1999. **13**(4): p. 914-921.

16. Boucher, M.E., et al., *Bio-oils obtained by vacuum pyrolysis of softwood bark as a liquid fuel for gas turbines. Part II: Stability and ageing of bio-oil and its blends with methanol and a pyrolytic aqueous phase.* Biomass Bioenergy, 2000. **19**(5): p. 351-361.

17. Bridgwater, A.V. and G.V.C. Peacocke, *Fast pyrolysis processes for biomass.* Renewable and Sustainable Energy Reviews, 2000. **4**(1): p. 1-73.

18. Diebold, J.P. and S. Czernik, *Additives To Lower and Stabilize the Viscosity of Pyrolysis Oils during Storage.* Energy & Fuels, 1997. **11**(5): p. 1081-1091.

19. Fahmi, R., et al., *The effect of lignin and inorganic species in biomass on pyrolysis oil yields, quality and stability.* Fuel, 2008. **87**(7): p. 1230-1240.

20. Oasmaa, A. and E. Kuoppala, *Fast Pyrolysis of Forestry Residue. 3. Storage Stability of Liquid Fuel.* Energy & Fuels, 2003. **17**(4): p. 1075-1084.

21. Oasmaa, A., et al., *Fast Pyrolysis of Forestry Residue and Pine. 4. Improvement of the Product Quality by Solvent Addition.* Energy & Fuels, 2004. **18**(5): p. 1578-1583.

22. Oasmaa, A.L., E.; Koponen P.;Levander, J. and Tapola E. (). , *Physical characterisation of biomass-based pyrolysis liquids – Application of standard fuel oil analyses.*, in *VTT Publications 306.*1997, Technical Research Centre of Finland.: Espoo, Finland.

23. Doshi, V.A., H.B. Vuthaluru, and T. Bastow, *Investigations into the control of odour and viscosity of biomass oil derived from pyrolysis of sewage sludge.* Fuel Process. Technol., 2005. **86**(8): p. 885-897.

24. Dufour, A., et al., *In Situ Analysis of Biomass Pyrolysis by High Temperature Rheology in Relations with 1H NMR.* Energy & Fuels, 2012. **26**(10): p. 6432-6441.

25. Stamatov, V., D. Honnery, and J. Soria, *Combustion properties of slow pyrolysis bio-oil produced from indigenous Australian species.* Renewable Energy, 2006. **31**(13): p. 2108-2121.

26. Yu, F., et al., *Physical and chemical properties of bio-oils from microwave pyrolysis of corn stover.* Applied Biochemistry and Biotechnology, 2007. **137-140**(1): p. 957-970.

27. Qi, Z.J., C.; Tiejun, W. and Ying, X., *Review of biomass pyrolysis oil properties and upgrading research.* Energy Conversion and Management., 2007. **48**: p. 87-92.

28. Majerski, P.A., *Method of upgrading biomass pyrolysis liquids for use as fuels and as a source of chemicals by reaction with alcohols.*, E.p. office, Editor 1996.

29. Neeft, J.P.A., *Rational for setup of Impinger Train, technical background report, Jan. 2005, CEN BT/TF 143.*, in *EuropeanStandard* 2005: The Netherlands.

30. EuropeanStandard, *Biomass gasification. Tar and particles in product gases. Sampling and analysis. DD CEN/TS 15439:2006.*, 2006.

31. Morgan, T.J., et al., *Characterization of Molecular Mass Ranges of Two Coal Tar Distillate Fractions (Creosote and Anthracene Oils) and Aromatic Standards by LD-MS, GC-MS, Probe-MS and Size-exclusion Chromatography.* Energy & Fuels, 2008. **22**(5): p. 3275-3292.

32. Del Rio, J.C., R.P. Philp, and J. Allen, *Nature and geochemistry of high molecular weight hydrocarbons (above C40) in oils and solid bitumens.* Organic Geochemistry, 1992. **18**(4): p. 541-553.

33. Hsieh, M. and R. Paul Philp, *Ubiquitous occurrence of high molecular weight hydrocarbons in crude oils.* Organic Geochemistry, 2001. **32**(8): p. 955-966.

34. Heath, D., et al., *Quantification of the C30+ fraction of North sea gas condensates by high temperature capillary gas chromatography.* Analytical Proceedings including Analytical Communications, 1995. **32**(12): p. 485-487.

35. Milne, T.A., Evans, R.J., Abatzoglou, N., *Biomass gasification tars: their nature, formation, destruction, and tolerance limits in energy conversion devices.*, in *Proceedings of 3rd biomass conference of the America's.*1997: Quebec, Canada. p. 729.

36. Parker, J.E., et al., *Identification of large molecular mass material in high temperature coal tars and pitches by laser desorption mass spectroscopy.* Fuel, 1993. **72**(10): p. 1381-1391.

37. Johnson, B.R., et al., *A test of the MALDI-MS calibration of SEC with N-methyl-2-pyrrolidinone for coal derived materials.* Fuel, 1998. **77**(14): p. 1527-1531.

38. Artor, L., Su, Y., Yoshihisa, H., Murata, S., Nomura, M., *Structural Characterization of asphaltene fraction from vacuum residue of Arabian crude mixture by spectroscopic and pyrolytic methods.* Sekiyu Gakkaishi., 1999. **42**: p. 206.

39. Janitschke, W., et al., *Investigations of coals by on-line coupled laser desorption/gas chromatography/mass spectrometry (LD/GC/MS).* Journal of Analytical and Applied Pyrolysis, 2000. **56**(1): p. 99-111.

40. Letzel, T., et al., *Phenyl-Modified Reversed-Phase Liquid Chromatography Coupled to Atmospheric Pressure Chemical Ionization Mass Spectrometry: A Universal Method for the Analysis of Partially Oxidized Aromatic Hydrocarbons.* Analytical Chemistry, 2001. **73**(7): p. 1634-1645.

41. Marin, N., et al., *Copyrolysis of wood biomass and synthetic polymers mixtures. Part II: characterisation of the liquid phases.* Journal of Analytical and Applied Pyrolysis, 2002. **65**(1): p. 41-55.

42. Sharypov, V.I., et al., *Co-pyrolysis of wood biomass and synthetic polymers mixtures. Part III: Characterisation of heavy products.* Journal of Analytical and Applied Pyrolysis, 2003. **67**(2): p. 325-340.

43. Bayerbach, R., et al., *Characterization of the water-insoluble fraction from fast pyrolysis liquids (pyrolytic lignin): Part III. Molar mass characteristics by SEC, MALDI-TOF-MS, LDI-TOF-MS, and Py-FIMS.* Journal of Analytical and Applied Pyrolysis, 2006. **77**(2): p. 95-101.

44. Lazaro, M.J., et al., *Fractionation of a wood tar pitch by planar chromatography for the characterisation of large molecular mass materials.* Journal of Chromatography A, 1999. **840**(1): p. 107-115.

45. Tanaka, R., et al., *Analysis of the Molecular Weight Distribution of Petroleum Asphaltenes Using Laser Desorption-Mass Spectrometry.* Energy & Fuels, 2004. **18**(5): p. 1405-1413.

46. Purevsuren, B., Davaajav, Y., Karaca, F., Morgan, T.J., George, A., Herod, A.A. and Kandiyoti, R. , *Pyrolysis of waste polypropylene and characterization of the tar.* European Journal of Mass Spectrometry, 2009. **15**: p. 23-33.

47. Herod, A.A., et al., *Analytical Methods for Characterizing High-Mass Complex Polydisperse Hydrocarbon Mixtures: An Overview.* Chem. Rev. (Washington, DC, U. S.),

2012. **112**(Copyright (C) 2012 American Chemical Society (ACS). All Rights Reserved.): p. 3892-3923.

48. Karaca, F., et al., *Molecular mass ranges of coal tar pitch fractions by mass spectrometry and size-exclusion chromatography.* Rapid Communications in Mass Spectrometry, 2009. **23**(13): p. 2087-2098.

49. Podgorski, D.C., et al., *Characterization of Pyrogenic Black Carbon by Desorption Atmospheric Pressure Photoionization Fourier Transform Ion Cyclotron Resonance Mass Spectrometry.* Analytical Chemistry, 2011. **84**(3): p. 1281-1287.

50. Jin, J.M., S. Kim, and J.E. Birdwell, *Molecular Characterization and Comparison of Shale Oils Generated by Different Pyrolysis Methods.* Energy & Fuels, 2011. **26**(2): p. 1054-1062.

51. Smith, D.F., et al., *Characterization of Acidic Species in Athabasca Bitumen and Bitumen Heavy Vacuum Gas Oil by Negative-Ion ESI FT–ICR MS with and without Acid–Ion Exchange Resin Prefractionation.* Energy & Fuels, 2008. **22**(4): p. 2372-2378.

52. McKenna, A.M., et al., *Identification of Vanadyl Porphyrins in a Heavy Crude Oil and Raw Asphaltene by Atmospheric Pressure Photoionization Fourier Transform Ion Cyclotron Resonance (FT-ICR) Mass Spectrometry.* Energy & Fuels, 2009. **23**(4): p. 2122-2128.

53. Karaca, F., et al., *The Calibration of Size Exclusion Chromatography Columns: Molecular Mass Distributions of Heavy Hydrocarbon Liquids.* Energy & Fuels, 2004. **18**(3): p. 778-788.

54. Berrueco, C., et al., *Calibration of Size-Exclusion Chromatography Columns with 1-Methyl-2-pyrrolidinone (NMP)/Chloroform Mixtures as Eluent: Applications to Petroleum-Derived Samples.* Energy & Fuels, 2008. **22**(5): p. 3265-3274.

55. Morgan, T.J., et al., *Isolation of Size Exclusion Chromatography Elution-Fractions of Coal and Petroleum-Derived Samples and Analysis by Laser Desorption Mass Spectrometry.* Energy & Fuels, 2009. **23**(12): p. 6003-6014.

56. Morgan, T.J., et al., *Estimating molecular masses of petroleum-derived fractions: High mass (>2000 u) materials in maltenes and asphaltenes from Maya crude oil.* Journal of Chromatography A, 2010. **1217**(24): p. 3804-3818.

57. Islas, C.A., et al., *Matching average masses of pitch fractions of narrow polydispersity, derived from matrix-assisted laser desorption ionisation time-of-flight mass*

spectrometry, with the polystyrene calibration of SEC. Journal of Separation Science, 2003. **26**(15-16): p. 1422-1428.

58. Pindoria, R.V., et al., *A two-stage fixed-bed reactor for direct hydrotreatment of volatiles from the hydropyrolysis of biomass: effect of catalyst temperature, pressure and catalyst ageing time on product characteristics.* Fuel, 1998. **77**(15): p. 1715-1726.

59. Somrang, Y., *Effect of Operating Conditions on Product Distributions and Bio-oil Ageing in Biomass Pyrolysis.*, in *Chemical Engineering.*2011, Imperial College: London, UK.

60. Morgan, T.J., *Molecular mass and structural characterization of heavy*

hydrocarbon materials, in *Chemical Engineering.*2008, Imperial College: London.

61. Morgan, T.J., et al., *Characterization of Maya Crude Oil Maltenes and Asphaltenes in Terms of Structural Parameters Calculated from Nuclear Magnetic Resonance (NMR) Spectroscopy and Laser Desorption–Mass Spectroscopy (LD–MS).* Energy & Fuels, 2010. **24**(7): p. 3977-3989.

62. P. Álvarez, C.B., S. Venditti, A. George, T.J. Morgan, M. Millan, A.A. Herod, R. Kandiyoti. *Syncrude Characterization* in *ACS Fuel Div, National meeting*. 2009. Salt Lake City, USA: ACS.

63. S. Kalisz, F.M., J. Martinec, J. Ungeheuer, L. Andersen, D. Baxter, *Air and air-steam biomass gasification in interconnected, internally circulating fluidized beds*, in *17th European Biomass Conference & Exhibition*2009: Hamburg, Germany. p. 980.

64. Miccio, F., et al., *Combustion of liquid bio-fuels in an internal circulating fluidized bed.* Chemical Engineering Journal, 2008. **143**(1–3): p. 172-179.

65. Li, C.-Z., et al., *UV-Fluorescence Spectroscopy of Coal Pyrolysis Tars.* Energy & Fuels, 1994. **8**(5): p. 1039-1048.

66. Mohan, D., C.U. Pittman, Jr., and P.H. Steele, *Pyrolysis of Wood/Biomass for Bio-oil: A Critical Review.* Energy Fuels, 2006. **20**(Copyright (C) 2012 American Chemical Society (ACS). All Rights Reserved.): p. 848-889.

67. Guilbault., G.G., *Practical Fluorescence, Second Edition.*1990: Marcel Dekker, New York, USA.

68. Metzinger, T. and K.J. Hüttinger, *Investigations on the cross-linking of binder pitch matrix of carbon bodies with molecular oxygen — Part I. Chemistry of reactions between pitch and oxygen.* Carbon, 1997. **35**(7): p. 885-892.

69. Álvarez, P., et al., *Characterization and Pyrolysis Behavior of Novel Anthracene Oil Derivatives.* Energy & Fuels, 2008. **22**(6): p. 4077-4086.

70. Fernández, A.L., et al., *Air-blowing of anthracene oil for carbon precursors.* Carbon, 2000. **38**(9): p. 1315-1322.

71. Álvarez, P., et al., *An insight into the polymerization of anthracene oil to produce pitch using nuclear magnetic resonance.* Fuel, 2012(0).

72. Lee, R.F., *Photo-oxidation and Photo-toxicity of Crude and Refined Oils.* Spill Science & Technology Bulletin, 2003. **8**(2): p. 157-162.

73. Thominette, F. and J. Verdu, *Photooxidative behavior of crude oils relative to sea pollution. Part I. Comparative study of various crude oils and model systems.* Mar. Chem., 1984. **15**(Copyright (C) 2012 American Chemical Society (ACS). All Rights Reserved.): p. 91-104.

74. Thominette, F. and J. Verdu, *Photooxidative behavior of crude oils relative to sea pollution. Part II. Photo-induced phase separation.* Mar. Chem., 1984. **15**(Copyright (C) 2012 American Chemical Society (ACS). All Rights Reserved.): p. 105-115.

75. Heitner., C., *Lignin and Lignans: Advances in Chemistry. Chapter 16. The photochemistry of lignin*2010: CRC Press.

76. Omais, B., et al., *Characterization of Oxygenated Species in Coal Liquefaction Products: An Overview.* Energy & Fuels, 2010. **24**(11): p. 5807-5816.

77. Strausz, O.P., I. Safarik, and E.M. Lown, *Cause of Asphaltene Fluorescence Intensity Variation with Molecular Weight and Its Ramifications for Laser Ionization Mass Spectrometry.* Energy & Fuels, 2009. **23**(3): p. 1555-1562.

References:

1. Aigner, I., C. Pfeifer, and H. Hofbauer, *Co-gasification of coal and wood in a dual fluidized bed gasifier.* Fuel, 2011. **90**(7): p. 2404-2412.

2. Vassilev, S.V., et al., *An overview of the organic and inorganic phase composition of biomass.* Fuel, 2012. **94**(Copyright (C) 2012 American Chemical Society (ACS). All Rights Reserved.): p. 1-33.

3. Morgan, T.J., et al., *Characterization of Molecular Mass Ranges of Two Coal Tar Distillate Fractions (Creosote and Anthracene Oils) and Aromatic Standards by LD-MS, GC-MS, Probe-MS and Size-exclusion Chromatography.* Energy & Fuels, 2008. **22**(5): p. 3275-3292.

4. Karaca, F., et al., *The Calibration of Size Exclusion Chromatography Columns: Molecular Mass Distributions of Heavy Hydrocarbon Liquids.* Energy & Fuels, 2004. **18**(3): p. 778-788.

5. Morgan, T.J., et al., *Isolation of Size Exclusion Chromatography Elution-Fractions of Coal and Petroleum-Derived Samples and Analysis by Laser Desorption Mass Spectrometry.* Energy & Fuels, 2009. **23**(12): p. 6003-6014.

6. Herod, A.A., et al., *Analytical Methods for Characterizing High-Mass Complex Polydisperse Hydrocarbon Mixtures: An Overview.* Chem. Rev. (Washington, DC, U. S.), 2012. **112**(Copyright (C) 2012 American Chemical Society (ACS). All Rights Reserved.): p. 3892-3923.

7. Morgan, T.J., et al., *Estimating molecular masses of petroleum-derived fractions: High mass (>2000 u) materials in maltenes and asphaltenes from Maya crude oil.* Journal of Chromatography A, 2010. **1217**(24): p. 3804-3818.

8. Strausz, O.P., I. Safarik, and E.M. Lown, *Cause of Asphaltene Fluorescence Intensity Variation with Molecular Weight and Its Ramifications for Laser Ionization Mass Spectrometry.* Energy & Fuels, 2009. **23**(3): p. 1555-1562.

9. Strausz, O.P., et al., *A Critique of Asphaltene Fluorescence Decay and Depolarization-Based Claims about Molecular Weight and Molecular Architecture.* Energy & Fuels, 2008. **22**(2): p. 1156-1166.

10. Morgan, T.J., et al., *Characterization of Maya Crude Oil Maltenes and Asphaltenes in Terms of Structural Parameters Calculated from Nuclear Magnetic Resonance (NMR) Spectroscopy and Laser Desorption–Mass Spectroscopy (LD–MS).* Energy & Fuels, 2010. **24**(7): p. 3977-3989.

11. Zander, M. and M.W. Haenel, *Regularities in the fluorescence spectra of coal-tar pitch fractions.* Fuel, 1990. **69**(9): p. 1206-1207.

12. P. Álvarez, C.B., S. Venditti, A. George, T.J. Morgan, M. Millan, A.A. Herod, R. Kandiyoti. *Syncrude Characterization* in *ACS Fuel Div, National meeting*. 2009. Salt Lake City, USA: ACS.

13. Morgan, T.J., et al., *Optimization of 1H and 13C NMR Methods for Structural Characterization of Acetone and Pyridine Soluble/Insoluble Fractions of a Coal Tar Pitch.* Energy & Fuels, 2008. **22**(3): p. 1824-1835.

14. Morgan, T.J., *Molecular mass and structural characterization of heavy*

hydrocarbon materials, in *Chemical Engineering.*2008, Imperial College: London.

15. Guilbault., G.G., *Practical Fluorescence, Second Edition.*1990: Marcel Dekker, New York, USA.

16. Álvarez, P., et al., *Characterization and Pyrolysis Behavior of Novel Anthracene Oil Derivatives.* Energy & Fuels, 2008. **22**(6): p. 4077-4086.


Sandia National Laboratories